CLONAL ANALYSIS OF COMPENSATORY PROLIFERATION IN DMHEXDC MUTANTS

by

Bilal Başdağ

B.S., Molecular Biology and Genetics, Istanbul Technical University, 2015

Submitted to the Institute for Graduate Studies in
Science and Engineering in partial fulfillment of
the requirements for the degree of
Master of Science

Graduate Program in Molecular Biology and Genetics

Bogazici University

2018

For those who live their life as a hobby…

ACKNOWLEDGEMENTS

Foremost, my profound thanks to my 9-membered BAŞDAĞ family I am the youngest one for their guidance by their priceless experiences. Also, special gratitude to momma who exerted oneself and encouraged my higher education.

I would like to thank my supervisor Assoc. Prof. Arzu Çelik Fuss. She provided me the opportunity to study in her laboratory.

I am also grateful to jury members Prof. Dr. Nesrin Özören, and Assoc. Prof. Gizem Dinler Doğanay for spending their time to evaluating this thesis.

A huge thank to my lab mates (Fly Lab people) for being superhuman, and making hard and stressful times tolerable. Also thanks a bunch for Fish Lab people especially Metin Adler for their invaluable supports and whatever. Moreover, thanks to my friends who spend their times with me.

A special gratitude to BUGEBİT organism for making this department more beautiful, and showing scientists can enjoy life via sports.

I am also grateful to the dining hall of the university for providing the best medium to us.

I also would like to thank deliverer Muhsin Tezcan who delivers sacks of hope for all of us.

Most importantly, a huge thank to persons who read this page.

This study was supported by the funds of Boğaziçi University (BAP No.7740, Project Number: 15B01P7)

ABSTRACT

CLONAL ANALYSIS OF COMPENSATORY PROLIFERATION IN dmHexDC MUTANTS

Recycling of sugar-containing organic compounds (saccharides) have importance for metabolic activity, cellular growth, and differentiation. During this recycling process, many enzymes, primarily lysosomal enzymes, play a role. We have discovered a novel hexosaminidase enzyme in *Drosophila*, dmHexDC that may have a role in ganglioside and glycosaminoglycan recycling. The function of dmHexDC was investigated in apoptosis-induced compensatory proliferation pathway in retinal development in *Drosophila melanogaster*.

As a result of this study, we show that lack of dmHexDC induces autophagy, which might trigger programmed cell death. Furthermore, we demonstrate by clonal analysis that in dmHexDC deficiency, compensatory proliferation mechanism is activated in neighboring cells. Defects of neuronal differentiation and glial migration were determined especially in the Notch-active equatorial region. Subcellular localization studies indicate that dmHexDC is localized mainly to the ER. Overall, our results indicate that dmHexDC plays a crucial role in *Drosophila* eye development and cell differentiation.

ÖZET

dmHexDC MUTANTLARINDA KOMPANSATUAR ÇOĞALMANIN KLONAL ANALİZİ

Şeker içeren organik bileşiklerin (sakkaritlerin) hücre içi geridönüşümü metabolizma faaliyeti, hücrelerin gelişimi ve farklılaşması için önem arz etmektedir. Bu geri kazanım sürecinde başta lizozom enzimleri olmak üzere pek çok enzim görev almaktadır. *Drosophila* sineklerinde daha önce araştırılmamış olan bir hexosaminidaz enzimi dmHexDC'nin gangliyosit ve glikozaminoglikan geri dönüşümünde rol alabileceğini keşfettik. dmHexDC'nin işlevini *Drosophila* göz gelişimindeki apoptoz ile indüklenen kompansatuar çoğalma yolağında araştırdık.

Bu çalışma sonucunda, dmHexDC enziminin eksikliği halinde, otofajinin aktifleştiğini ve otofajinin de programlanmış hücre ölümünü tetikleyebildiğini gösterdik. Ayrıca, dmHexDC eksikliği halinde komşu hücrelerde komapsatuar çoğalma mekanizmasının aktifleştiğini klonal analiz ile gösterdik. Özellikle Notch aktif ekvator bölgede sinir hücresi farklılaşmasında ve glia hücrelerinin göçünde bozulmalar tespit edildi. Hücre içindeki konum belirleme çalışmaları dmHexDC'nin çoğunlukla ER'da bulunduğunu gösterdi. Genel olarak, sonuçlarımız dmHexDC'nin *Drosophila* göz gelişiminde ve hücre farklılaşmasında muhim rolü olduğunu göstermektedir.

TABLE OF CONTENTS

LIST OF FIGURES

LIST OF TABLES

LIST OF SYMBOLS

bp	Base pair
g	Gram
kb	Kilo base
L	Liter
mL	milliliter
M	Molarity
ng	Nano gram
pH	Power of Hydrogen
rpm	Round per minute
v	Volume
w	Weight
µg	Micro gram
µm	Micro meter
µL	Micro liter

LIST OF ACRONYMS/ABBREVIATIONS

A	Anterior
CP	Compensatory proliferation
D	Dorsal
DNA	Deoxyribonucleic Acid
dsRED	Discosoma Species Red Fluorescent Protein
FRT	Flippase Recognition Target
GFP	Green Fluorescent Protein
L3	Third instar larva
MF	Morphogenetic Furrow
P	Posterior
PBS	Phosphate Buffered Saline
PFA	Paraformaldehyde
RFP	Red Fluorescent Protein
RNA	Ribonucleic Acid
RNAi	RNA Interference
TM	Trans Membrane
UAS	Upstream Activating Sequence
V	Ventral

1. INTRODUCTION

One of the most prominent question in biology is how the fate of cells is determined and how cells differentiate. Neurons are terminally differentiated cells and understanding of differentiation of neuron one of the milestone to understand general differentiation of cells. Unfortunately, the human neuronal system contains tens of neuron type and much more sub-types of neurons (Martini, 2007), which makes it too complicated to understand the mechanism by which each lineage of neuron arises. Nonetheless, simpler models help us to uncover mechanisms underlying neuronal differentiation. The compound eye of the fruit fly, *Drosophila melanogaster*, is one of the best models to study cell differentiation as it includes a small number of cell types and only 8 sub-types of neurons (photoreceptors). Differentiation of neuronal subtypes occurs sequentially and makes it easier to follow changes in normal development. Moreover, rapid development (short life-cycle) and availability of genetic manipulation tools make *Drosophila* a very appropriate model organism to study in this field (Çelik and Wernet, 2017).

1.1. The Life cycle of *Drosophila melanogaster*

The lifespan of a single *Drosophila melanogaster* is approximately 30 days at 29ºC. Development and metamorphosis take about 10 days. During development, the stationary egg hatches after less than one day after fertilization. The larval stage consists of three sub-stages named as first instar, second instar, and third instar. During the first, second, and early third instar stage, larvae crawl inside and around the food. At the late stage of the third instar, larvae crawl away from the food, its cuticle begins to harden and it turns into a still pupa. During the pupal stage, adult organs develop by metamorphosis. Ten days after fertilization, the adult fly ecloses from the pupal case (Hales *et al.*, 2015). Adult *Drosophila* can fly and walk around, start mating after as early as 8 hours post eclosion, and lay new eggs (Greenspan, 1997).

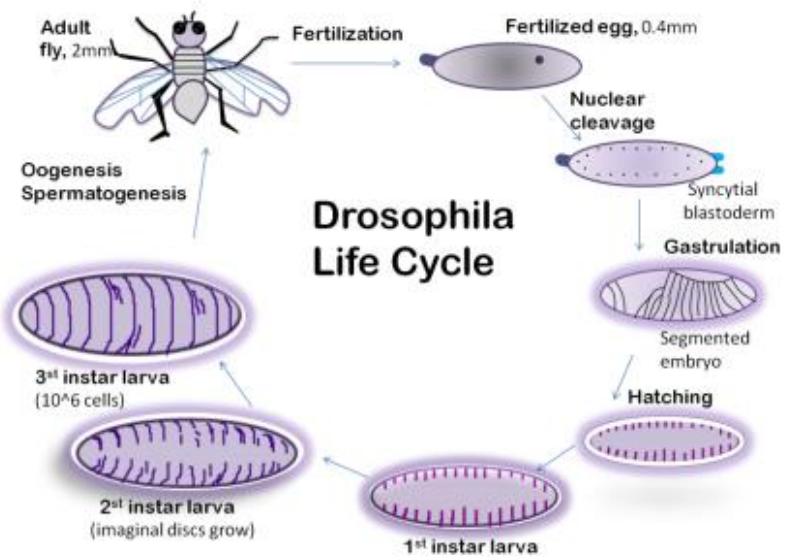

Figure 1.1. The Life cycle of *Drosophila melanogaster* (Vijayalakshmi, 2012)

1.2. Eye Morphology and Development in *Drosophila*

The compound eye is common among insects. Distinct from a vertebrate camera-type eye, the compound eye is composed of 800 hexagonal-shaped units called ommatidia. Each ommatidium includes 8 photoreceptor neurons (also called retinula cells or R cells), and 11 supporting cells such as cone cells, pigment cells, and bristle cells. Photoreceptor neurons have the ability to detect light using specific light-sensitive rhodopsin proteins. PR neurons are named as R1 to R8 according to their rhabdomere, optically active rod-like cell body structure, position, and function. R1 to R6 cells represent the outer photoreceptors, which are sensitive to broad wavelengths of light (see Figure 1.2). Outer PRs have functions that are equivalent to rod cells in vertebrates. R7 and R8 are inner PR cells and are functionally equivalent to cone cells in vertebrates. R7 cells are sensitive to ultraviolet light, and R8 cells are sensitive to the blue and green spectrum of light. Axons of each sub-type of PR cells project to a specific region in the medulla (Voas and Rebay, 2004). Eight PRs are capped by four non-neuronal cone cells and two primary pigment cells which form an iris. 8 cell containing ommatidial cores are insulated from neighboring ommatidium by a

hexagonal lattice of secondary and tertiary pigment cells which blocks leaking of light between ommatidia (Cagan, 2010).

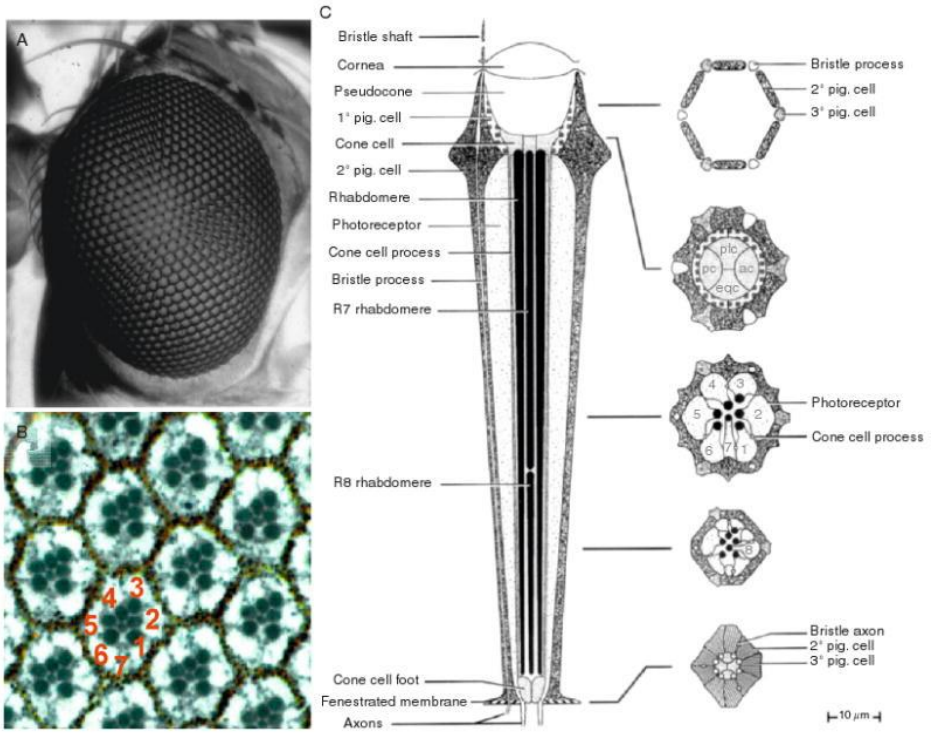

Figure 1.2. Morphological structure of the *Drosophila* eye. A) External morphology of the compound eye. B) Section image of adult eye 30 µm below eye surface, seven apical PR of one ommatidium are labeled C) Schematic representation of a single ommatidium (From Cagan 2010).

The eye and other organs develop from small monolayered epithelial tissues called imaginal discs. During early developmental stages (first and second instar larval stage), the cells in the eye disc proliferate asynchronously. Determination of the dorsal-ventral midline, or equator, of the eye disc is critical for eye morphogenesis. The initiation site of the morphogenetic furrow is delimited to the posterior margin on the equator. The dorsal and ventral side of the eye is determined during embryogenesis by a GATA transcription factor, which is necessary for *wingless* (*wg*) expression (Lee and Treisman, 2002). At the dorsal margin, Hedgehog and wingless activate the expression of the Iroquois complex (Iro-C) genes. Iro-C expression is delimited to the dorsal side of the eye. Fringe expression is repressed by dorsally expressed Iro-C, thus expression of Fringe defines the ventral side of the eye disc. Fringe is a glucosyltransferase and one of its vital functions is to modify the

membrane receptor Notch by converting N-acetylglucosamine to O-linked fucose residues. This modification increases the affinity of Notch to its ligand Delta. There are two main ligands of Notch in the eye disc; Delta and Serrate. Delta is restricted to the dorsal, and Serrate to the ventral side of the eye disc. These restrictive regulations are controlled by wg and Hh signals from peripodial cells. Notch activation can only take place in the dorsoventral (D-V) midline, where modified ventral Notch can interact with dorsal Delta, and unmodified dorsal Notch can interact with ventral Serrate. By the activation of Notch, one of the Notch effector genes, *eyegone* (*eyg*), is also activated at the equator. Studies show that *eyg* supports the growth of the eye disc by promoting the expression of *unpaired* (*upd*). Upd is a diffusible ligand for the JAK/STAT pathway, which plays an important role in tissue growth (Figure 1.3B). Briefly, Notch activation at the equator of the eye disc provides proper tissue growth (Hales *et al.*, 2015; Voas and Rebay, 2004).

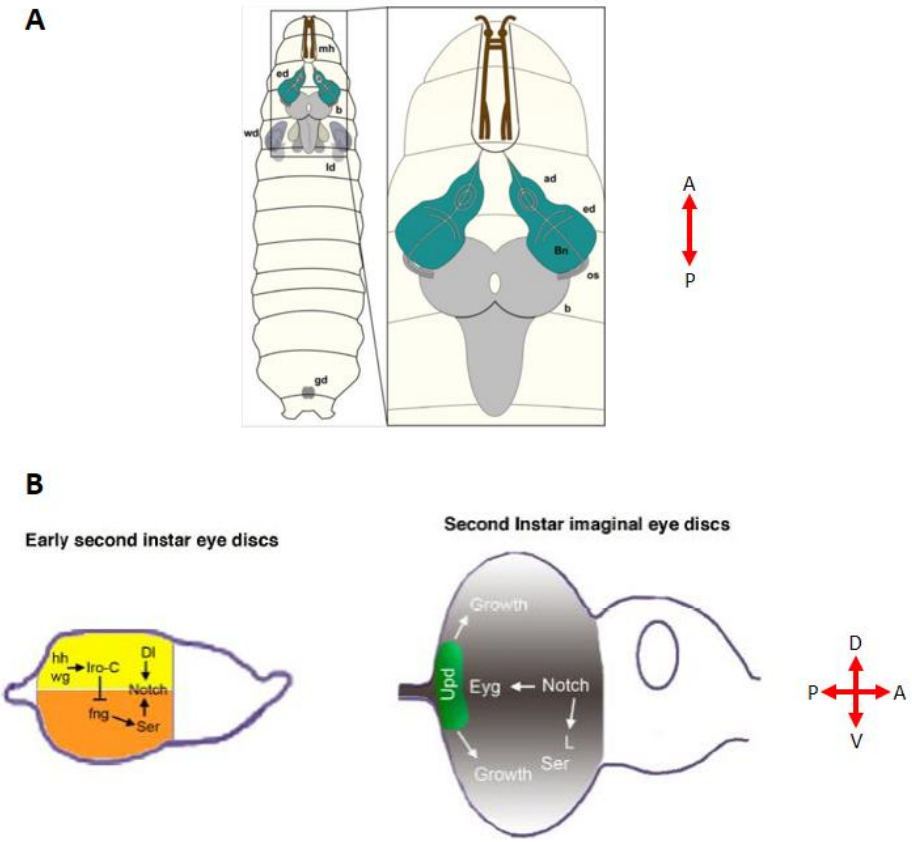

Figure 1.3. Schematic of *Drosophila melanogaster* eye development A) Imaginal discs in third instar larva of *Drosophila melanogaster* (Jeibmann and Paulus, 2009). B) Eye imaginal disc representation of second instar larva, and signaling pathways important for growth (Estella and Baonza, 2015).

After that, differentiation of cells starts at the posterior margin of the tissue by the formation of a morphogenetic furrow (MF). The MF is a visible differentiation wave. It forms a boundary between undifferentiated cells located anteriorly and developing PRs located posteriorly. The anterior zone of the MF is composed of proliferative precursor cells. During development, MF progresses from posterior to anterior and cells in the MF are arrested in the G1 phase of the cell cycle. Just posterior to the MF, five-cell preclusters are produced, which will eventually give rise to the PRs. In a restricted zone posterior to the MF, cells outside the preclusters undergo one additional proliferation cycle. This process is called the second mitotic wave (SMW), and is necessary for producing the rest of the cells in each ommatidial cluster. In each ommatidium, PRs are formed sequentially. First, R8 cells are formed, then R2 and R5 are recruited into the ommatidium. PR recruitment is followed by R3 and R4 then R1 and R6. Finally, R7 is recruited into each ommatidium. Sequential differentiation of the PR in the ommatidium cluster is controlled through the lateral inhibition by Delta and Spitz signalling. Sevenless and boss signaling are critical for R7 formation (Wernet and Desplan, 2014). After the formation of PRs, cone cells and other cells are recruited into ommatidium latter.

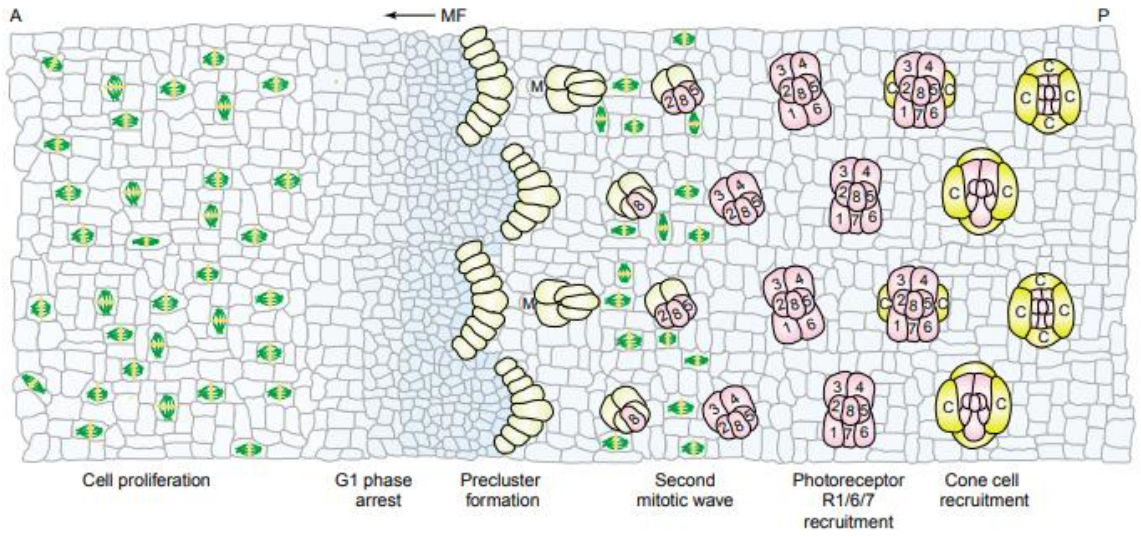

Figure 1.4. Representation of cells in eye imaginal disc, cell proliferation MF progression and ommatidia differentiation. Two proliferation zones are seen in the figure, where anterior of MF and SMW. Proliferating cells are shown by green mitotic spindles. (Ou *et al.*, 2003)

Morphogenesis is strictly regulated by many signaling molecules such as dpp, Wg, Hh, and Ato. Notch activation defines the MF initiation point, and hedgehog is essential for MF sweeping. Dpp promotes MF movement, while Wg inhibits MF movement (Lee and Treisman, 2002). Hh is also required for MF progression, and Ato initiates the R8 specification (Greenwood and Struhl, 1999).

1.3. Apoptosis and Apoptosis-induced Compensatory Proliferation in *Drosophila*

Apoptosis is a genetically regulated cell death process conserved in all metazoans (Martín *et al.*, 2009). Generally, it occurs by activating caspases, which are cell death proteases. There are two types of caspases, initiator and effector caspases. Initiator caspases are responsible for activating effector caspases by cleaving them. In *Drosophila*, Dronc is the most studied initiator caspase, and Dcp-1 (Death Caspase-1) and DrICE are well-known effector caspases. All caspases are inhibited by Diap-1 (*Drosophila* inhibitor of apoptosis-1) protein to prevent apoptosis. If apoptosis is induced by any apoptotic stimulus, pro-apoptotic proteins (well-known pro-apoptotic proteins are Grim, Reaper, and Hid) are activated, and active pro-apoptotic proteins inhibit Diap-1. Thus, Dronc can freely cleave and activate the effector caspases, and effector caspases drive cells to death by destroying vital cell structures (Li *et al.* 2016).

Maintenance of tissue homeostasis is crucial for the survival of multi-cellular organisms during development. Cell growth, cell death, and proliferation are strictly controlled especially during development. To form an appropriate morphology excess, non-functional, injured, or dangerous cells are removed by activating cell death mechanisms. On the other hand, stress conditions such as irradiation, heat, or a mutation during development can result in apoptosis, yet full organ development can still be observed under these conditions. Studies in *Drosophila* show that irradiation during development causes apoptosis in more than 50% of cells in the wing imaginal disc, but still almost normal sized wings are formed after metamorphosis (Martín *et al.*, 2009).

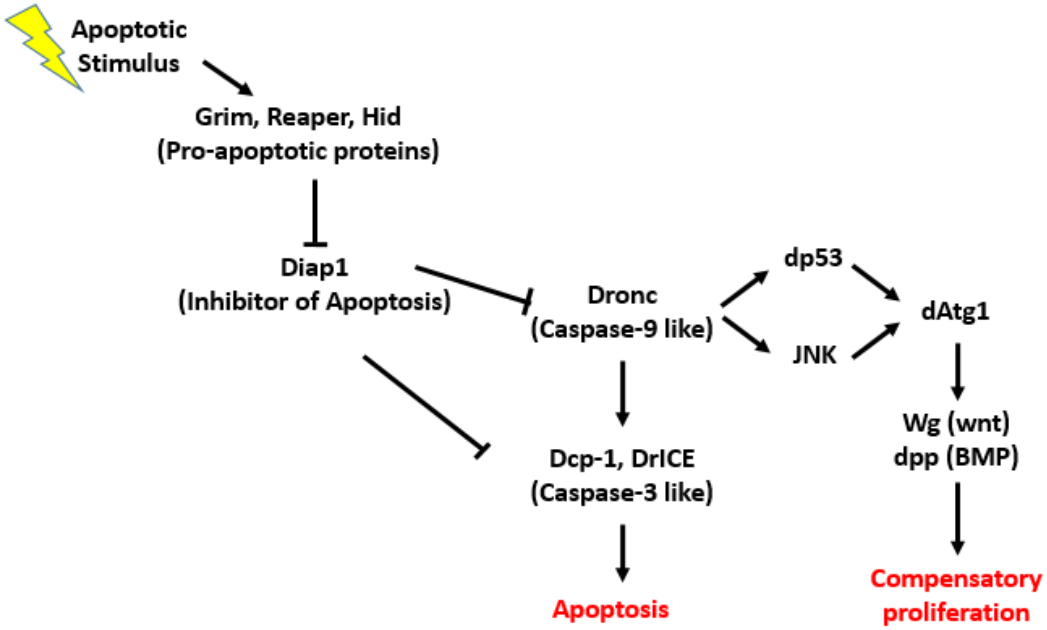

Figure 1.5. Apoptosis and compensatory proliferation pathways in *Drosophila*

Interestingly, stress-mediated cell loss is compensated by additional proliferation of the surviving cells during development. This phenomenon is known as apoptosis-induced compensatory proliferation (CP). The same phenomenon is also observed in the eye imaginal discs (Fan and Bergmann, 2008a). However, the mechanism by which CP takes place is not completely understood yet. However, some studies indicate that signals such as Wg and Dpp from dying cells induce CP in neighboring cells. To observe and study signals involved in CP, p35, which is a cleaved apoptosis effector inhibitor, is commonly utilized. In this way, cells surviving apoptosis (so-called undead cells) continuously secrete apoptotic signals and provide a chance to observe what happens under these circumstances. Such experiments show that compensatory proliferation induced by undead cells results in overgrowth and impaired differentiation (Fan and Bergmann, 2008a; Kondo *et al.*, 2006; Martín *et al.*, 2009).

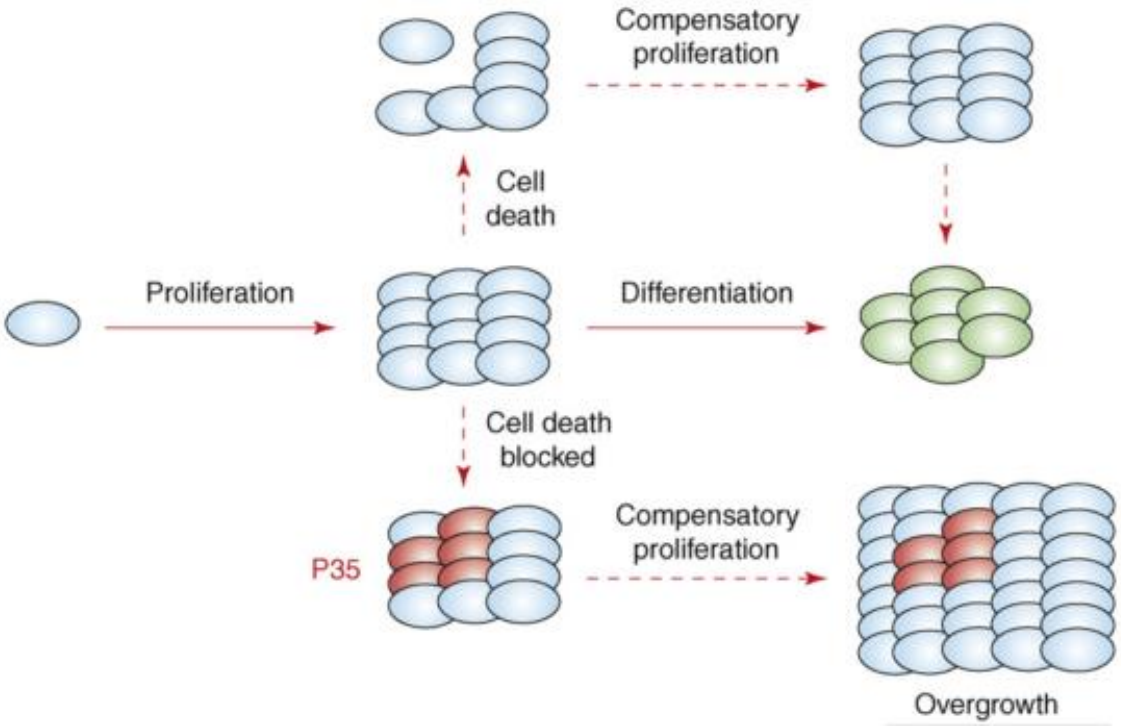

Figure 1.6. Developmental process in a tissue with compensatory proliferation after apoptosis (Top) and without cell death (Middle). Developing tissue with p35 apoptosis inhibitor (Bottom) (Fan and Bergmann, 2008a).

1.4. Autophagy in *Drosophila*

Autophagy is a lysosomal degradation process in eukaryotic cells. Generally, the term autophagy refers to macroautophagy, which is a non-selective degradation process of macromolecules and cell compartments. During autophagy, cellular components are sequestered by a double membrane vesicle, the autophagosome, which fuses with a lysosome becoming an autolysosome where enzymatic degradation of the encapsulated material takes place. The autophagy process provides the survival of organisms under stress conditions and energy saving during starvation. Alteration and deficiencies in autophagy (*Atg*) genes are primarily responsible for autophagosome formation and autophagy. However, Atg proteins also play a role in development and cell death as well (Li *et al.*, 2016; McPhee and Baehrecke, 2010). In *Drosophila*, the molecular mechanism by which autophagy is triggered begins by formation of the Atg1 complex. With the activation of other Atg proteins and Vsp34 proteins, a phagophore forms, and assembles to form a double membrane autophagosome. A Syntaxin17-containing SNARE complex and HOPS tethering complex

provide the autolysosome formation. After the formation of the autolysosome, the degradation of autophagic cargo takes place. The Atg8 complex localizes to the membrane during phagophore and autophagosome formation, and remains there until autolysosome fusion. Then, Atg8 is released from the complex and localizes to the outer membrane of the autolysosome. Based on this fact, Atg8 (or LC3) is used as a common marker protein for autophagy (McPhee and Baehrecke, 2010) (Figure 1.7).

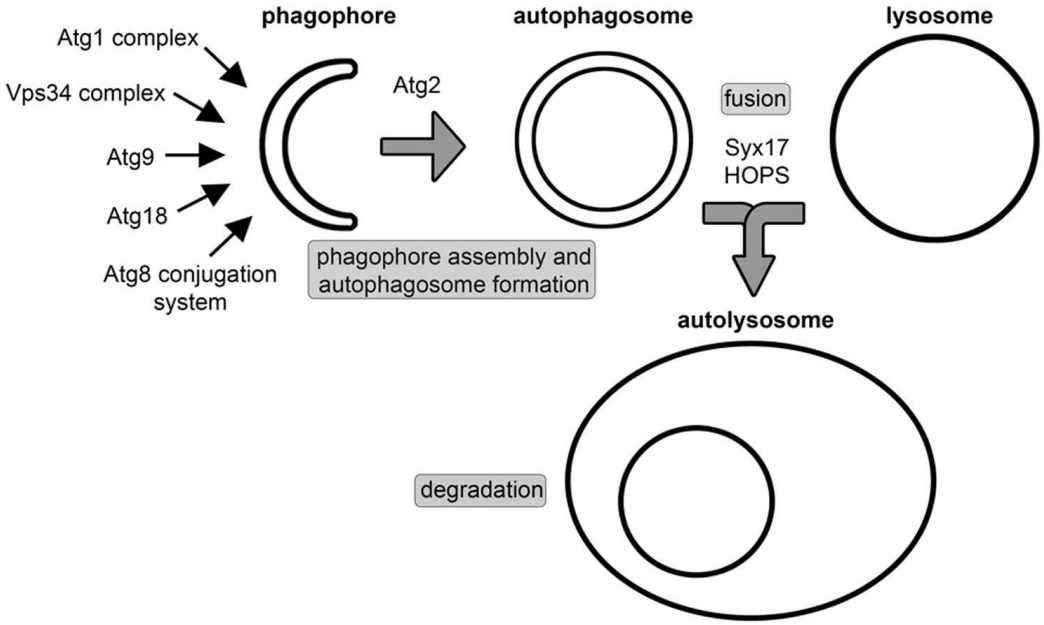

Figure 1.7. Autolysosome formation in *Drosophila.* Sequential coordination of Atg proteins to form double-membraned autophagosome. Syntaxin17-containing SNARE and the HOPS tethering complex are required for autophagosome fusion with the lysosome. (Nagy *et al.*, 2015)

Larval fat body cells are commonly used as an autophagy model in *Drosophila*. Autophagy can be easily induced by starvation in larval fat body tissue, and autolysosomes can be labeled by lysotracker staining (Scott *et al.*, 2004).

1.5. Hexosaminidases and Their Roles in Glycosylation Pathways

Hexosaminidases (β-N-acetylhexosaminidase; EC 3.2.1.52) are enzymes that are involved in the hydrolysis of terminal non-reducing N-acetyl-D-hexosamine residues in N-

acetyl-β-D-hexosaminides. Many types of hexosaminidases exist, and they play important roles in cell-to-cell communication, glycosaminoglycan (GAG) metabolism and ganglioside degradation. The most known hexosaminidases are hexosaminidase A (HexA), hexosaminidase B (HexB) and Hexosamindase S (HexS). These enzymes consist of the different combination of α and β subunits, which are encoded by *HEXA* and *HEXB* (*HEXO1* and *HEXO2* homologs in insects) genes, respectively. HexA and HexB are lysosomal enzymes, have high affinity to terminal N-acetyl-D-glucosamine residues, and are responsible for ganglioside degradation (Pennybacker *et al.*, 1996). A less known member of the hexosaminidase family is hexosaminidase D (HexD) encoded by *HEXDC* gene. It is shown that HexD is a nucleocytoplasmic enzyme in humans. It has high affinity to terminal N-acetyl-D-galactosamine residues (Gutternigg, Rendic, Voglauer, Iskratsch, and Wilson, 2010), and plays a role in degradation of sulfated GAG pathways ("Dermatan Sulfate Degradation (Metazoa)," n.d.; Trowbridge and Gallo, 2002).

1.5.1. The Degradation of Gangliosides

Gangliosides are membrane molecules that consist of hydrophobic carbon tails (Ceramide) and branched oligosaccharide chains as hydrophilic head-group. A common feature of the ganglioside head group is that it consists of a sialic acid (N-acetylneamunaricacid, NANA is the most common sialic acid in gangliosides) hexose, and hexosamine residues. Generally, gangliosides are found in lipid rafts on cellular membranes, and are involved in various cellular processes such as cell-to-cell signaling and cell differentiation. Gangliosides are predominantly present in cells of the nervous system. Many types of gangliosides are found, and classified according to their number of sialic acid residues. These molecules are continuously synthesized and degraded. The balance between the rate of degradation and synthesis is highly important for its function. Degradation of gangliosides takes place in lysosomes, and is catalyzed by lysosomal enzymes. In mammals, one of the best characterized lysosomal enzymes for ganglioside degradation is Hexosaminidase A (HexA) (Posse de Chaves and Sipione, 2010).

HexA consists of two subunits, α and β. It is responsible for lysosomal degradation of GM2 ganglioside. Degradation of GM2 ganglioside is provided by recognition of the ganglioside by the GM2 adaptor protein (GM2AP), and the ganglioside molecule is taken

from the lysosomal membrane. HexA enzyme, GM2AP, and the ganglioside form a Michaelis Menten complex and the terminal GalNac (N-acetylgalactosamine) residues are cleaved by the HexA enzyme (Figure 1.8A). Also, HexB and some other lysosomal enzymes participate in the ganglioside degradation to ceramide process (Seyrantepe *et al.*, 2018; Werth *et al*., 2001) (Figure 1.8B). Hexosaminidase D may also be involved in ganglioside degradation.

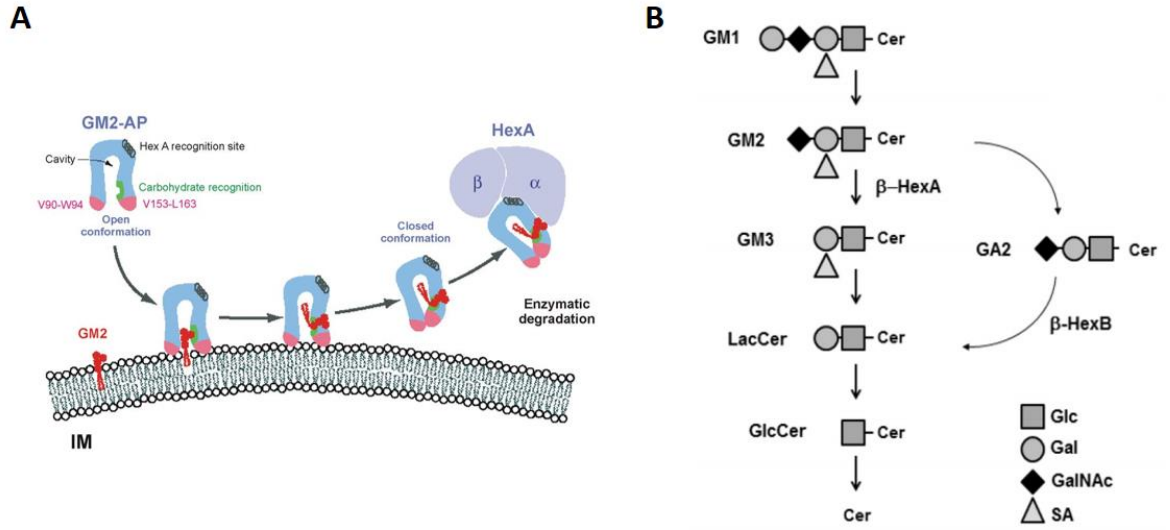

Figure 1.8. Enzymatic degradation of gangliosides. A) Degradation of GM2 ganglioside occurs by recognition of ganglioside by an adaptor protein and formation of a Michaelis Menten Complex (Sandhoff and Harzer, 2013). B) Enzymatic degradation pathway of gangliosides into ceramide (Seyrantepe *et al.*, 2018).

1.5.2. The Degradation of Glycosaminoglycans

Glycosaminoglycans (GAGs) are one of the most abundant macromolecule types (saccharides). They have characteristic oligosaccharide chains, generally found in the extracellular matrix and the cell membrane surface on proteins (proteoglycans). GAGs have various function in cells from affecting compressive properties of tissues to receiving growth factor signals. Studies in *Drosophila* show that glypican (one major family of heparan sulfate proteoglycans), and *dally* (*division abnormally delayed*), have crucial effects on Wg and Dpp signaling molecules. Many enzymes take part in GAG metabolic pathways in *Drosophila*. For instance, Sugarless is a GAG biosynthetic enzyme and affects multiple

growth factors including wingless, Dpp, Heartless, and Breathless. In another example, Sulfateless is required for Wg-mediated Fibroblast Growth Factor signaling. Recycling of GAGs is necessary for GAG metabolism. Various enzymes play roles in GAG metabolism, and most of the enzymatic degradation processes take place in the lysosomes (Lindahl *et al.*, 2017).

Sulfated GAGs such as heparan sulfate, dermatan sulfate, and chondroitin sulfate are common sulfated glycosaminoglycans composed of repeating disaccharide units with various composition. They have the important function in protecting tissues against compression, and are generally found in cartilage and skin in vertebrates. While the existence of these molecules in *Drosophila* has also been described (Toyoda *et al.*, 2000), very little is known about the metabolic processes they are involved in and their mechanism of action. Multiple enzymes play a role in sulfated GAG degradation. Hyoluronon glucosaminidase hydrolyzes the sulfated GAGs into sulfated disaccharide units. After that a sulfatase, which for instance can be iduronate-2-sulfatase for dermatan sulfate, and N-acetyl-galactosamine-4/6 sulfatase for chondroitin sulfate, pull of the sulfates from the disaccharide units. After removal of the sulfate moiety, the products are expelled from the lysosome. It has been hypothesized that a hexosaminidase, possibly hexosamindase D, plays a role in hydrolysis of GalNac-glycan into N-acetyl-β-D-Galactosamine and Glycan at the last step of dermatan sulfate (Figure 1.9A; "Dermatan Sulfate Degradation (Metazoa)," n.d.) and chondroitin sulfate degradation (Figure 1.9B; "Chondroitin Sulfate Degradation (Metazoa)," n.d.) outside the lysosome (Gerhold *et al.* , 2011).

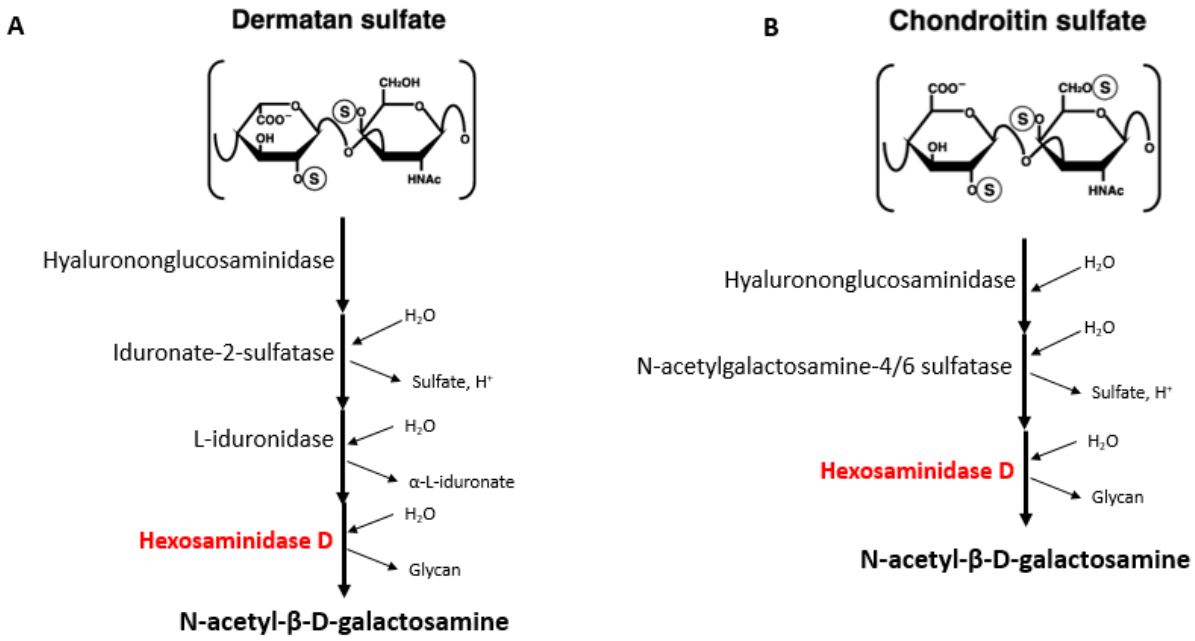

Figure 1.9. Degradation of Sulfated GAG molecules. Dermatan sulfate (A), and Chondroitin Sulfate (B) ("Chondroitin Sulfate Degradation (Metazoa)," n.d., "Dermatan Sulfate Degradation (Metazoa)," n.d.)

1.5.3. Lysosomal Storage Disorders

Lysosomal storage disorders (LSDs), are rare inherited metabolic recessive diseases that result in dysfunction of lysosomal hydrolases. There are more than 50 types of LSDs. Impaired function of acidic enzymes in lysosomes cause accumulation of secondary metabolites in lysosomes. Enlargement of lysosome size and number are observable phenotypes of LSD (Figure 1.10). Gaucher's syndrome is the most common LSD and is caused by the accumulation of glucocerebroside (a sphingolipid molecule) in cells. Another common LSD is Tay-Sachs disease caused by autosomal recessive mutations in *HexA*, which is lethal at the early ages. Mutations in *HexB* causes Sandhoff LSD, which is also an autosomal recessive genetic disease (Posse de Chaves and Sipione, 2010). Mutations in some genes namely *dnpc1a* (Scott *et al.*, 2004), *benchwarmer* (Dermaut *et al.*, 2005), and *spinster* (Nakano *et al.*, 2001), are related to LSD in *Drosophila*.

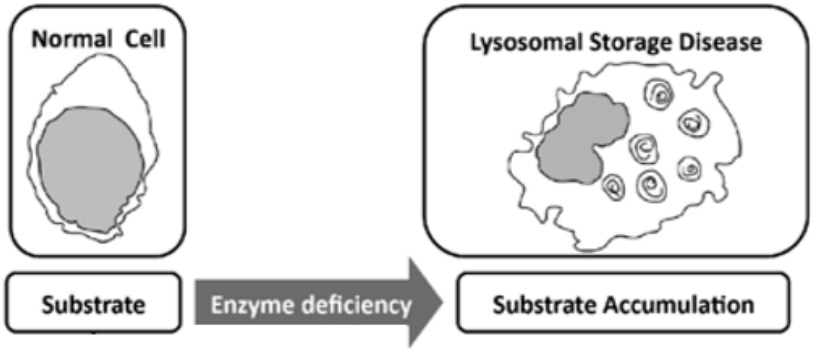

Figure 1.10. Schematic illustration of cells with a lysosomal storage disease with enlarged number of lysosomes (Modified from Urbanelli *et al.* 2013).

1.5.4. CG7985, A Novel Hexosaminidase D in *Drosophila*

CG7985 is a hexosaminidase protein encoded by the uncharacterized *CG7985* gene. Since its amino acid sequence analysis of CG7985 indicated significant homology to the mammalian HexDC protein, we named it as *Drosophila melanogaster* HexDC or dmHexDC for short. Hexosaminidase D is a highly conserved protein in the animal kingdom (Kıral, 2015). The dmHexDC gene consist of 5 exons; Exon 1.1, Exon 1.2, Exon 2, Exon 3, and Exon 4. Two alternative forms of transcripts are generated from the dmHexDC gene, one of the first two untranslated exons (Exon1.1 and Exon 1.2) is alternatively spliced. A long intron with putative enhancer elements is found between the first Exon 1.2 and Exon 2. The translation start site is found at the 5' end of Exon 2 and the translation stop site is found in Exon 3. The last exon (Exon 4) encodes for the 3'UTR of the mRNA.

The dmHexDC protein consist of 708 aminoacid residues. A conserved putative catalytic domain spans the region between amino acids 188 and 517. In contrast to mammalian HexDC, dmHexDC contains a transmembrane domain between amino acid residues 13 and 35 (Figure 1.11B). *In vitro* biochemical enzymatic tests show that dmHexDC has a high affinity to the substrate p-nitrophenyl-N-acetyl-D-galactosamide and low affinity to p-nitrophenyl-N-acetyl-D-glucosamide in the range of pH 4.5 to pH 6 (Erkol, unpublished). dmHexDC is expressed in R7 PRs, in cells anterior to the MF in the eye disc and in a subset of glia (Kıral, 2015), Kenyon cells in the larval brain (Öztürk, 2010), hinge region of leg disc, haltere disc (see Appendix A), and neuromuscular junctions (Sönmez,

unpublished) during development. However, the sub-cellular localization of dmHexDC has not been completely elucidated yet. While mitochondrial localization has been reported in *Drosophila* embryos using a YFP protein trap screen (Lye, Naylor, and Sanson, 2014), localization to the Golgi apparatus and endosomes has also been reported in our lab using subcellular markers (Kıral, 2015). Furthermore, our laboratory has shown that loss of dmHexDC function results in neuronal loss, lipid accumulation, lysosomal enlargement and apoptosis in eye imaginal discs using the protein trap mutant. Additionally, there are findings that indicate apoptosis induced compensatory proliferation via wg signaling (Kıral, 2015).

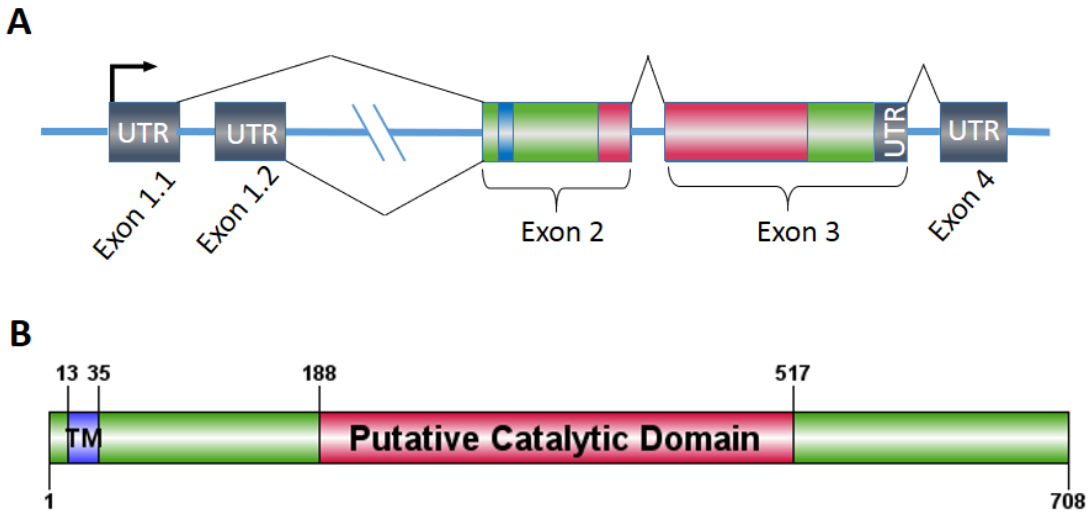

Figure 1.11. Schematic illustration of *dmHexDC* gene and protein product. A) Gene structure of *dmHexDC*. Exons are shown with boxes. Gray regions represent the UTR. Exons encoding the different domains are shown with matching color in the protein structure. B) Protein structure of dmHexDC. Numbers represent the amino acid positions. Transmembrane and catalytic domains are shown in blue and red respectively.

1.6. Genetic Tools Used in This Study

1.6.1. Gal4/UAS system

The Gal4/UAS system is a powerful gene expression tool that consists of two components. Gal4 is a yeast transcription factor that binds to an Upstream Activating

Sequence (UAS). Tissue or cell specific expression of genes can be achieved by crossing driver lines, which are fly lines that express Gal4 under the control of a tissue or cell-specific promoter to responder lines that express an effector gene (which can encode either protein or RNAi) under UAS control. In this way, effector gene activation is achieved in a tissue or cell-specific manner in the F1 generation (Hales *et al.*, 2015) (Figure 1.12). Many Gal4 and UAS lines are commercially available from *Drosophila* stock centers all around the world.

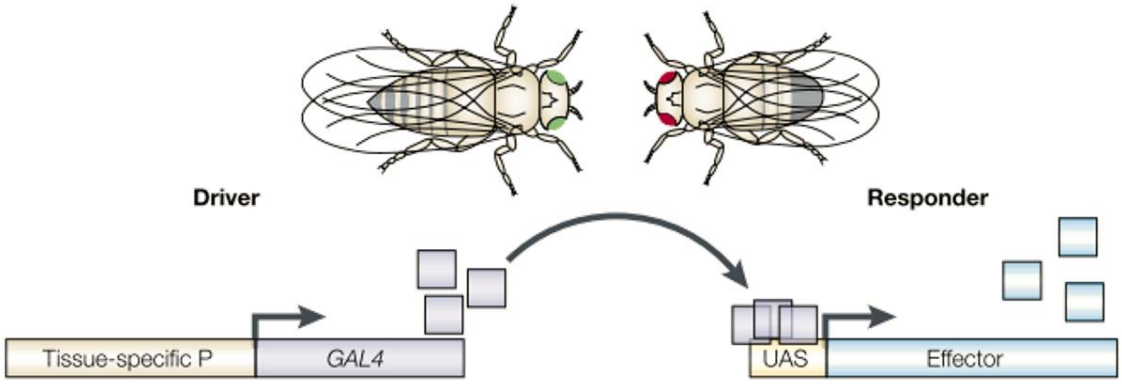

Figure 1.12. Gal4-UAS binary system for *Drosophila melanogaster*. Gal4-UAS system is used for expressing effector genes in a specific manner by crossing specific driver and responder lines

1.6.2. Enhancer Trap versus Protein Trap Lines

An enhancer trap line represents a transgenic line that is generated by random integration of a transposable element that carries the coding sequence of Gal4 with a minimal promoter into the genome near an enhancer element. Thus, the expression of the integrated Gal4 is controlled by that enhancer and represents most likely the expression pattern of the nearby gene. This method is widely used for the detection of the expression pattern of a gene. It can also be used to ectopically express desired proteins under the control of this specific enhancer when these lines are crossed to the desired responder line (Mayer *et al.*, 2013) (Figure 1.13A).

A protein trap line represents a transgenic fly line that has been generated by random integration of a transposable element that contains splice acceptor and splice donor sites

flanking a GFP sequence. If the transposable element integrates into an intron it will likely be spliced like an additional exon and integrated into the coding sequence of the gene it was inserted into. The generated protein will be fused to GFP and can be used to track the localization of the protein, which in the process might or might not disrupt the function of the protein (Sineshchekova *et al.*, 2004) (Figure 1.13B).

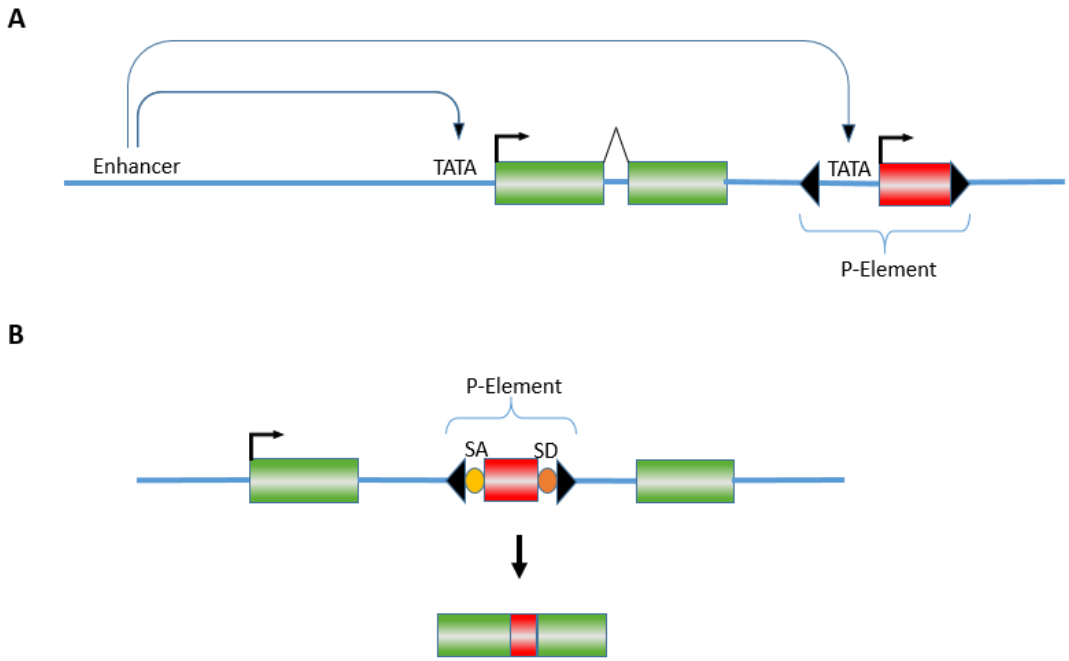

Figure 1.13. Schematic illustration of enhancer trap and protein trap lines. A) Enhancer trap of inserted red gene with TATA box (minimal promoter) near the enhancer of the green gene. B) Protein trap of red protein into green protein by integrating coding sequence of the red gene with splicing sites (SA: splicing acceptor; SD: splicing donor) in the intron of the green gene.

1.6.3. FRT/FLP System

The FRT (Flippase Recognition Target) / FLP (Flippase) system is similar to the Cre/LoxP system in mice and is used for generation of tissue-specific homozygous cell populations, clones, in a heterozygous background. In this way, homozygous lethal mutations can be generated in a tissue-specific manner at the desired time. It can also be used to study autonomous and non-autonomous effects of a mutation as the effects of a mutation can be observed in the surrounding normal tissue. Homozygous mutant clones can

be easily visualized by labeling with a reporter gene (Hales *et al.*, 2015; Pastor-Pareja and Xu, 2013) (Figure 1.14).

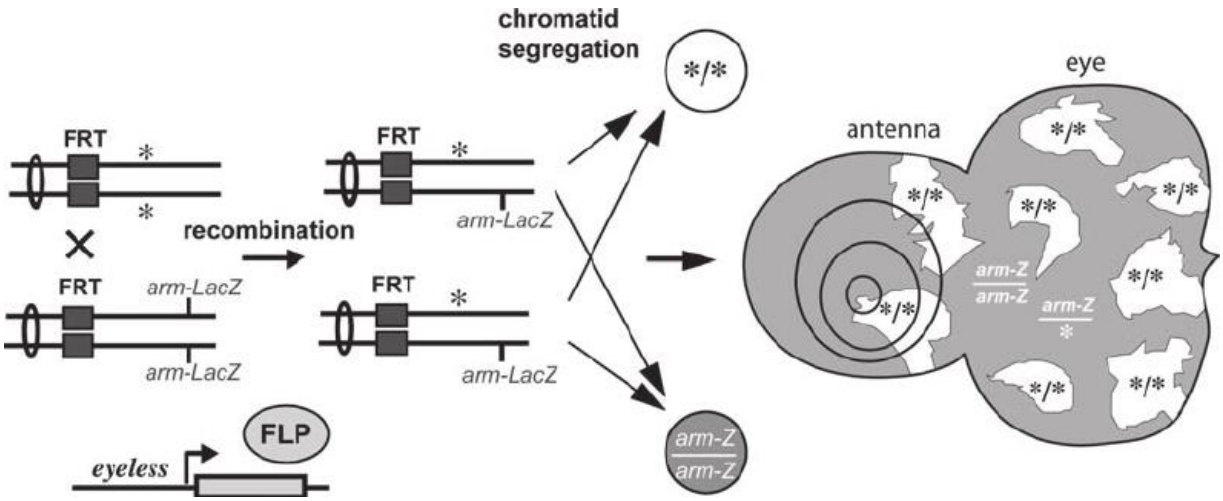

Figure 1.14. Schematic illustration of FRT/FLP system for mitotic recombination. Mutant clone generation in the eye-antenna imaginal disc by using ey-FLP, FRT allele of a mutation, and FRT allele of arm-LacZ which expresses LacZ reporter under the control of *Drosophila* β-catenin, Armadillo (Arm) (Legent and Treisman, 2009).

FLP is expressed under the control of a tissue-specific or a temperature-sensitive promoter. The flippase enzyme then recombines the homologous chromosome arms at FRT sites during mitosis. In this way, homozygous mutant cells can be obtained in specific tissues (Figure 1.14).

1.6.4. CRISPR/Cas9

In recent years, the possibilities for genome editing have enormously improved by the development of the CRISPR/Cas9 technology. Using the conventional CRISPR method genes are edited by creating a double-strand break. The generated break can be repaired by the organism via non-homologous end joining (NHEJ) or homology-directed repair (HDR). HDR can be used for introducing new specific sequences to DNA by providing a donor DNA as template for the repair event. NHEJ-mediated repair is used to generate random nucleotide mutations and knockout of genes disturbing the gene and/or protein functions (Figure 1.15).

A 20-nucleotide long DNA sequence adjacent to a NGG sequence, which represents a so-called protospacer adjacent motif (PAM), can be easily targeted and cleaved by a designed gRNA and the Cas9 complex. In *Drosophila*, gene editing via CRISPR/Cas9 is performed by injection of gRNA into the fly embryos and generation of gRNA expressing transgenic fly lines. These lines are then crossed to transgenic fly lines that express Cas9 in germline cells. The F1 generation is then screened for the introduced mutation after removal of gRNA and Cas9 carrying alleles (Gratz *et al.*, 2016).

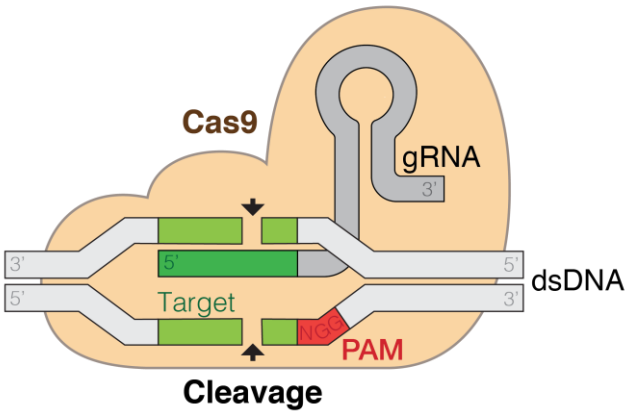

Figure 1.15. Cutting of double-stranded DNA by Cas9/gRNA complex.

2. PURPOSE

One key attribute for cellular differentiation may be the composition of saccharides in the cell. To understand the effect of saccharides behind cellular differentiation, we focused on a novel hexosaminidase, dmHexDC function in developing eye of *Drosophila melanogaster*.

In a previous study we identify dmHexDC as a necessary protein for proper development of the eye imaginal disc. Mutant analysis shows that loss of dmHexDc leads to loss of neurons by causing lipid accumulation, lysosomal disfunction and increased apoptosis. Furthermore, an increase in cell proliferation and wg signaling indicate the possibility of compensatory proliferation.

To further investigate the causal relationship between these observations we perform clonal analysis of dmHexDC mutants. We find that loss of dmHexDC triggers autophagy and apoptosis pathways in precursor cells. Compensatory proliferation is activated in neighboring cells by apoptosis. Moreover, loss of dmHexDC causes defects in glial migration in Notch-active equator line. These results indicate the importance of dmHexDC function in neuronal development and migration and that some of these functions might be mediated by modifications in Notch signaling.

3. MATERIALS AND METHODS

3.1. Biological Material

Drosophila melanogaster lines were kept in air-permeable transparent vials with fly food at constant temperature (25^{o}C or 18^{o}C) and humidity (70%) with 12h:12h light and dark cycle. Commercially available fly food (Genesee Scientific Nutri-Fly^{TM} Bloomington Formula) was prepared and used according to company's instruction for the *Drosophila* lines.

Table 3.1. Transgenic constructs in *Drosophila melanogaster* lines used in this study.

Transgene	**Inserted Chr. No.**	**Description**
Gal4 Drivers		
AC887-Gal4	3	*Gal4* sequence is inserted in the first intron of *CG7985* gene. Gal4 activity depends on the enhancer elements of *CG7985* gene.
ey-Gal4	2	Expresses Gal4 under the control of *eyeless* gene enhancer. Gal4 expressed in all eye cells except glia.
eyGMR-Gal4	2	Expresses Gal4 under the control of either *eyeless* or *GMR* promoter. Gal4 expressed in all eye cells.
DE-Gal4	3	Expresses Gal4 under the control of *mirror* gene enhancer. Gal4 expressed in the dorsal part of eye.
ubi-Gal4	2	Expresses Gal4 ubiquitously in all cells.
UAS Constructs		
UAS-GFPnls	3	Encodes GFP with nuclear localization signal under the control of *UAS*. Expressed GFP labels the nucleus.
UAS-dicer2	1	Encodes dicer2 protein enhances RNAi mediated silencing mechanism.
UAS-CG7985^{RNAi}	2	Encodes double-stranded RNAi of *CG7985* gene under the control of *UAS*.

Table 3.1. Transgenic constructs in *Drosophila melanogaster* lines used in this study (cont.).

Transgene	Inserted Chr. No.	Description
UAS-dmHexDC	2	Encodes CDS of *CG7985* under the control of *UAS*.
UAS-p35	2	Encodes apoptosis inhibitor protein p35 under the control of *UAS*.
UAS-FLP	2	Encodes flippase under the control of *UAS*.
General Stocks		
dmHexDC::eGFP (BAC)	2	GFP fused with transgenic *dmHexDC* construct inserted in the genome by BAC recombineering.
$CG7985^{CPTI100032}$ (Protein Trap)	3	Protein trap line of dmHexDC. YFP sequence with splice acceptor and splice donor site is inserted in the first intron of *dmHexDC* gene. Null mutant allele of *dmHexDC* ($dmHexDC^{null}$).
ey-FLP	1	Expresses flippase under the control of the *eyeless* promoter. It expresses in all eye cells except glia.
FRT82B	3	Flippase recognition target site on 82B map position.
FRT82B sb'	3	Flippase recognition target site on 82B map position with *sb'* marker mutation.
FRT82B sb' dmHexDC^{null}	3	Recombined construct of Protein trap of dmHexDC with FRT82B.
FRT82B ubi-RFP	3	Recombined construct of ubiquitously expressed RFP with FRT82B.
FRT82B GMR-hid	3	Recombined construct of pro-apoptotic gene *hid* under the control of *GMR* promoter with FRT82B.
Nos-Cas9	1	Expresses Cas9 protein under the control of the promoter of *nanos* gene. Cas9 expressed in germline cells.
U6:1-gRNA(T1) *U6:3-gRNA*(T2)	2	Expresses gRNA under the control of RNA promotor U6:1 and U6:3. Expressed gRNAs specific to target sequences (T1 and T2) on *dmHexDC* gene.

Table 3.1. Transgenic constructs in *Drosophila melanogaster* lines used in this study (cont.).

Transgene	Inserted Chr. No.	Description
Markers and Balancers		
w^{1118} *(w)*	1	Marker mutation in *white* gene which causes white eye phenotype.
yw	1	Marker mutation which causes yellow body and white eye phenotype.
v' (v)	1	Vermillion marker mutation which causes vermillion red eye phenotype.
Sp	2	Speck marker mutation which causes increased bristle number.
CyO	2	Balancer chromosome with curled wing marker.
TM2	3	Balancer chromosome with ubx marker which causes bigger haltere and extra bristle(s) on it.
TM3	3	Balancer chromosome.
TM6B	3	Balancer chromosome with *tb* and *Hum* marker.
tb	2/3	Marker mutation which causes the tubby size of larvae and pupae.
sb'	3	Stubble marker mutation which causes short bristles.
e	3	Ebony marker mutation which causes dark body color.
Ser'	3	Serrate marker mutation which causes wings with nick.

3.2. Chemicals and Supplies

Chemicals used in this study were obtained commercially from companies listed under the corresponding titles.

3.2.1. Chemical Supplies

Chemicals used in this study are listed in Table 3.2.

Table 3.2. Chemical list used in this study.

Chemical	Producing Company
1 kb Marker	NEB, USA (N3232L)
100 bp Marker	NEB, USA (B7025)
Bovine Serum Albumin	Sigma-Aldrich, USA (A9647)
EDTA	Sigma-Aldrich, USA (59417C)
Ethidium Bromide solution	Sigma Life Sciences, USA (E1510)
$MgCl_2$	Riedel-de Haen, Germany (13152)
NaCl	Sigma-Aldrich, USA (S7653)
OCT Compound	Fisher HealthCare, USA
Paraformaldehyde	Sigma-Aldrich, USA (P6148)
Sodium Deoxycholate	Sigma-Aldrich, USA (30970)
Tris	Sigma-Aldrich, USA (T6066)
Triton X-100	AppliChem, USA (A4975)

3.2.2. Solutions and Buffers

Solutions and buffers used in this study are listed in Table 3.3.

Table 3.3. Solution and buffers list used in this study.

Solution / Buffers	Ingredient
Formaldehyde Solution (4%)	2 g Paraformaldehyde in 50 ml dH_2O 1M NaOH until solution becomes transparent pH 7.4
LB Agar	5 g/L NaCl 10 g/L Tryptone 5 g/L Yeast extract 14 g/L Agar
LB Broth	5 g/L NaCl 10 g/L Tryptone 5 g/L Yeast extract
Non-ionic Lysis Buffer	20 mM Tris-Cl pH 8.0 50 mM NaCl 1% NP-40 2 mM EDTA 1X Roche Protease Inhibitor Cocktail
PAXD	10 g BSA 3 g Sodium Deoxycholate 3 ml Triton X-100 100 ml 10X PBS dH_2O to 1 L
PBS (1X)	137 mM NaCl 2.7 mM KCl 10 mM Na_2HPO_4 1.8 mM KH_2PO_4
PBX3	0.3% Triton X-100 in 1X PBS
Squish Buffer	10 mM Tris, pH 8.0 1 mM EDTA 25 mM NaCl

3.2.3. Oligonucleotides

Oligonucleotides were synthesized commercially at Macrogen (South Korea, Inc.), and produced lyophilized oligonucleotides were dissolved in dH_2O at a final concentration of 100 pmol/μL. Dissolved oligonucleotides were stored at -20^{o}C as stock solutions. For

PCR, 1:10 diluted (10 pmol/μL) stock oligonucleotides were used. Oligonucleotides used in this study are listed in Table 3.4.

Table 3.4. Oligonucleotide list used in this study.

Name	Sequence
dmHexDC_CRISPR_ secreening_Close_Fwd	5'-GAAACTTTCCTTCCTGCTCG-3'
dmHexDC_CRISPR_ secreening_Close_Rev	5'-GAGCACCCTTCAAGTCCAGA-3'
dmHexDC_CRISPR_ secreening_Wide_Fwd	5'-GGGGGCTACTTGTTGGATCT-3'
dmHexDC_CRISPR_ secreening_Wide_Rev	5'-AACTCCGCTGTAGGGAAACA-3'
pCFD4_Target1_Fwd	5'-TATATAGGAAAGATATCCGGGTGAACTTCGGCTGTCG TATCGATTAGTAGTTTTAGAGCTAGAAATAGCAAG-3'
pCFD4_Target2_Rev	5'-ATTTTAACTTGCTATTTCTAGCTCTAAAACCCACCGG CACGCCCATCCCCGACGTTAAATTGAAAATAGGTC-3'
pU6_BbsI_chiRNA_ sense	5'-CTTCGCCAGACACGACGAGCAGGA-3'
pU6_BbsI_chiRNA_ antisense	5'-AAACTCCTGCTCGTCGTGTCTGGC-3'

3.2.4. Antibodies

Antibodies used in this study are listed in Table 3.5.

Table 3.5. Antibodies used in this study.

Name	Antigen	Species	Dilution	Source
Primary Antibodies				
Anti-dsRed	RFP	Rabbit	1:1000	Cell Signaling
Anti-Elav	Elav	Mouse	1:20	DSHB (9F8A9)
Anti-Elav	Elav	Rat	1:20	DSHB (7E8A10)
Anti-GFP	GFP	Chicken	1:1000	Abcam (ab13970)
Anti-GFP	GFP	Rabbit	1:500	Torrey Pines (TP401)
Anti-GFP	GFP	Mouse	1:1000	Promega
Anti-Pros	Prospero	Mouse	1:20	DSHB (MR1A)
Anti-Repo	Repo	Mouse	1:20	DSHB (8D12)
Anti-Wg	Wingless	Mouse	1:20	DSHB (4D4-s)
Anti-pH3	Phospho-histone H3 (ser10)	Mouse	1:200	EMD Millipore
Anti-pH3	Phospho-histone H3 (ser10)	Rabbit	1:100	Cell Signaling (S10)
Anti-Casp3	Caspase 3	Rabbit	1:200	BD Pharmingen
Anti-dcp-1	Dcp-1	Rabbit	1:200	DSHB
Anti-Arl8	Arl8	Rabbit	1:500	DSHB
Anti-Cnx99a	Calnexin	Mouse	1:2000	DSHB
Anti-Golgin84	Golgin	Mouse	1:2000	DSHB
Anti-Hrs	hrS	Mouse	1:2000	DSHB
Anti-Rab7	Rab7	Mouse	1:2000	DSHB
Anti-Yan	Yan	Mouse	1:50	DSHB
Secondary Antibodies				
Alexa 405	Rat	Goat	1:800	Invitrogen
Alexa 405	Rabbit	Goat	1:800	Invitrogen
Alexa 488	Rabbit	Goat	1:800	Invitrogen
Alexa 488	Rabbit	Donkey	1:800	Invitrogen
Alexa 488	Chicken	Donkey	1:200	Invitrogen
Alexa 555	Mouse	Donkey	1:800	Invitrogen
Alexa 555	Rabbit	Goat	1:800	Invitrogen
Alexa 633	Rat	Goat	1:800	Invitrogen
Alexa 647	Rat	Donkey	1:800	Invitrogen
Alexa 647	Rabbit	Goat	1:800	Invitrogen
Cy3	Mouse	Goat	1:800	Invitrogen

3.2.5. Embedding Media

Stained tissues were embedded in Vectashield embedding medium (Vector Laboratories, Inc) or Fluoromount-G embedding medium (SouthernBiotech). Embedded tissues were kept at 4^{o}C until visualization using confocal microscopy.

3.2.6. Disposable Labware

Disposable labware used in this study is listed in Table 3.6.

Table 3.6. Disposable labware used in this study.

Material	**Manufacturer**
Culture tubes (14 ml)	Greiner Bio-One, Belgium
Filter Tips	Greiner Bio-One, Belgium
Microscope cover glass	Fisher Scientific, UK
Microscope slides	Fisher Scientific, UK
PCR tubes (200 µl)	Bio-Rad, USA
Petri Dishes, 60 x 15 mm	TPP Techno Plastic Products AG, Switzerland
Pipette Tips	VWR, USA
Plastic Pasteur pipettes	TPP Techno Plastic Products AG, Switzerland
Test Tubes, 0.5 ml	Citotest Labware Manufacturing, China
Test Tubes, 1.5 ml	Citotest Labware Manufacturing, China
Test Tubes, 2 ml	Citotest Labware Manufacturing, China
Test Tubes, 15 ml	Becton, Dickinson and Company, USA
Test Tubes, 50 ml	Becton, Dickinson and Company, USA

3.2.7. Equipment

Equipment used in this study is listed in Table 3.7.

Table 3.7. Equipment used in this study.

Equipment	Manufacturer
Autoclave	Astell Scientific Ltd., UK
Centrifuges	Eppendorf, Germany (Centrifuge 5424, 5417R)
Confocal Microscopes	Leica Microsystems, USA (TCS SP5) Leica Microsystems, USA (TCS SP8 *Inverted*)
Electrophoresis Equipment	Bio-Rad Labs, USA
Fluorescence Stereomicroscope	Leica Microsystems, USA (MZ16FA)
Freezers	Arçelik, Turkey
Gel Documentation System	Bio-Rad Labs, USA (Gel Doc XR)
Heating Block	Fisher Scientific, France
Heating Magnetic Stirrer	IKA, China (RCT Basic)
Incubator	Weiss Gallenkamp, USA (Incubator Plus Series)
Laboratory Bottles	Isolab, Germany
Micropipettes	Eppendorf, Germany
Microwave oven	Vestel, Turkey
pH meter	WTW, Germany (Ph330i)
Refrigerators	Arçelik, Turkey
Stereo Microscope	Olympus, USA (SZ61)
Thermal Cycler	Bio-Rad Labs, USA (C1000 Thermal Cycler)

3.3. Histological Techniques

3.3.1. Dissection of Third Instar Eye Imaginal Disc and Immunohistochemistry

All tissues were dissected in one drop (40µL) pre-chilled PBS on a dissection pad. Antenna-eye imaginal discs of third instar larvae were dissected together with mouth hook and larval brain (Figure 3.1). Dissected tissues were collected in fresh PBS (200 µL) in a glass chamber placed on ice. All larval dissections were performed in max. 20 min period. After that, the PBS was replaced with cold (4-8ºC) 4% PFA. The tissues were fixed with 4% PFA for 15-20 min at RT and 50-100 rpm on a shaker. Next, the PFA was replaced with 200 µL cold PBX3 for washing. Washing step was performed for 10-15 min and three times on a shaker at 50-100 rpm. After completion of washing steps, tissues were blocked in 200 µL PAXD for 2 hours at RT at 100 rpm on a shaker. Next, tissues were incubated with primary antibody, diluted in PAXD, for overnight at 4°C and 50-100 rpm on a shaker. After a day, the tissues were washed three times with cold PBX3 for 10-15 min at 50-100 rpm and RT. Then, remaining PBX3 was replaced with diluted secondary antibody in PAXD, and incubated for 2 hours at RT at 50-100 rpm on a shaker. During secondary antibody incubation, samples were protected from light by using aluminum foil or a light-proof box. After that, tissues were washed with PBX3 three times for 15 min. Then, antenna-eye imaginal discs were separated from mouth hook, larval brains, and other tissue parts, and mounted on a microscope slide with embedding medium. Finally, eye imaginal discs were visualized under a confocal microscope.

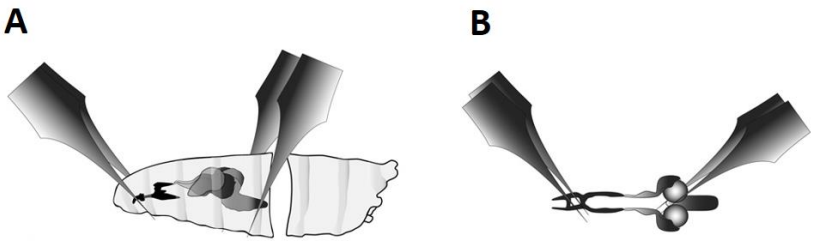

Figure 3.1. Schematic illustration of eye imaginal disc dissection (Legent and Treisman, 2009).

3.3.2. Starvation Assay and LysoTracker Staining of Larval Fat Body

Second instar larvae were transferred to dietary food (40 g fly food mixture, 15 g yeast, and 5 g agar per liter) for starvation. After 3-4 hours, larvae were dissected and fat body tissues were isolated. Dissected tissues were incubated with 1:1000 LysoTracker Red DND99 in PBS for 10 min. After several quick washes with PBS, tissues were fixed in 4% PFA for 15 min. Fixed tissues were washed three times with PBS for 10 min. Finally, the tissues were mounted on a slide and stored at +4ºC degree until visualization under the confocal microscope.

3.3.3. Cryosectioning of Adult Eye and Phalloidin Staining

Adult fly heads were separated from the body, and proboscis was removed from the head. The head without proboscis was fixed with 4% PFA for 2 hours at 4ºC. Then the heads were incubated with 20% sucrose solution for overnight at 4ºC. After that, the heads were embedded in OCT containing molds. The mold was frozen at -20ºC until it became rigid. At this step, the frozen molds can be stored at -80º C until sectioning. For cryosectioning, 12 µm frozen sections were taken and mounted on a positively charged slide. The slide was incubated at 65ºC for 1 hour to fix the tissues on the slide. To prevent flowing of liquid from the slide, edges of it were drawn with hydrophobic ink for next steps. Next, 4% PFA was put on the slide as form a thin layer on it for 15 min at RT. Then, the slide was placed into a PBX3 containing jar, and the slide was washed for 15 on a 50 rpm shaker at RT. Washing step was repeated with fresh PBX3 for three times. After that, samples were blocked by putting PAXD on the slide as a thin layer and incubated for 30 min at RT without shaking. 1:100 diluted fluorophore-conjugated Phalloidin in PAXD was put on the slide as a thin layer, and incubated for 2 hours at RT without shaking in a lightproof box. After incubation, the slide was washed three times again. Finally, tissues were mounted in Vectashield.

3.4. Molecular Biological Techniques

3.4.1. Agarose Gel Electrophoresis

Agarose gels were prepared as 1% (w/v) with 1X TAE buffer unless otherwise stated. After mixing the necessary amount of powder agarose and 1X TAE in a flask, it was boiled and dissolved in a microwave. 1 µL 1:10 10 mg/mL EtBr were added for each 10 mL in the flask, and mixed. After pouring the liquid mixture to the appropriate tank with a comb, it was allowed to solidify inside the hood. Meanwhile, samples were prepared by adding the appropriate volume of 6X loading dye to a final concentration of 1X. The solidified gel was placed in a 1X TAE containing tank, and the comb was removed. 1 kb or 100 bp marker was loaded to the first well, and the appropriate amount of prepared samples loaded to other wells. The gel was run at 90 V for 30-60 min and visualized under UV.

3.4.2. Genomic DNA Extraction

A single fly was placed in a 200 µL test tube and frozen at -20ºC for at least 10 min. 1 µL proteinase K (18 mg/mL) was added to 50 µL Squish buffer, the proteinase K containing Squish buffer was sucked up with a micropipette tip. The frozen fly was squished with a micropipette tip until it becomes unrecognizable, then the Squish buffer was slowly added to the test tube. The mixture was incubated at 37ºC for 30 min and 95ºC for 2 min in a thermocycler. The extract was kept in -20ºC until further use.

3.4.3. Plasmid DNA Isolation

3.4.3.1. Small Scale Plasmid DNA Isolation. Thermo-Scientific GeneJET Plasmid Miniprep Kit was used. Plasmid purification protocol was carried out at RT, and max rpm (13200 rpm) was used for tabletop centrifugation. 3-4 mL overnight *E. coli* culture in LB media were used for the purification protocol. Firstly, bacterial culture was harvested in 2mL test tube by centrifugation at 8000 rpm for 2 min at RT. After removing the remaining medium, pelleted cells were resuspended in 250 µL of the RNase-A containing Resuspension Buffer by vortexing. After that, 250 µL of the Lysis Solution was added, and mixed by inverting

the tube 4-6 times. After 5 min incubation 350 µL of the Neutralization Solution was added to the test tube immediately, and mixed by inverting the tube 4-6 times. Next, the sample was centrifuged for 5 min to pellet cell debris and chromosomal DNA. After that, the supernatant was transferred to the supplied GeneJET spin column by pipetting. Then, the column was centrifuged for 1 min, and the flow-through was discarded. 500 µL of the Wash Solution was added to the column, and centrifuged for 1 min. The washing step was performed two times. Then the column was placed into a fresh 1.5 mL test tube, and 50 µL of the Elution Buffer was added to the center of the column membrane. After incubation for 2 min, the column and the tube were centrifuged for 2 min. Collected Plasmid DNA was stored in -20ºC.

3.4.3.2. Medium Scale Plasmid DNA Isolation. QIAGEN Plasmid Plus Midi Kit was used for medium scale plasmid DNA isolation. 50 mL overnight *E. coli* culture in LB were harvested in 50 mL test tubes by centrifuging at 6000xg for 15 min at 4ºC. After that, pelleted bacteria were resuspended in 2 mL cold Buffer P1. Then, 2 mL Buffer P2 were added, and mixed by inverting the tube several times until the lysate appears viscous. After incubation for 3 min, 2 mL Buffer S3 was added to the lysate, and mixed by inverting the tube 4-6 times. Next, the lysate was transferred to the QIA filter Cartridge, and incubated at RT for 10 min. By using the supplied plunger, the cell lysate was filtered into a 15 mL tube, a 2 mL Buffer BB was added, and mixed by inverting the tube 4-6 times. Then, the lysate was transferred to QIAGEN Plasmid Plus columns placed on a vacuum manifold. Approximately 300 mbar of vacuum was applied until the liquid was drawn through all columns. For washing, 700 µL Buffer ETR was added, and vacuum was applied. A second washing with 700 µL Buffer PE was performed. For removing residual wash buffer, the column was centrifuged at 9700 rpm (10000 x g) for 1 min. The column was placed into a fresh 1.5 mL tube. For the elution of DNA, 200 µL Buffer EB or water to the center of the column. It was incubated for 2 min. and centrifuged for 1 min. Collected plasmids were kept at -20ºC.

3.4.4. Restriction Digestion of DNA

Restriction enzymes were used according to manufacturers' instructions. Generally, 1 µL restriction enzyme was used to digest 1 µg of DNA in a volume of 30 µL at 37ºC for 1 h.

3.4.5. Transformation

3.4.5.1. Chemical Transformation. 50 µL competent *E. coli* (TOP10 strain) cells stored at -80ºC were thawed on ice for approximately 30 min. 50-100 ng plasmid was gently mixed with the competent cells and kept on ice for 30 min. The cells were heat-shocked by incubation at 42ºC for 45 sec and incubated on ice for 2 min. 1 mL LB was added to the cells and incubated at 37ºC for 1 h. After that, 100 µL culture was spread on LB agar plates containing the appropriate antibiotic, and incubated at 37ºC overnight. Transformed colonies were used for further studies.

3.4.5.2. Transformation with Electroporation. Electro-competent *E. coli* (TOP10 strain) cells stored at -80ºC were thawed on ice. Meanwhile, an electroporation cuvette was kept on ice for chilling. 50 ng plasmid was gently mixed with the cells, and cells were kept on ice for 10 min. The cells were transferred to the pre-chilled electroporation cuvette. Humidity outside the cuvette was swiped, and the cuvette was placed into the electroporation device. Ec1 set up was selected, and the cells were electroporated by pressing the pulse button. 1 mL LB was rapidly added to the cuvette. The cells were transferred to the 1.5 mL test tube, and incubated at 37ºC for 60 min. After that, the 100 µL culture was spread on the appropriate antibiotic plate and incubated overnight. Transformed colonies were used for further studies.

3.4.6. Ligation

0.020 pmol Vector DNA, 0.060 pmol insert DNA, 1x Ligation Buffer, and 1 U of T4 DNA ligase were mixed in a microcentrifuge tube and incubated at 25ºC for 2 h or at 16-18ºC for 16h. Finally, the ligated construct was transformed to the *E.coli*.

3.4.7. Gibson Assembly

NEB Gibson Assembly Kit was used according to manufacturers' protocol. In summary, 0.02-0.5 pmol insert and backbone fragments, 10 µL 2x Gibson Assembly Master Mix were mixed and the total volume was completed to 20 µL with dH_2O. The samples were

incubated at 50ºC for 15 min. The samples were stored at -20ºC for subsequent transformation.

3.4.8. Polymerase Chain Reaction (PCR)

For Taq polymerase chain reactions, each reaction was performed in 25 µL volume which contains 1xTaq buffer, 1.5 mM $MgCl_2$ 0.5 mM dNTP, 10 mM forward primer, 10 mM reverse primer ~100 ng of template genomic DNA, and 5 U of Taq polymerase. Following thermocycler program was used for Taq PCR:

Table 3.8. Thermocycler program for Taq polymerase chain reaction

Temperature (ºC)	Duration	Cycle
95	3 min	-
95	30 sec	35 cycles
50-55	30 sec	
68	1-1.5 min	
68	5 min	-
4	∞	-

3.4.9. Gel Purification

After agarose gel electrophoresis, the DNA band of interest was cut out from the gel using a razor blade on a UV light box, and the gel slice was placed in 1.5 mL test tube. The weight of the gel slice was determined. The Roche gel purification kit was used for DNA isolation from the gel. For each 100 mg of gel, 300 µL binding buffer was added, and vortexed. The tube was incubated in a heat-block at 56ºC for 10 min at 900 rpm. During the incubation, the mixture was vortexed several times for 10-15 sec. For each 100 mg of gel 150 µL isopropanol was added to the tube, and vortexed. A high filter tube was placed in a collection tube, and the mixture (max 700 µL) was transferred to the high filter tube. It was centrifuged at max speed for 60 sec. in a tabletop centrifuge at RT. The flow-through in the

collection tube was discarded. 500 µL of wash buffer was added to the high filter tube, and it was centrifuged for 1 min at max. speed. After that, a second washing step was performed with 200 µL of wash buffer, and the collection tube was discarded. The high filter tube was placed in a 1.5 mL test tube. 50 µL elution buffer was added to the center of the filter. After, incubation for at least 5 min at RT, the high filter tube with 1.5 mL test tube was centrifuged at max speed for 1 min (to increase yield, the elution step was repeated with collected elution in 1.5 mL test tube). The isolated DNA containing elution was stored in -20ºC for further experiments.

3.4.10. Sequencing Analysis

Purified PCR products were sent to MACROGEN (Korea, Inc.) for sequencing, and sequence results were analyzed with MUSCLE alignment tool and ExPasy *in silico* translation tool.

3.5. Generation of NHEJ Mediated dmHexDC Knockout Allele by CRISPR/Cas9

3.5.1. Selection of sgRNA Target

Two different gRNA target sites (T1 and T2) were selected as close as possible to translation start site by using online available designing tools: MIT CRISPR design, and CRISPRscan. Both tools identified possible gRNA target sites, and gave scores between 0-100 to each target site according to their complex algorithms. Higher scores indicate less gRNA off-target sites in the genome, and higher binding and cutting efficiency of the gRNA/Cas9 complex.

3.5.2. Cloning of gRNA Expressing Plasmid

72 bp long forward and reverse primers which contain gRNA target sequences and homology sequences according to pCFD4 backbone were commercially synthesized. Then, polymerase chain reaction was performed with the aforementioned primers and pCFD4 template and a product of the expected 600bp was obtained. Later, pCFD4 plasmid was

digested with the *Bbs*I restriction enzyme. The PCR product and the digested plasmid were run on a 1% Agarose gel, and 600 bp and 6.4 kb bands were isolated from the gel. Isolated fragments were assembled using the Gibson Assembly kit (NEB) and transformed into competent *E. coli* bacteria and plated on ampicillin plates. Transformed *E. coli* were isolated and DNAs were sent to sequencing for verifying the construct.

3.5.3. Embryo Injection

PhiC31 Embryo injection and transformant selection were performed at GenetiVision (USA, Inc.). pCFD4-dmHexDC_gRNA-T1-T2 construct was injected to 200 embryos of the *Drosophila melanogaster* strain *yw*; *attB* (VK37 line). After adult G0 flies were obtained from injected embryos, male G0 flies were crossed with *v*'; *BcE*/*CyO* virgin female flies. After screening for *vermillion* in F1 males, the positive males were balanced with *v*'; *BcE*/*CyO*.

3.5.4. Generation of NHEJ-mediated *dmHexDC* mutants

To generate NHEJ mediated mutant flies, gRNA-expressing males were crossed with germline-specific Cas9 expressing females. Germ cells of F1 females represent putative *dmHexDC* mutants. After obtaining adult F2 flies that carry putative NHEJ-mediated mutations, each *vermillion*-positive putative mutant F2 male was balanced separately with *w*;;*TM3*/*TM6B* flies (Figure 3.2). In the next generation, putative mutant lines were screened by PCR and sequencing analysis was performed on each population to observe mutations in the desired genomic region.

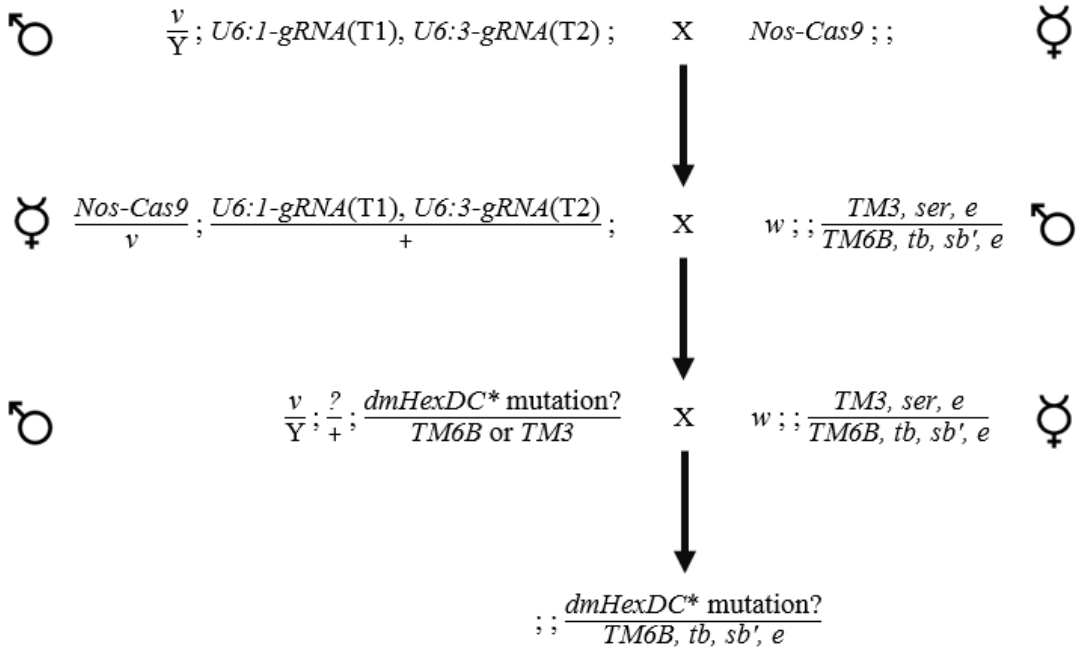

Figure 3.2. Cross scheme for generation of dmHexDC mutants. NHEJ mediated mutation is induced in germline cells of F1 generation. Cas9 and gRNA coding transgenes are got rid of by crossing with balancer line.

3.6. Crosses for Experiments

3.6.1. Downregulation of dmHexDC in the Whole Eye

To downregulate *dmHexDC* expression specifically in the eye, dicer-2 and RNAi of dmHexDC were overexpressed using eye-specific drivers. Ey-Gal4, GMR-Gal4 (eyGMR-gal4) and UAS-*dicer2* carrying transgenic virgin females were crossed with UAS-*dmHexDC*^{RNAi} carrying transgenic males. GFP-negative third instar larvae from F1 generation were selected under a fluorescent microscope. EyGMR-Gal4 carrying second chromosome cannot be homozygous for the line, so that transgenic construct is found heterozygous with *CyO* balancer chromosome with GFP marker. Because of that, to select eyGMR-Gal4 carrying larvae from F1 generation GFP negative larvae were selected (Figure 3.3).

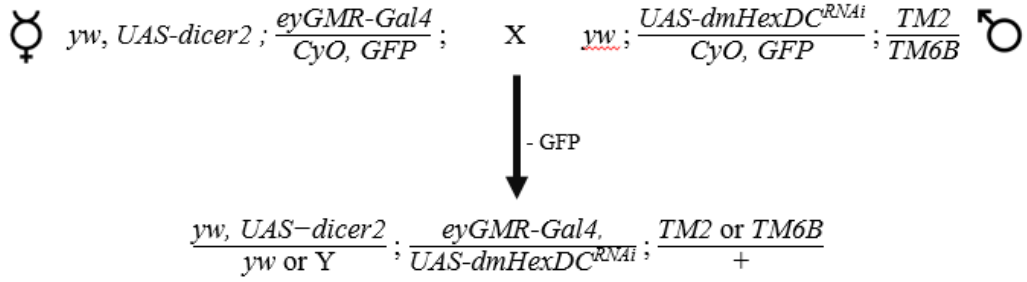

Figure 3.3. Cross scheme for downregulation of *dmHexDC* in the eye. dmHexDC is downregulated by *UAS-dicer2* and *UAS-dmHexDC*^{RNAi} transgenic constructs under the control of both *ey-Gal4* and *GMR-gal4*.

3.6.2. Downregulation of dmHexDC in Dorsal Part of the Eye Imaginal Disc

To downregulate the *dmHexDC* specifically in the dorsal part of the eye, RNAi of dmHexDC (UAS-*dmHexDC*^{RNAi}) was induced using the dorsal eye-specific driver DE-Gal4 (Figure 3.4).

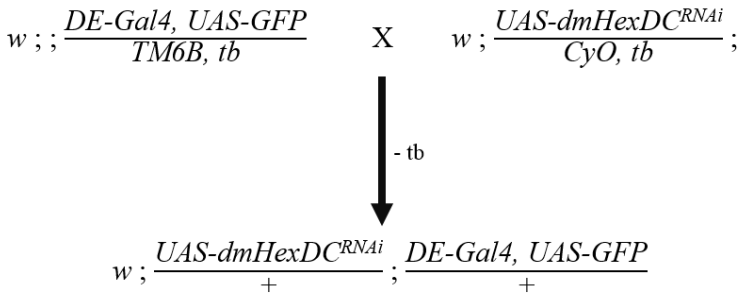

Figure 3.4. Cross scheme for downregulation of dmHexDC in the dorsal eye. dmHexDC downregulated by *UAS-dmHexDC*^{RNAi} construct under the control of DE-Gal4. Expressed GFP provides the visualization of dmHexDC knockdown in the dorsal region.

3.6.3. Generation of *dmHexDC*^{null} Clones in the Eye Imaginal Disc

Females of a transgenic line carrying an eye-specific flippase (*ey-FLP*) and an FRT allele carrying a ubiquitously expressed RFP (*FRT82B ubi-RFP*) were crossed with males of a transgenic line carrying an FRT82B with sb' marker chromosome to which the P. trap

line has been recombined (*FRT82B sb' dmHexDC*^{null}). Eye imaginal discs of non-tubby larvae from the F1 generation were used for analysis as clonal eye discs (Figure 3.5).

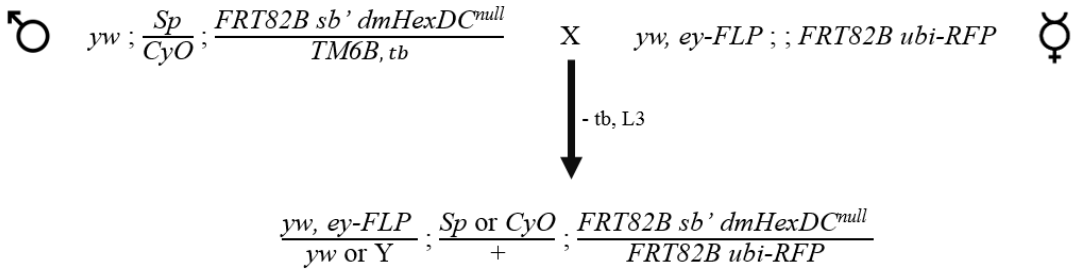

Figure 3.5. Cross scheme for the generation of *dmHexDC*^{null} clones in eye imaginal discs. FLP causes mitotic recombination and clone formation under the control of the *eyeless* promoter

3.6.4. Generation of *dmHexDC*^{null} Clones in Apoptosis Inhibited Eye Imaginal Disc

Ey-Gal4, UAS-FLP (EGUF) carrying *FRT82B sb' dmHexDC*^{null} line was crossed with *UAS-p35* carrying *FRT82B ubi-RFP* line. Eye discs of larvae without tubby marker were selected from the F1 generation (Figure 3.6).

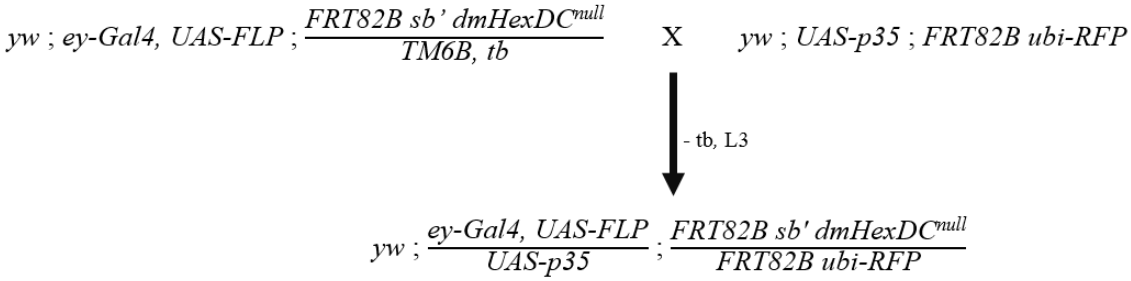

Figure 3.6. Generation of *dmHexDC*^{null} clones in apoptosis inhibited eye. p35 is expressed under the control of ey-GAL4 and used for apoptosis inhibition in the eye disc.

3.6.5. Generation of Flies Over-expressing dmHexDC

Flies carrying homozygous *Ubi-Gal4* transgenic construct were crossed with flies with the homozygous UAS-dmHexDC transgenic construct. Larvae from the F1 generation were used for analysis (Figure 3.7).

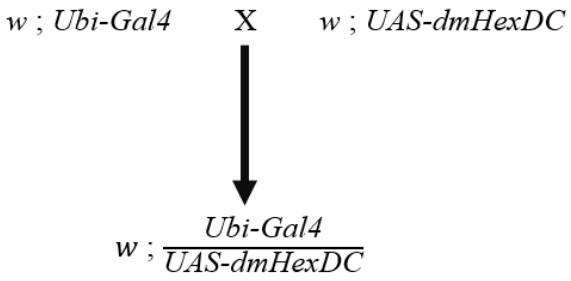

Figure 3.7. Cross scheme for generation dmHexDC overexpressed fly. dmHexDC is expressed ubiquitously in the F1 progeny.

4. RESULTS

dmHexDC is a novel protein in *Drosophila* that is expressed in R7 photoreceptors and undifferentiated cells in the eye imaginal discs. Our lab has previously shown that loss of dmHexDC causes photoreceptor loss, overproliferation and increased apoptosis in eye imaginal discs with an increase in wg signaling. Furthermore, lipid accumulation and lysosomal disfunction were also observed. We hypothesize that the observed phenotypes might be explained by compensatory proliferation (Kıral, 2015).

4.1. Generation of NHEJ Mediated dmHexDC Knockout by CRISPR/Cas9

The protein trap line that was used in the initial experiments acts like an enhancer-trap line and interferes with some of our analysis. Thus, we aimed to generate novel mutants by CRISPR/Cas9.

4.1.1. Designing and Cloning of dmHexDC Targeting sgRNAs

The rationale behind the design was to delete a portion of the coding sequence and thus eliminating a functional dmHexDC expression. To achieve this, two separate gRNAs were designed targeting bp 100 and 566 from the beginning of the dmHexDC CDS. Among the possible candidate guide RNAs that were provided by the MIT CRISPR and CRISPRscan, “5’-GGCTGTCGTATCGATTAGTATGG-3’ (T1, + strand, cutting position is 100 bp after TSS) and 5’- GGGGATGGGCGTGCCGGTGGTGG-3’ (T2, -strand, cutting position is 566 bp after TSS) were selected since they were with the highest scores and least off target hits. (Figure 4.1).

A

	score	sequence	
Guide #1	99	GGCTGTCGTATCGATTAGTA	TGG
Guide #2	98	TGCTTCTCGGCCTCTGGACA	TGG
Guide #3	98	GTGCACCTGCTGGTAACCCG	TGG
Guide #4	98	GCAGTCCACGGGTTACCAGC	AGG
Guide #5	98	GCCAGACACGACGAGCAGGA	AGG
Guide #6	97	TCCTTCCTGCTCGTCGTGTC	TGG
Guide #7	97	GCTTCTCGGCCTCTGGACAT	GGG
Guide #8	97	GTGTCTGGCCTGGTGCTTCT	CGG
Guide #9	96	TTAGTATGGCCCATGTCCAG	AGG
Guide #10	96	AGCTTATCGAGCAGGCAAAC	CGG
Guide #11	96	CTGCTGCTGGCGCTCAGAAT	TGG
Guide #12	96	CCAGGCCAGACACGACGAGC	AGG
Guide #13	95	GGCGGCAGGAGGCTGTGCTG	AGG
Guide #14	95	GCCTGGTGCTTCTCGGCCTC	TGG
Guide #15	95	CTGGCGCTCAGAATTGGAAA	TGG
Guide #16	95	TCCAGAGGCCGAGAAGCACC	AGG
Guide #17	95	GGCGCTCAGAATTGGAAATG	GGG
Guide #18	94	TGGCGCTCAGAATTGGAAAT	GGG
Guide #19	94	CATCCAGAAGCTTATCGAGC	AGG
Guide #20	94	TTGCCTGCTCGATAAGCTTC	TGG
Guide #21	94	CGAGCAGGAAGGAAAGTTTC	CGG
Guide #22	93	TTTGGATATTTATTTGGCGC	CGG
Guide #23	93	TCTGGATGATGTGCACCTGC	TGG
Guide #24	93	GCTTATCGAGCAGGCAAACC	GGG
Guide #25	92	CTCAGAATTGGAAATGGGGG	CGG
Guide #26	91	GCGCTCAGAATTGGAAATGG	GGG
Guide #27	91	CCTGCTCGTCGTGTCTGGCC	TGG
Guide #28	90	GAATTGGAAATGGGGGCGGC	AGG
Guide #29	87	TTGGAAATGGGGGCGGCAGG	AGG
Guide #30	86	CAAATCTTTGGATATTTATT	TGG
Guide #31	27	GCAGCAGCAGCAGCAGTCCA	CGG
Guide #32	25	CAGCAGCAGCAGCAGTCCAC	GGG
Guide #33	9	TGGACTGCTGCTGCTGCTGC	TGG

B

CRISPRscan score	Locus	Oligo
57	yourseq:3R:18212860-18212883 (+)	taatacgactcactataGGACGAGCGAATGCTCAGTTgttttagagctagaa
78	yourseq:3R:18212815-18212838 (+)	taatacgactcactataGGGCCAGAGAAACGCCGGTAgttttagagctagaa
63	yourseq:3R:18212523-18212546 (-)	taatacgactcactataGGCGGCAGGAGGCTGTGCTGgttttagagctagaa
78	yourseq:3R:18212544-18212567 (-)	taatacgactcactataGGGCTCAGAATTGGAAATGGgttttagagctagaa
58	yourseq:3R:18212546-18212569 (-)	taatacgactcactataGGGCGCTCAGAATTGGAAATgttttagagctagaa
57	yourseq:3R:18213099-18213122 (-)	taatacgactcactataGGGCTGAAGAACTCCGCTGTgttttagagctagaa
61	yourseq:3R:18212586-18212609 (-)	taatacgactcactataGGGCACCTGCTGGTAACCCGgttttagagctagaa
62	yourseq:3R:18212638-18212661 (-)	taatacgactcactataGGCGCTCGGCACGCAGCACCgttttagagctagaa
63	yourseq:3R:18212652-18212675 (-)	taatacgactcactataGGCGTTATCCTTGAGCCGCTgttttagagctagaa
75	yourseq:3R:18212716-18212739 (+)	taatacgactcactataGGGTTCCCTGCGACCCACACgttttagagctagaa
56	yourseq:3R:18212725-18212748 (+)	taatacgactcactataGGGACCCACACAGGCCAAGAgttttagagctagaa
61	yourseq:3R:18212730-18212752 (-)	taatacgactcactataGGCGCCTTCTTGGCCTGTGgttttagagctagaa
85	yourseq:3R:18212730-18212753 (-)	taatacgactcactataGGGCGCCTTCTTGGCCTGTGgttttagagctagaa
57	yourseq:3R:18212829-18212852 (-)	taatacgactcactataGGCGTTCAGTTCCTCCATACgttttagagctagaa
61	yourseq:3R:18212479-18212502 (+)	taatacgactcactataGGTTCTCGGCCTCTGGACATgttttagagctagaa
66	yourseq:3R:18212863-18212886 (+)	taatacgactcactataGGAGCGAATGCTCAGTTCGGgttttagagctagaa
58	yourseq:3R:18212898-18212921 (+)	taatacgactcactataGGTACGAGCACGAGCTTCAGgttttagagctagaa
74	yourseq:3R:18212903-18212926 (+)	taatacgactcactataGGGCACGAGCTTCAGAGGATgttttagagctagaa
57	yourseq:3R:18212911-18212934 (+)	taatacgactcactataGGTTCAGAGGATGGGCGTGCgttttagagctagaa
109	yourseq:3R:18212917-18212940 (+)	taatacgactcactataGGGGATGGGCGTGCCGGTGGgttttagagctagaa
77	yourseq:3R:18212927-18212950 (+)	taatacgactcactataGGGCCGGTGGTGGCTGGCATgttttagagctagaa
58	yourseq:3R:18212928-18212951 (+)	taatacgactcactataGGCCGGTGGTGGCTGGCATCgttttagagctagaa
67	yourseq:3R:18212930-18212953 (-)	taatacgactcactataGGCCCGATGCCAGCCACCACgttttagagctagaa
70	yourseq:3R:18212932-18212955 (+)	taatacgactcactataGGTGGTGGCTGGCATCGGGCgttttagagctagaa
66	yourseq:3R:18212936-18212959 (+)	taatacgactcactataGGGGCTGGCATCGGGCCGGAgttttagagctagaa
64	yourseq:3R:18212951-18212974 (-)	taatacgactcactataGGGGGAGCTCTCGGACCATCgttttagagctagaa
80	yourseq:3R:18213086-18213109 (+)	taatacgactcactataGGGGACATGTTTCCCTACAGgttttagagctagaa
66	yourseq:3R:18213041-18213064 (-)	taatacgactcactataGGTCCCAGTGCCCGCAGCACgttttagagctagaa
60	yourseq:3R:18213063-18213086 (-)	taatacgactcactataGGACTCTATGAGCAGACCAGgttttagagctagaa
41	yourseq:3R:18212757-18212780 (-)	taatacgactcactataGGACAGGAAGCTCTCGGACAgttttagagctagaa
34	yourseq:3R:18212764-18212787 (+)	taatacgactcactataGGAGAGCTTCCTGTTCGAGCgttttagagctagaa
44	yourseq:3R:18212773-18212796 (-)	taatacgactcactataGGAGGCGCTCCTGCTCGAACgttttagagctagaa
43	yourseq:3R:18213098-18213121 (-)	taatacgactcactataGGCTGAAGAACTCCGCTGTAgttttagagctagaa
28	yourseq:3R:18212791-18212814 (-)	taatacgactcactataGGTGCTGCTCCAGAATCTTGgttttagagctagaa
49	yourseq:3R:18212451-18212474 (-)	taatacgactcactataGGCAGACACGACGAGCAGGAgttttagagctagaa
42	yourseq:3R:18213124-18213147 (+)	taatacgactcactataGGCCGCGCACAATGCCTACAgttttagagctagaa
30	yourseq:3R:18212839-18212862 (+)	taatacgactcactataGGAACTGAACGCCAATGCCGgttttagagctagaa
54	yourseq:3R:18212440-18212463 (-)	taatacgactcactataGGAGCAGGAAGGAAAGTTTCgttttagagctagaa
37	yourseq:3R:18213099-18213121 (-)	taatacgactcactataGGCTGAAGAACTCCGCTGTgttttagagctagaa
43	yourseq:3R:18212581-18212604 (+)	taatacgactcactataGGAGTCCACGGGTTACCAGCgttttagagctagaa
39	yourseq:3R:18212902-18212925 (+)	taatacgactcactataGGAGCACGAGCTTCAGAGGAgttttagagctagaa
37	yourseq:3R:18212502-18212525 (-)	taatacgactcactataGGCTGTCGTATCGATTAGTAgttttagagctagaa
46	yourseq:3R:18212619-18212642 (+)	taatacgactcactataGGCTTATCGAGCAGGCAAACgttttagagctagaa
46	yourseq:3R:18212620-18212643 (+)	taatacgactcactataGGTTATCGAGCAGGCAAACCgttttagagctagaa
48	yourseq:3R:18212465-18212488 (+)	taatacgactcactataGGGTCTGGCCTGGTGCTTCTgttttagagctagaa
42	yourseq:3R:18212644-18212667 (+)	taatacgactcactataGGTGCGTGCCGAGCGGCTCAgttttagagctagaa
52	yourseq:3R:18212537-18212560 (-)	taatacgactcactataGGATTGGAAATGGGGGCGGCgttttagagctagaa
22	yourseq:3R:18212686-18212709 (+)	taatacgactcactataGGCATCGCCAGTCCAGCGGCgttttagagctagaa
44	yourseq:3R:18212472-18212495 (+)	taatacgactcactataGGCTGGTGCTTCTCGGCCTCgttttagagctagaa
48	yourseq:3R:18212545-18212568 (-)	taatacgactcactataGGCGCTCAGAATTGGAAATGgttttagagctagaa
45	yourseq:3R:18212960-18212983 (-)	taatacgactcactataGGACGCTCGGCGGGAGCTCTgttttagagctagaa
47	yourseq:3R:18212969-18212992 (-)	taatacgactcactataGGATGAACGAGACGCTCGGCgttttagagctagaa
23	yourseq:3R:18212971-18212994 (+)	taatacgactcactataGGCCGAGCGTCTCGTTCATCgttttagagctagaa
44	yourseq:3R:18212973-18212996 (-)	taatacgactcactataGGCCAGATGAACGAGACGCTgttttagagctagaa
26	yourseq:3R:18213011-18213034 (-)	taatacgactcactataGGCTTGAGAAAGCTTAGCTTgttttagagctagaa
34	yourseq:3R:18213030-18213053 (+)	taatacgactcactataGGCAACTGCTGCCCGTGCTGgttttagagctagaa
38	yourseq:3R:18212729-18212752 (-)	taatacgactcactataGGCGCCTTCTTGGCCTGTGTgttttagagctagaa
31	yourseq:3R:18213068-18213090 (+)	taatacgactcactataGGTCTGCTCATAGAGTACGgttttagagctagaa
40	yourseq:3R:18212546-18212568 (-)	taatacgactcactataGGCGCTCAGAATTGGAAATgttttagagctagaa
40	yourseq:3R:18213042-18213065 (-)	taatacgactcactataGGCTCCCAGTGCCCGCAGCAgttttagagctagaa
29	yourseq:3R:18212478-18212501 (+)	taatacgactcactataGGCTTCTCGGCCTCTGGACAgttttagagctagaa
49	yourseq:3R:18213067-18213090 (+)	taatacgactcactataGGGTCTGCTCATAGAGTACGgttttagagctagaa
55	yourseq:3R:18213127-18213150 (+)	taatacgactcactataGGCGCACAATGCCTACAAGGgttttagagctagaa
62	yourseq:3R:18213037-18213060 (+)	taatacgactcactataGGTGCCCGTGCTGCGGGCACgttttagagctagaa
43	yourseq:3R:18213031-18213054 (+)	taatacgactcactataGGAACTGCTGCCCGTGCTGCgttttagagctagaa
36	yourseq:3R:18212782-18212805 (+)	taatacgactcactataGGAGGAGCGCCTCAAGATTCgttttagagctagaa
50	yourseq:3R:18212569-18212592 (+)	taatacgactcactataGGAGCAGCAGCAGCAGTCCAgttttagagctagaa
43	yourseq:3R:18212566-18212589 (-)	taatacgactcactataGGGACTGCTGCTGCTGCTGCgttttagagctagaa
31	yourseq:3R:18212566-18212588 (-)	taatacgactcactataGGACTGCTGCTGCTGCTGCgttttagagctagaa

Figure 4.1. Suggested gRNAs for dmHexDC. A) MIT CRISPR results. B) CRISPRscan results. Candidate gRNA sequences and their fitness scores are listed. Selected gRNAs with the highest score are marked.

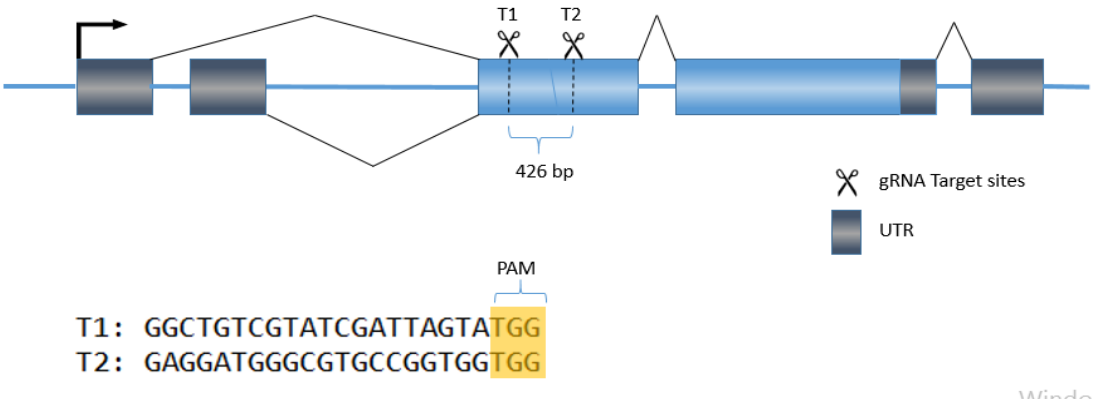

Figure 4.2. Schematic drawing indicating dmHexDC gRNA targeting sites, T1 and T2. Blue exons belong to the CDS of the gene. Splicing regions are shown with cursed lines. PAM sequences are highlighted in yellow

The 600 bp long segment of the vector containing the gRNA was generated through PCR using 72 bp oligonucleotides as primers and pCFD4 as a template and this fragment was used later to replace the original piece within the pCFD4 vector, thus resulting in the gRNA-inserted pCFD4 vector (Figure 4.3). The cloning procedure was carried out by Ecem Çayıroğlu.

In parallel, the pCFD4 vector was digested with the restriction enzyme *Bbs*I and the 600 bp insert and 6.4 kb long backbone fragments were isolated from the agarose gel (Figure 4.5A and B). The insert and backbone fragments were then assembled using Gibson assembly, and the construct containing the dmHexDC target sites was obtained successfully. Cloning of pCFD4-T1-T2 was verified by *Xba*I and *Sac*II analytical digestion, and sequencing analysis. Restriction digestion of gRNA-inserted pCFD4 with *Xba*I and *Sac*II results in fragments of 2340 and 4885 bps (Figure 4.5C).

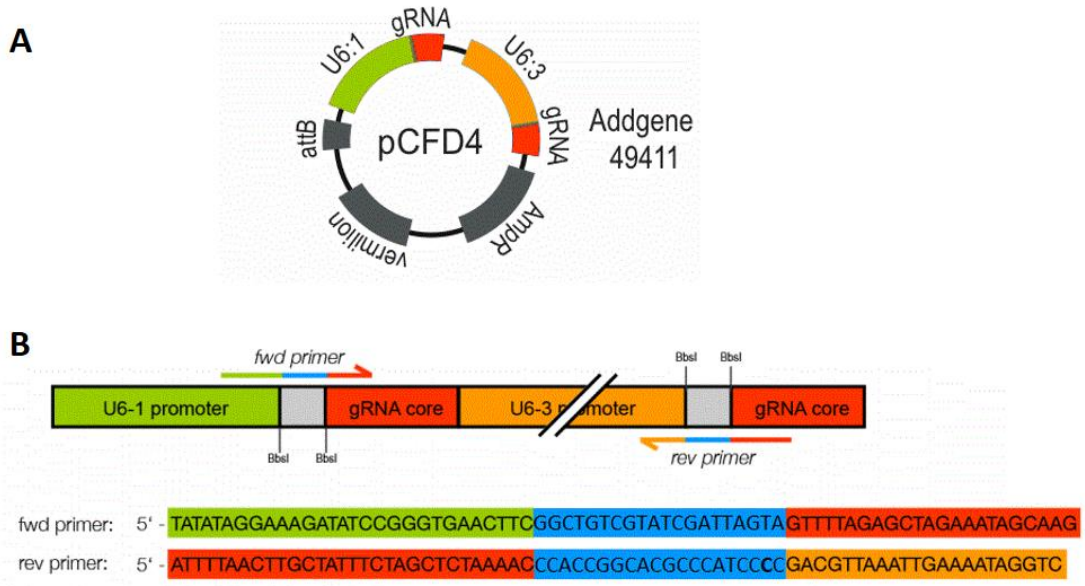

Figure 4.3. Schematic illustration of cloning of target sites into pCFD4 vector. A) Schematic illustration of pCFD4 vector. B) Schematic illustration of generation of target site containing insert fragment by PCR.

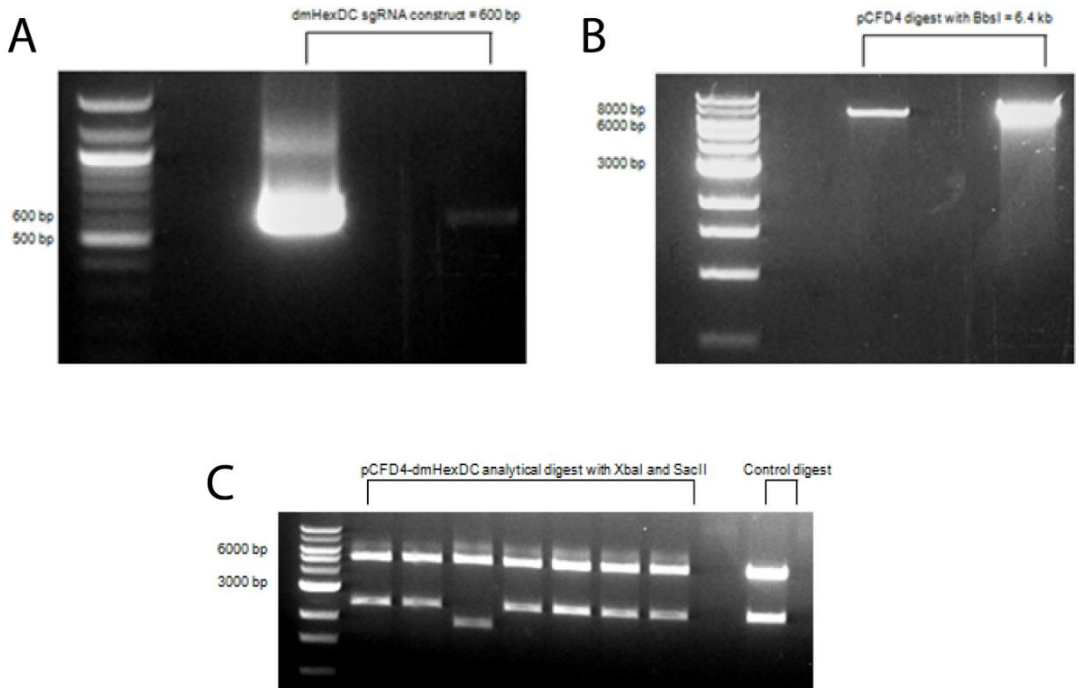

Figure 4.4. Gel images of cloning steps for cloning of target sites into pCFD4. A) Gel image of target site containing insert fragment. B) Gel image of *Bbs*I digested pCFD4 backbone fragment. C) Gel image of generated dmHexDC target site containing pCFD4 constructs.

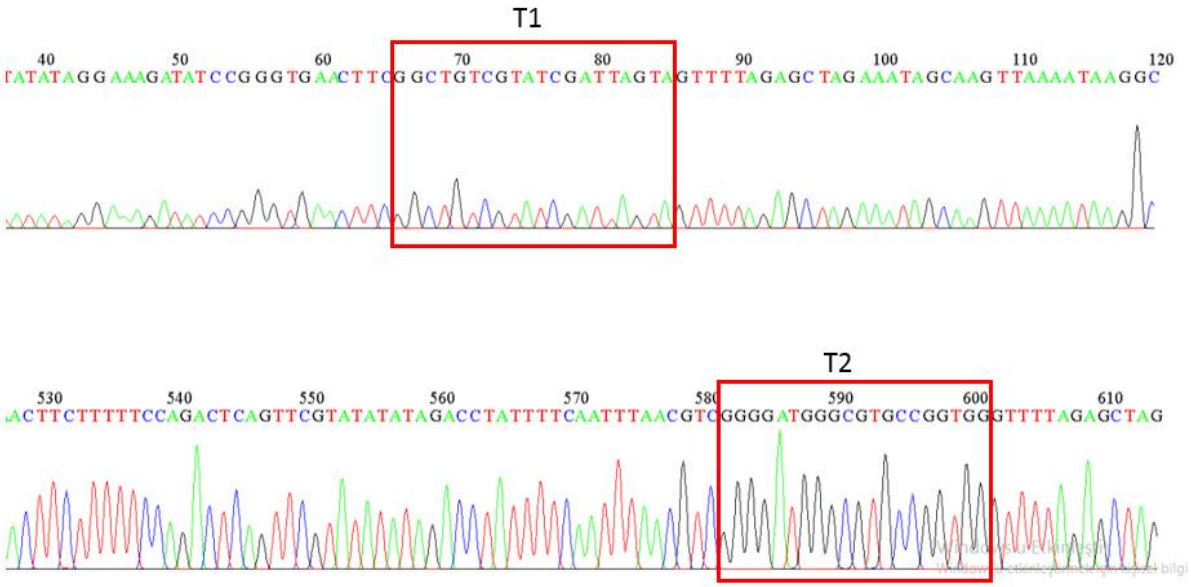

Figure 4.5. Sequencing result of the generated pCFD4-T1-T2 construct. Red boxes show integrated target sequences.

4.1.2. Generation and Screening of Mutants

For embryo injection the pCFD4 plasmid containing T1 and T1 gRNAs was isolated in large scale using QIAGEN midiprep kit. After embryo injections, two *v'; U6:1-gRNA(T1), U6:3-gRNA(T2)/CyO* stock line were received from the injection company GenetiVision. The injected flies were crossed with Nos-Cas9 carrying flies. After necessary crosses were performed, 79 different possible mutant flies were obtained, and they numbered as 1 to 79. 61 of them were gave viable offspring. The progeny was screened for a deletion between gRNA target sites by genomic PCR of single male flies. A 566 bp region in *dmHexDC* gene was amplified using primers flanking the gRNA target sites. In cases in which both of the gRNAs were utilized by Cas9 and the desired deletion was induced, 140 bp long band was expected with the same set of primers (Figure 4.6).

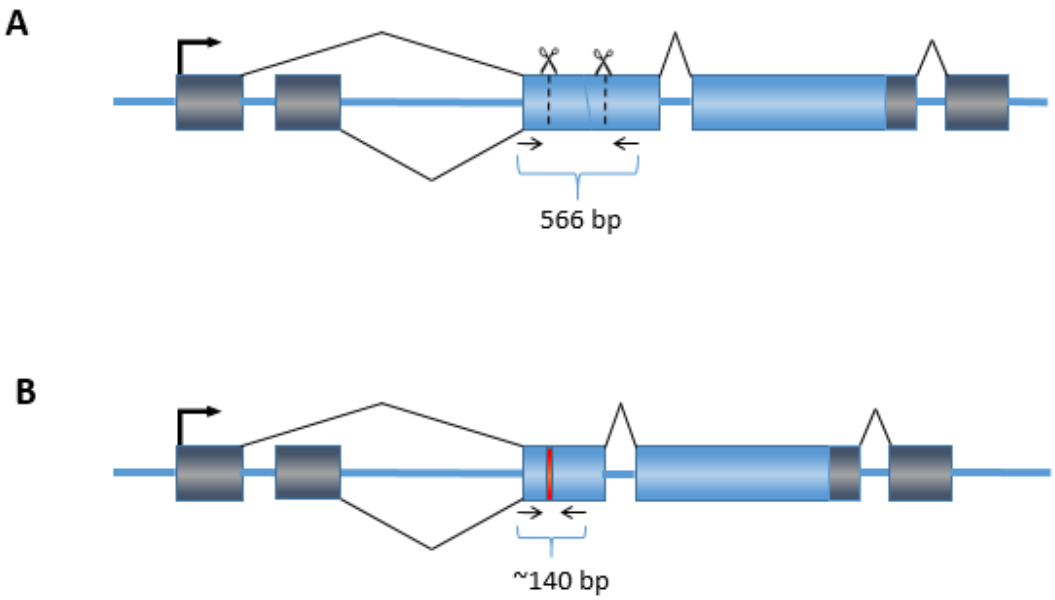

Figure 4.6. Illustration of designed screening primers and amplified genomic regions in genomes of wt (A) and mutant (B) lines.

After the screening, the desired deletion was observed in five different flies which belonged to lines 13, 22, 35, 61, and 79 (Figure 4.7).

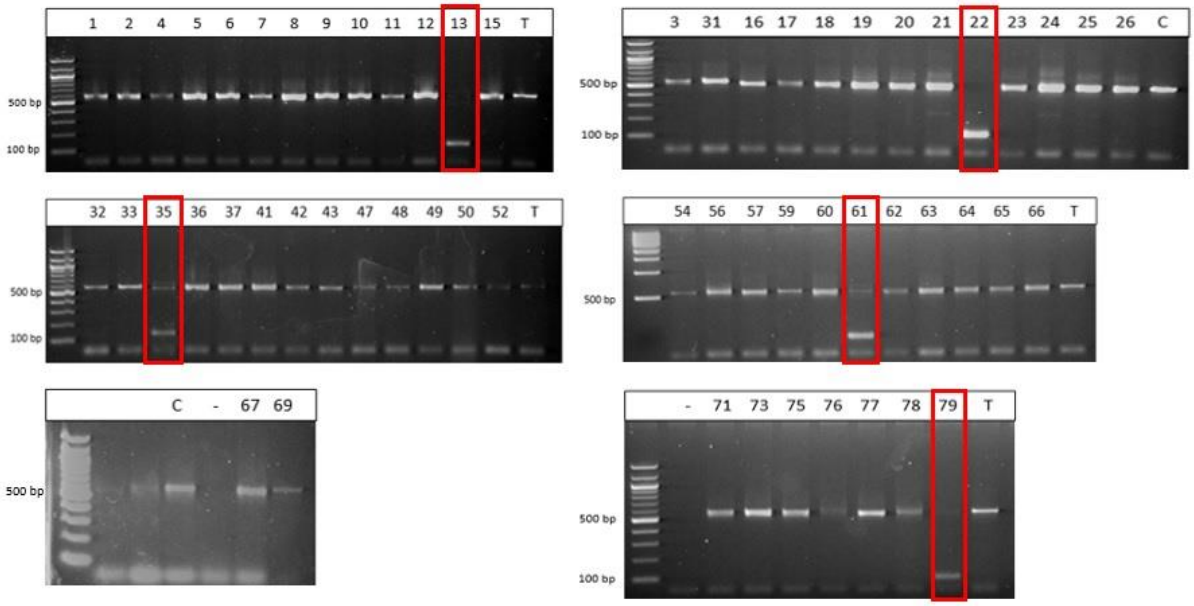

Figure 4.7. Agarose gel images of genomic PCR screening. 566 bp region of a wt fly were amplified. Expected band size for mutants with expected deletion is approximately 140 bp. Expected deletions were observed in 5 different lines (marked with red boxes).

4.1.3. Analysis of Generated Mutants

600 bp long genomic region of mutants were sequenced, and approximately 466 bp deletion between target sites were verified (Figure 4.8).

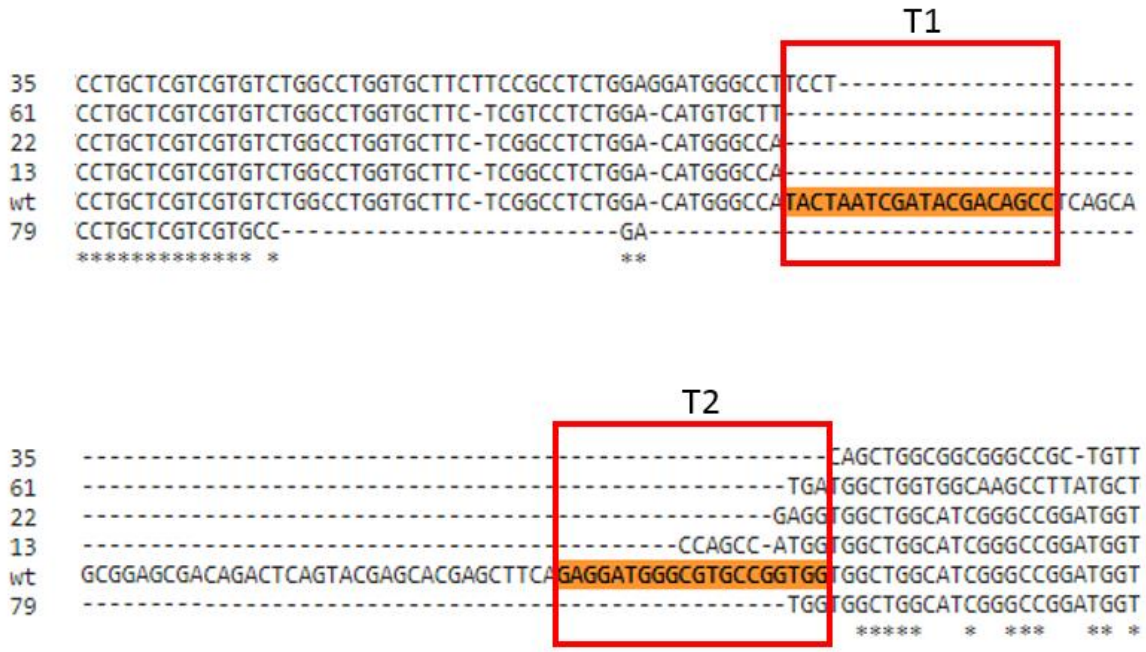

Figure 4.8. Aligned sequence result of generated mutants. Red boxes show gRNA target sites, T1 and T2.

The mutant lines generated by CRISPS/Cas9 method in this study were named as *dmHexDC*^{13}, *dmHexDC*^{22}, *dmHexDC*^{35}, *dmHexDC*^{61}, and *dmHexDC*^{79}. The effect of each deletion in relation to the resulting protein sequence was investigated by using *in silico* translation service provided by the MUSCLE alignment tool. The analysis showed that the primary structures of dmHexDC^{13}, dmHexDC^{22}, and dmHexDC^{35} were highly similar: each carried a frameshift mutation at amino acid residue 27, resulting in a truncated version of the protein due to the formation of an early stop codon. This truncated version of the protein lacks the putative catalytic domain resulting in a knockout of the gene in a functional sense. The lengths of dmHexDC^{13}, dmHexDC^{22}, and dmHexDC^{35} are 61, 59, and 60 amino acid residues respectively. The primary structures of the remaining two mutant alleles dmHexDC^{61} and dmHexDC^{79} were relatively similar. Unlike other mutants, these two alleles were still coding for a protein harboring the putative catalytic domain, yet with a deletion of

approximately 150 amino acid residues from the N terminus of the protein. For dmHexDC^{61}, 145 amino acid residues were deleted and 2 random amino acid residues (leucine and methionine) were inserted. For dmHexDC^{79} 161 amino acid residues were deleted and 7 random amino acid residues were inserted (Figure 4.9).

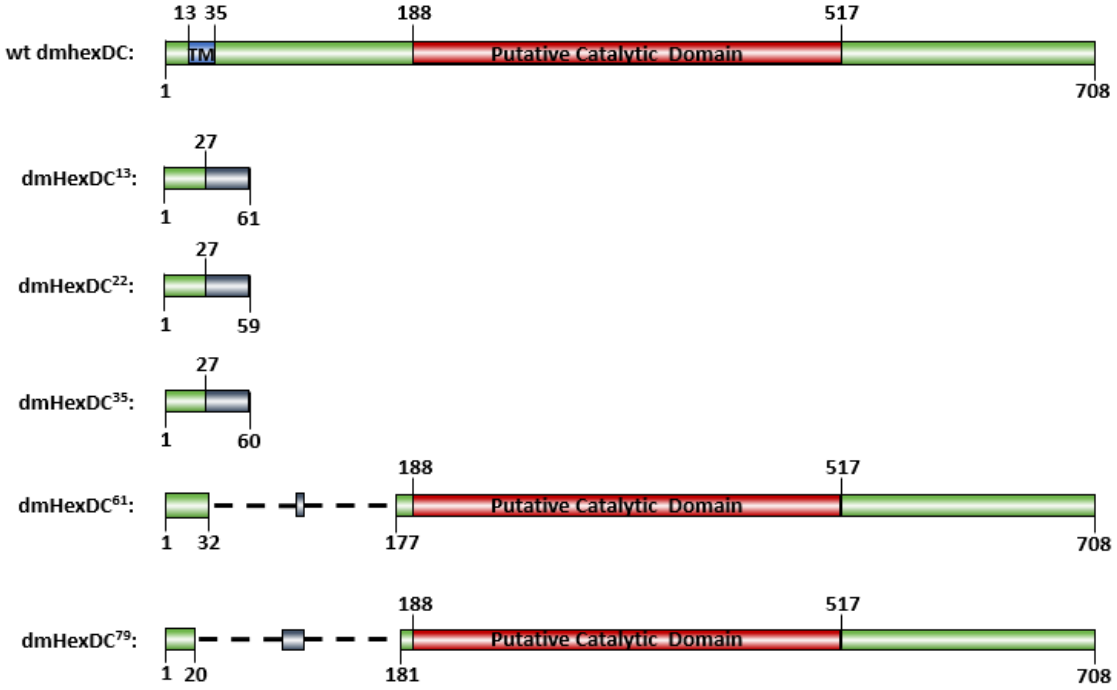

Figure 4.9. Primary structures of wild-type and mutant dmHexDC protein. Red region shows putative catalytic domain, blue region is the transmembrane domain, and green region is frameshift region.

dmHexDC^{13} and dmHexDC^{22} alleles were homozygous lethal similar to *dmHexDC^{null}* allele (Protein Trap allele of dmHexDC). However, different from *dmHexDC^{null}* allele, *dmHexDC^{13}* and *dmHexDC^{22}* are embryonic lethal. Surprisingly, homozygous *dmHexDC^{35}* flies appeared to be viable. As expected, homozygous *dmHexDC^{61}* and *dmHexDC^{79}* alleles were viable.

4.2. Analysis of the *dmHexDC^{null}* allele

Further analysis of CRISPR mutants could not be performed, because of problems in generating stable stock lines. Thus, the clonal analyses were performed using the protein trap line, which we showed to be a *dmHexDC^{null}* allele (Kıral, 2015).

4.2.1. Clonal Analysis of dmHexDC Mutant for Compensatory Proliferation

We hypothesize that loss of dmHexDC might lead to apoptosis-induced compensatory proliferation. To investigate this further cell autonomous and non-autonomous effect of *dmHexDC^{null}* allele was analysed for apoptosis and proliferation.

To analyze the autonomous and non-autonomous effect of loss of dmHexDC on CP, apoptosis and cell proliferation were analyzed in 8 imaginal discs from 4 third instar larvae, which contain mosaic homozygous mutant regions. Apoptotic cells were observed in heterozygous (marked by presence of RFP) as well as homozygous regions (marked by absence of RFP). However, an increased level of apoptosis was observed in mutant clones particularly in clones encompassing the morphogenetic furrow. These results are consistent with a cell-autonomous function of dmHexDC. Analysis of mitotic cells showed an increase of cell proliferation in both heterozygous tissue and homozygous mutant clones (Figure 4.10). Apoptotic cells in anterior tissue causes compensatory proliferation in neighboring cells. However, increased proliferation level in neighboring wt tissue was not by itself enough to conclude the apoptosis-induced CP as the driving force.

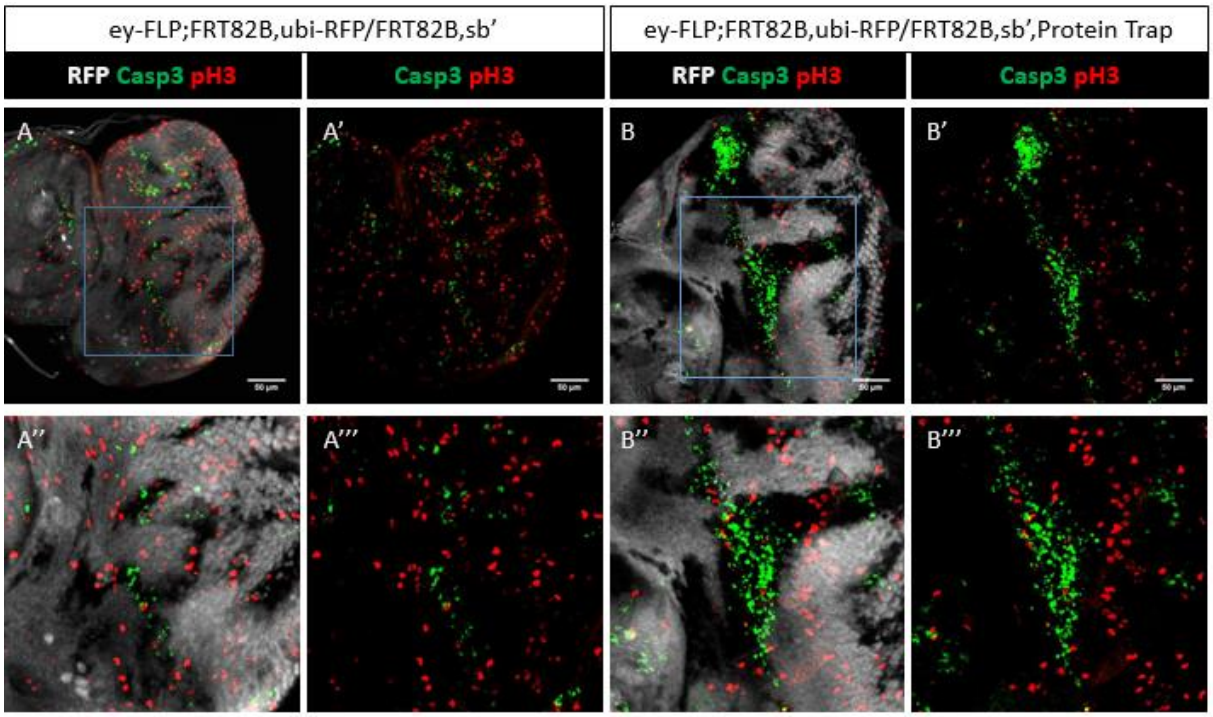

Figure 4.10. Clonal analysis of apoptosis and proliferation in mutant clones. Caspase3 (green) and phosphohistone H3 (red) staining of control (A-A''') and *dmHexDC*^{null} (B-B''') clonal eye disc of third instar larva. Homozygous clones are negatively labeled with RFP (grey). Blue rectangles mark regions that are shown in higher magnification in the bottom row.

4.2.2. Clonal Analysis of Compensatory Proliferation in Apoptosis Inhibited Eye

In the literature, apoptosis inhibited cells are used to prove the presence and the necessary signaling events for CP. Thus, undead cells were generated by overexpressing the apoptosis inhibitor p35. Two eye discs were investigated and an increase in mitotic cell density and size of tissue within or near the clone region were observed (Figure 4.11).

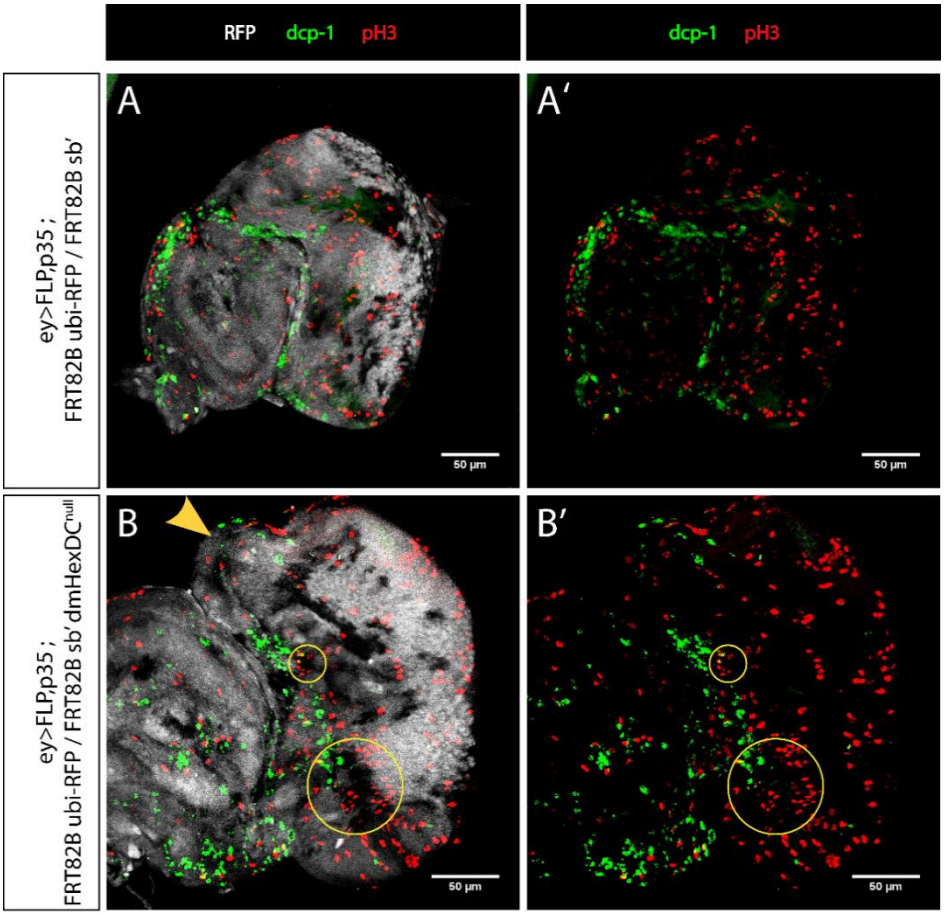

Figure 4.11. Clonal analysis for CP in apoptosis inhibited eye. dcp-1 (green) and pH3 (red) staining of control (A and A') and *dmHexDC*^{null} (B and B') clonal eyes of third instar larva. Homozygous mutant clones are negatively labeled with RFP (gray). Arrowhead indicates a region of tissue with overgrowth, and circles delineate increased density of mitotic cells near clonal regions.

Four imaginal discs with clones for loss of dmHexDC and overexpressed p35 were stained with anti-mCherry to visualize the clones and anti-Wg antibody. Additional Wg signal was observed near mutant clones in the ey-Gal4 domain where overexpression of p35 was achieved. Interestingly, the Wg overexpression was localized around the equator. (Figure 4.12. Clonal analysis of compensatory proliferation signal in imaginal discs where apoptosis was inhibited by overexpression of p35.).

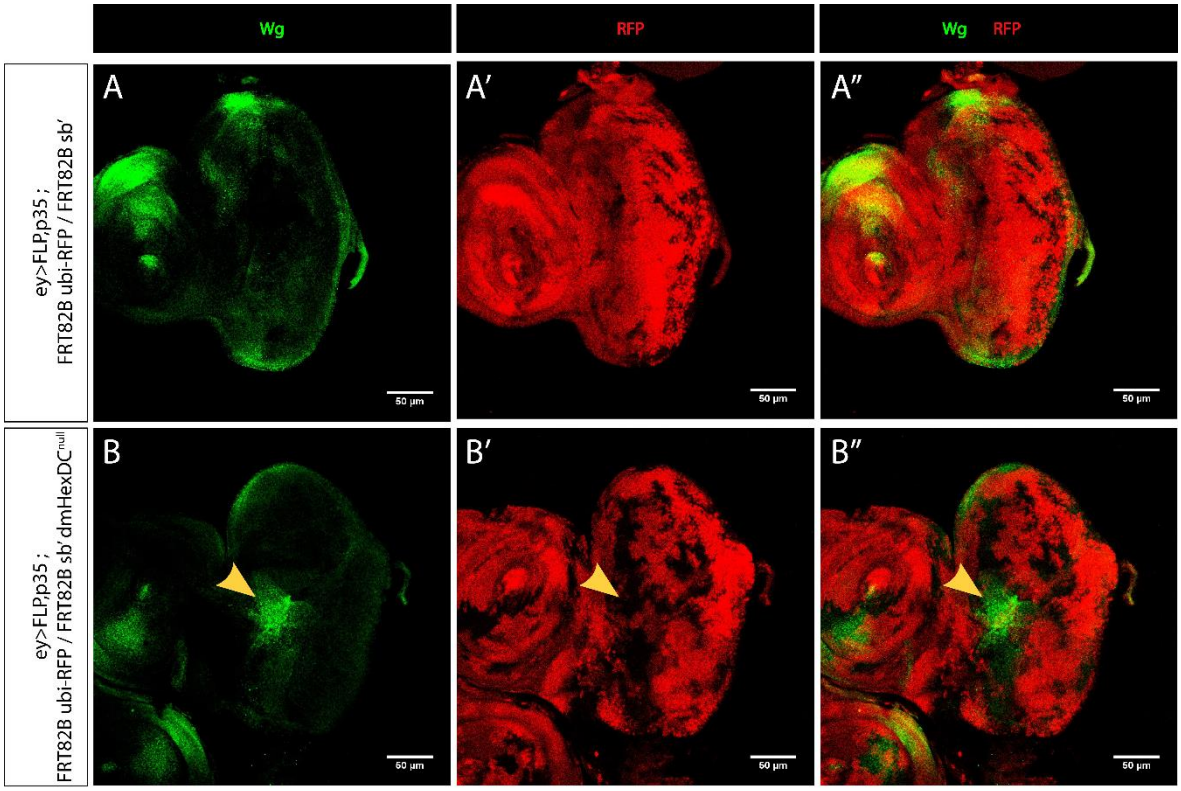

Figure 4.12. Clonal analysis of compensatory proliferation signal in imaginal discs where apoptosis was inhibited by overexpression of p35. Wingless (green) staining of control (A-A'') and *dmHexDC*^{null} (B-B'') clonal eye discs. The clones are negatively labeled with RFP.

4.2.3. Analysis of Undifferentiated Cells in *dmHexDC*^{null} Eye Imaginal Disc

To assess the state of undifferentiated cells within and posterior to the MF, a marker for undifferentiated cells, Yan, was used. Yan is a transcription factor that is highly expressed by undifferentiated cells in the posterior of the MF in eye imaginal disc. Two imaginal discs were stained with antibodies against Yan and Elav. As seen in Figure 4.8 Yan expression within the MF is lost and decreased posterior to the MF in *dmHexDC*^{null} mutants (Figure 4.13).

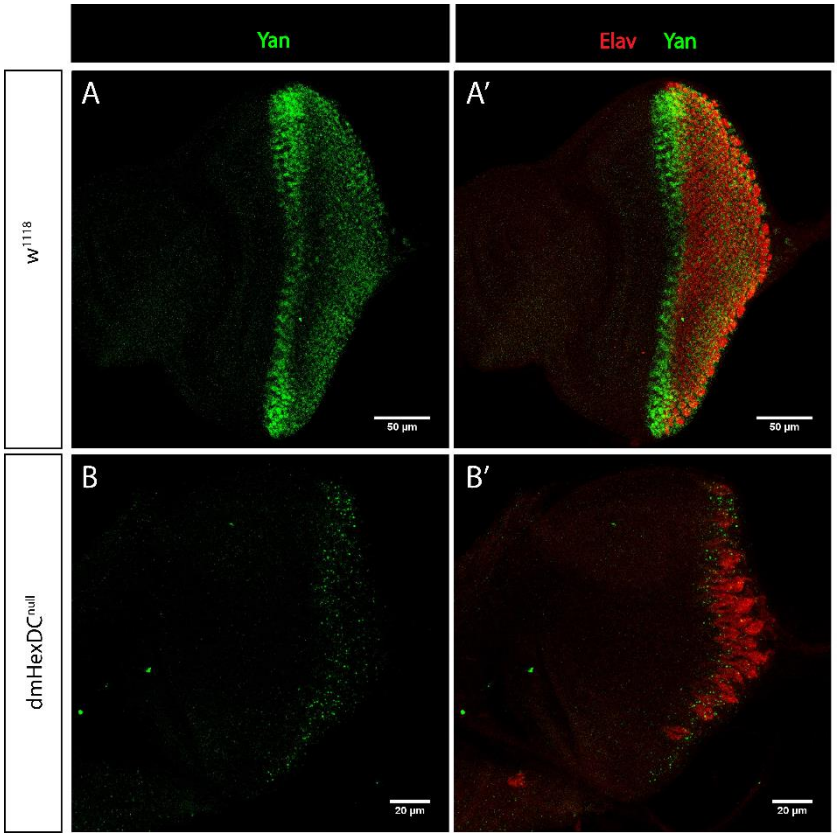

Figure 4.13. IHC to visualize undifferentiated cells. Yan (green) and Elav (red) staining of w^{1118} (A and A') and *dmHexDC*^{null} eye disc (B and B'). Decrease in Yan signal was observed in *dmHexDC*^{null} eye disc.

4.2.4. Clonal Analysis of Yan as an Undifferentiated Cell Marker

To further understand if the effect of *dmHexDC*^{null} mutation on Yan expression is cell-autonomous or non-autonomous *dmHexDC*^{null} clones were generated in the third instar larval eye using the FRT-FLP method, and stained with the Yan antibody. Elav was used to visualize neurons and RFP was used to mark wild-type tissue. The analysis of six imaginal discs showed that there was no difference between the Yan signal in wt and homozygous mutant clones (Figure 4.14B and B'). This presents a discrepancy with the previous experiment. As the previous experiment was performed on a very low number of imaginal discs the experiment needs to be repeated. From the clonal analysis experiments we can conclude that dmHexDC has no effect on undifferentiated cells.

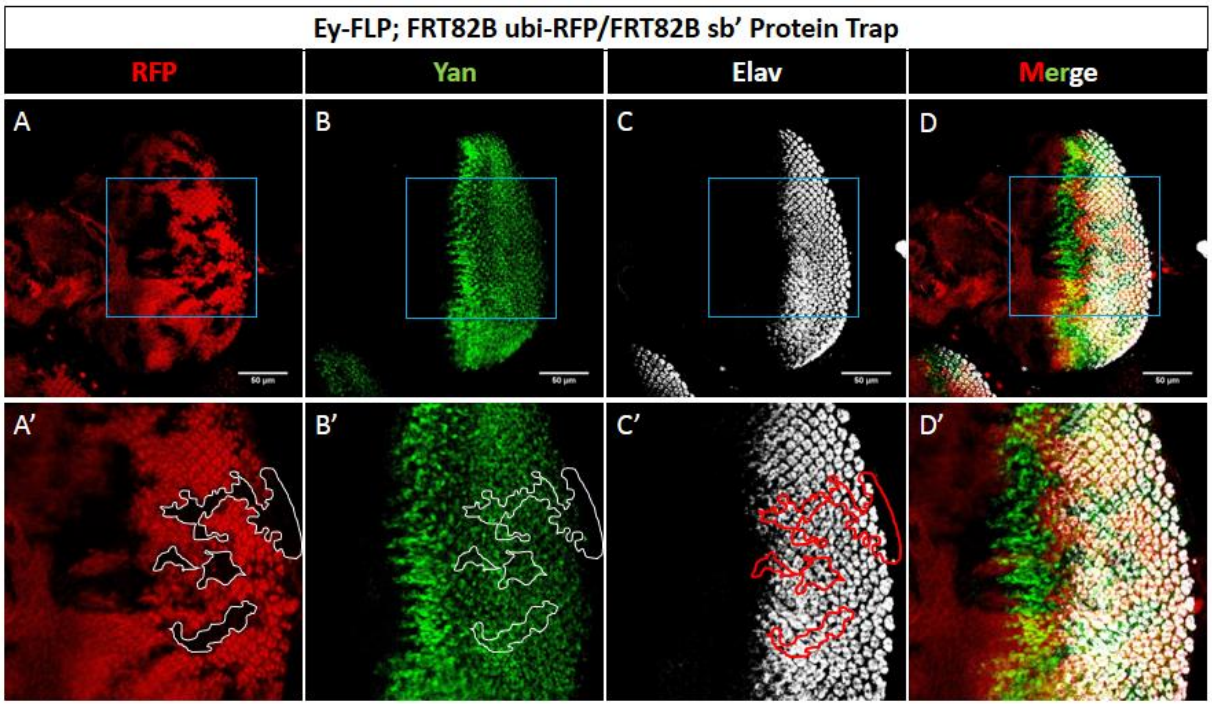

Figure 4.14. Clonal analysis of undifferentiated cells. Yan (green) and Elav (gray) staining of *dmHexDC*^{null} clonal eye disc. Light blue square shows zoom in region. There is no significant difference between *dmHexDC*^{null} clonal and wt regions.

4.2.5. Clonal Analysis of Morphogenetic Furrow Progression

Although Yan expression shows no difference in the clones, another indication for differentiation is morphogenetic furrow progression. The effect of loss of dmHexDC on MF progression was analyzed by generating homozygous *dmHexDC*^{null} clones, and analyzing the Yan and Elav boundary in six eye imaginal discs. The result shows that the MF progression was slightly attenuated at the equator of mutant clones of the eye (Figure 4.15, red arrow). As a conclusion, dmHexDC is necessary for the proper MF progression in the Notch active region.

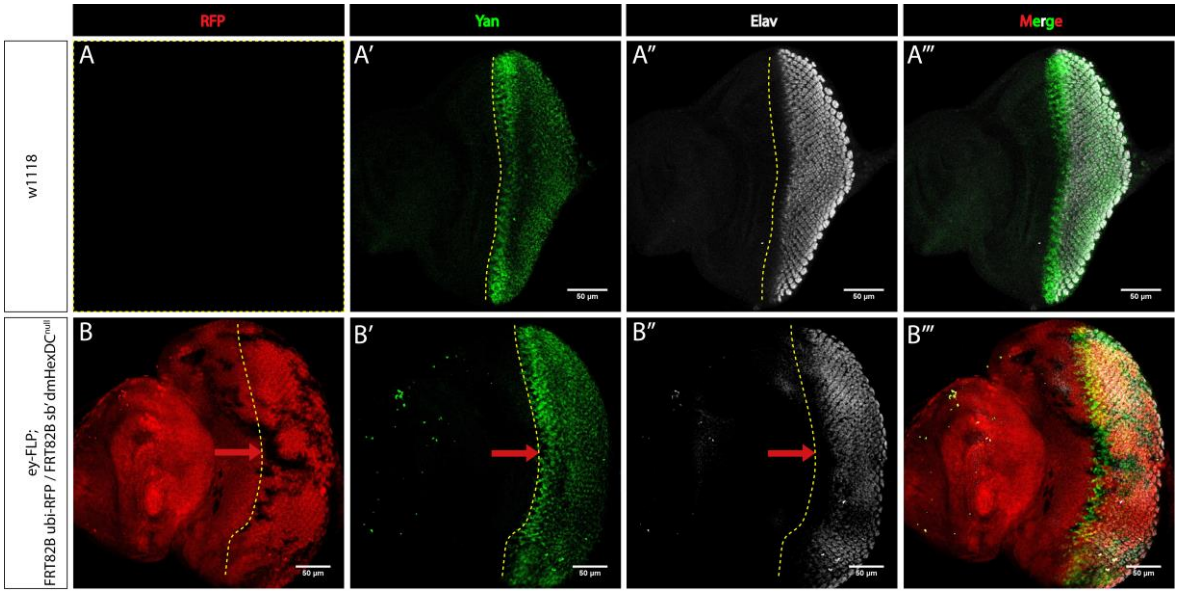

Figure 4.15. Morphogenetic furrow analysis in clonal eye discs. Yan (green) and Elav (gray) staining of control (A-A’’’) and *dmHexDC*^{null} (B-B’’’) clonal eye discs. Homozygous mutant clones are negatively labeled with RFP (red).

4.2.6. Clonal Analysis of Morphogenetic Furrow Progression in Apoptosis Inhibited Eye

We previously suggested that there can be a relation between apoptosis-induced CP and dmHexDC (Kıral, 2015). To understand the effect of apoptosis and CP on MF progression further, MF was analyzed by visualizing Yan and Elav expression boundary in three apoptosis inhibited *dmHexDC*^{null} clonal eye discs from third instar larva. An apparent disruption in MF progression and neuronal differentiation was observed in the middle of *dmHexDC*^{null} clonal eye disc with a large clone (Figure 4.16, B’ and B’’). The disrupted region in the MF belongs to a homozygous mutant clone region (Figure 4.16B). Eyes with wild type clones were used as negative control (Figure 4.16, A-A’’’). As a conclusion, newborn cells by compensatory proliferation blocks the MF progression in the Notch active region.

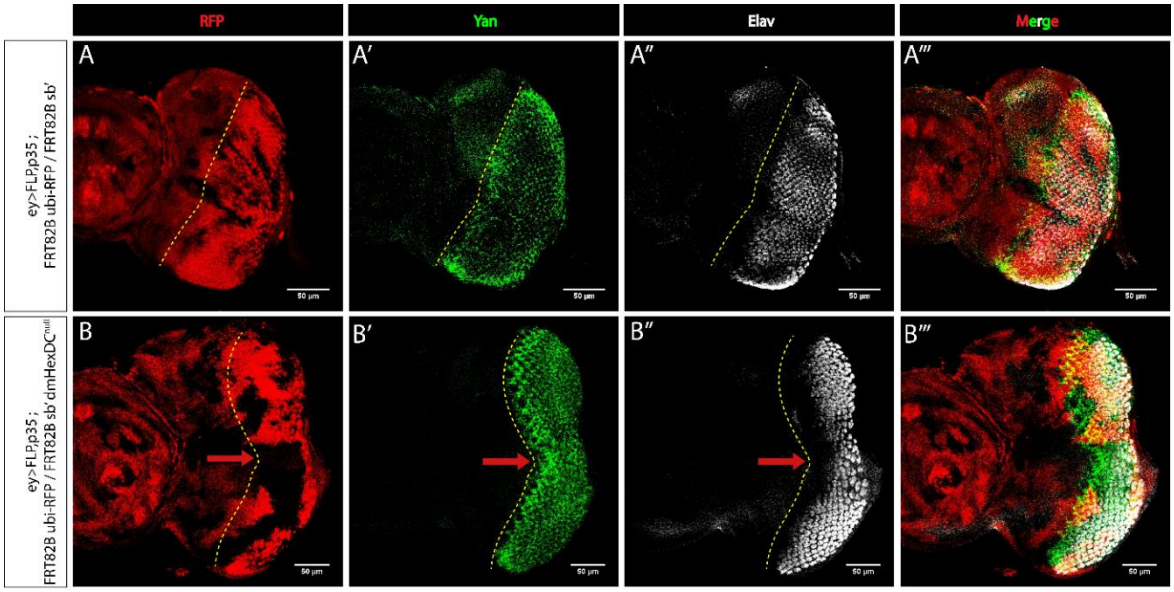

Figure 4.16. IHC of morphogenetic furrow. Yan (green) and Elav (gray) staining of control (A-A’’’) and *dmHexDC*^{null} (B-B’’’) clonal eye disc. Homozygous clones are negatively labeled with RFP (red).

4.2.7. Immunohistochemistry Analysis of Glial Cells in *dmHexDC*^{null} Eye Imaginal Discs

Previously, poor expression of dmHexDC was reported in glial layer of eye imaginal disc (Kıral, 2015). To understand the effect of dmHexDC on glial cells, we checked the gilal marker Repo in dmHexDC^{null} eye discs.

Impairment in neuronal differentiation was observed as expected mostly near the D-V midline in eye imaginal discs by IHC analysis using the neuronal antibody Elav (Figure 4.17B, arrowhead). Unexpected over-migration of glial cells to anterior of MF in the equator was observed (Figure 4.17B’, arrowhead). *w*^{1118} flies were used as negative control. Four *dmHexDC*^{null} eye imaginal discs were analyzed. As a conclusion, dmHexDC is necessary for proper glial migration in the D-V midline of eye disc.

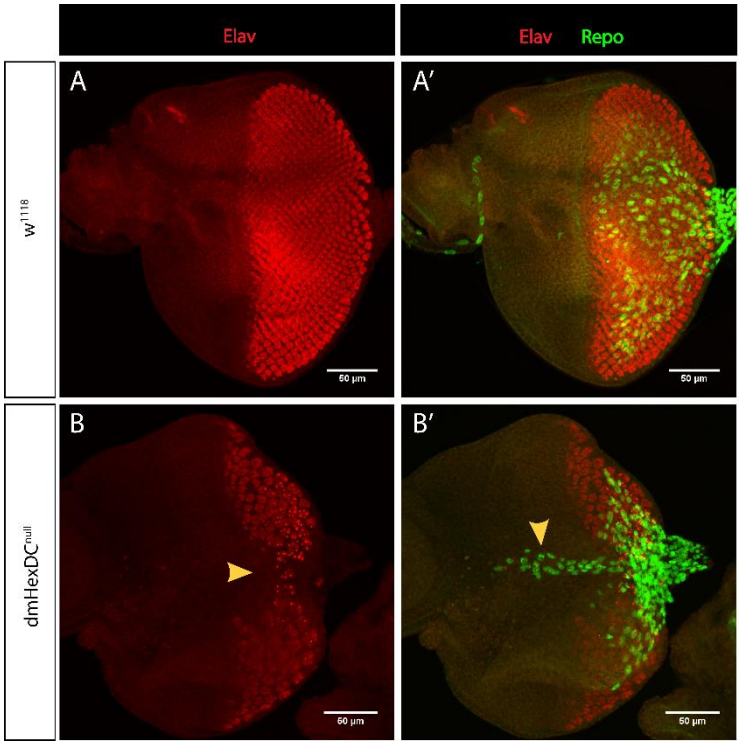

Figure 4.17. IHC analysis of PR and Glial cells. Elav (red), Repo (green) staining of w^{1118} (A-A') and $dmHexDC^{null}$ eye disc (B-B').

4.2.8. External Morphology of *dmHexDC*^{null} Clone Adult Eye

To examine the effect of dmHexDC loss in adult flies, complete homozygous $dmHexDC^{null}$ mutant adult eyes were generated using the FRT-FLP system. To generate whole mutant adult eyes a GMR-hid allele was used. Hid is a dominant apoptotic gene that drives cells to apoptosis. Under the control of the eye-specific promoter GMR, hid will only be activated in the eye and drive those cells to apoptosis. When combined with the FRT-FLP system the only cells that can survive in this genetic background are homozygous mutant cells.

Heterozygous dmHexDC mutants do not display any sign of abnormality in their external morphology (Figure 4.18A). The presence of a GMR-hid allele even in the heterozygous state causes an almost complete loss of the eye (Figure 4.18B). The hid phenotype is significantly suppressed in the presence of a wild-type or $dmHexDC^{null}$ allele. However, the differences in external morphology observed with both alleles were not

significantly different (Figure 4.18C and D). More than 10 flies for each group were analyzed.

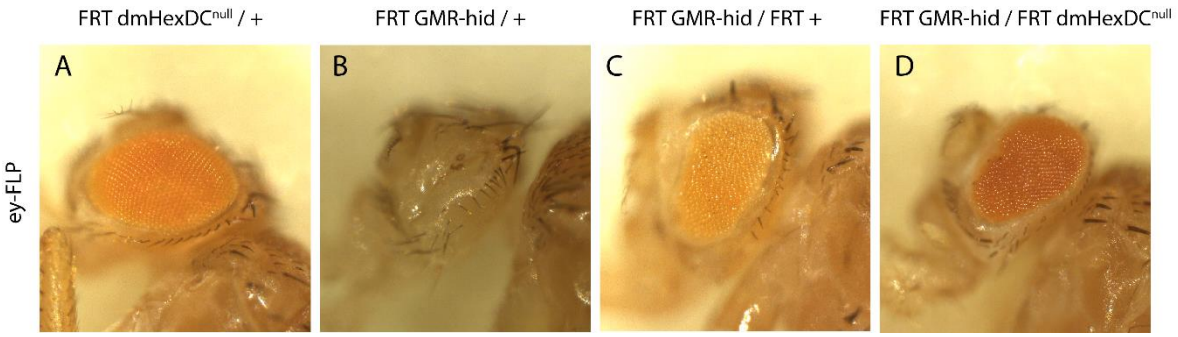

Figure 4.18. Light microscopy images of FRT-FLP carrying adult eyes. Heterozygous FRT mutant (A), heterozygous GMR-hid (B), *wt* clone (C), and *dmHexDC*^{null} clone (D) adult

4.3. Down-regulation of dmHexDC in the Eye

In the clonal analysis experiments, apoptosis induced-CP also observed in the mutant clones less than the mutant clones. To verify and quantify the CP in dmHexDC loss, dmHexDC down regulated eye discs were used.

4.3.1. Eye-specific dmHexDC Knockdown Function in Apoptosis and Proliferation

Imaginal discs where dmHexDC has been downregulated using the eye-specific drivers ey-Gal4 and GMR-Gal4 was analyzed for apoptosis using the apoptosis marker activated cleaved caspase-3 and the proliferation marker phosphohistone H3. Immunohistochemical staining of four eye imaginal discs revealed an increase in the number of caspase3-positive cells especially in the anterior region of the MF (Figure 4.19A and B). Furthermore, the number of mitotic cells within the anterior region increased approximately three-fold (Figure 4.19D). Downregulation of Hexo1, was used as a control. Hexo1 encodes HEX1 hexosaminidase which is similar to mammalian isozyme A (HexA). It was expected a similar result with dmHexDC downregulation in the anterior region. Because, role of HexA in ganglioside degradation is already known, and we expect dmHexDC also have a role in ganglioside degradation. Similar to downregulation of dmHexDC, downregulation of

Hexo1 results in an approximately two-fold increase in apoptotic and mitotic cells in the anterior. Also, a higher number of apoptotic cells were observed in Hexo1 downregulated eye discs. The calculated median number of mitotic cells in the anterior region in control, dmHexDC downregulated, and Hexo1 downregulated eye discs are 57, 145, and 100.5 respectively (Figure 4.19D). Four eye imaginal discs were analyzed for each group.

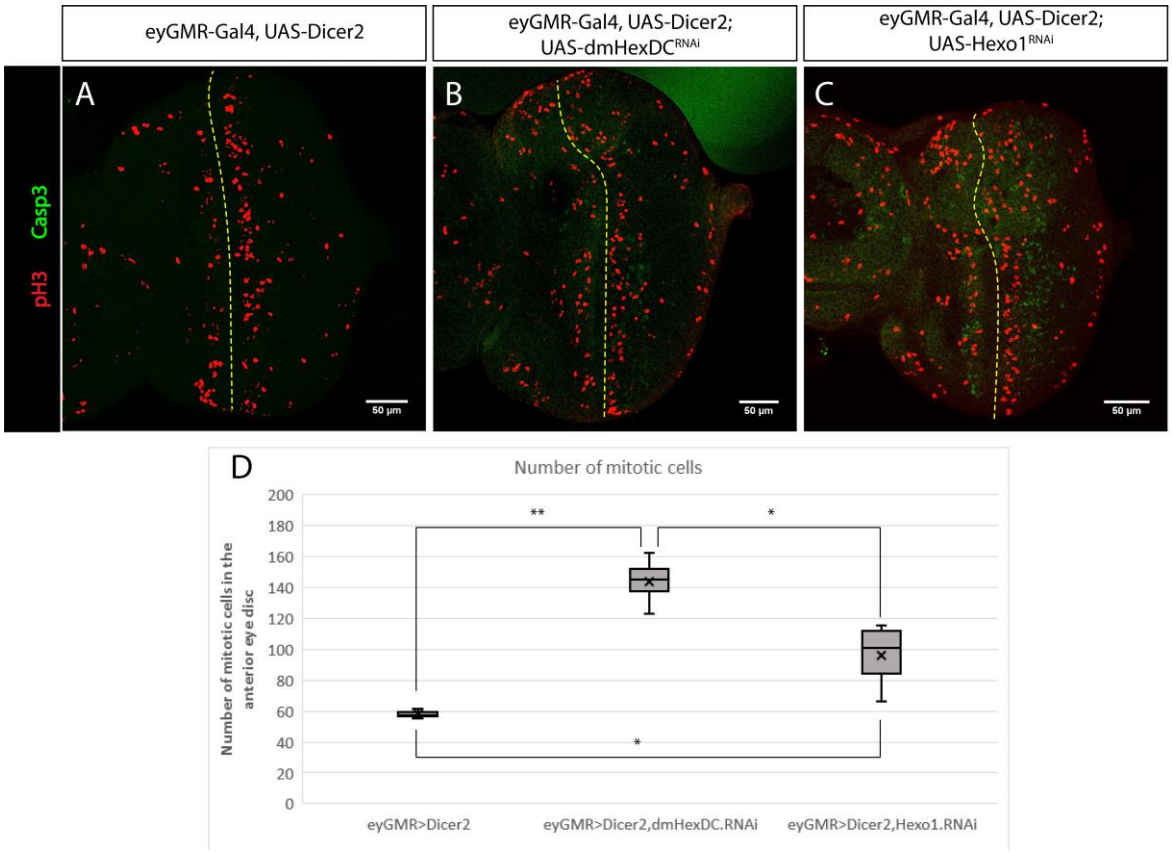

Figure 4.19. Compensatory proliferation analysis of dmHexDC down-regulated eyes. Caspase 3 (green) and phosphohistone H3 (red) staining of control (A), dmHexDC knockdown (B), and Hexo1 knockdown (C) third instar larval eyes. Yellow dashed lines show MF. D) Quantification of the number of mitotic cells in the anterior proliferative zone. *: $p<0.05$, **: $p>0,005$

4.3.2. Dorsal Knockdown of dmHexDC Function in Apoptosis and CP

One of the best ways to observe apoptosis-induced CP is through generation experimental tissue with an internal control. To observe apoptosis-induced CP with an internal control, dmHexDC downregulated only in dorsal part of the eye disc. In the observed

eye discs, the density of mitotic cells and apoptotic cells increased in dmHexDC knockdown in the dorsal part of the developing eye (Figure 4.20, B-B' and C). In control eye discs where only GFP was overexpressed in the dorsal region, apoptosis and mitotic cell signal is similar in dorsal and ventral regions (Figure 4.20, A-A' and C). The ratio of mitotic cell density is approximately 1 as expected. However, mitotic cell density in the dmHexDC downregulated dorsal part increased about 25%. The median value of the ratio between dorsal and ventral sides for control and *DE>dmHexDC^{RNAi},GFP* discs are 1.02 and 1.27 respectively (Figure 4.20C).

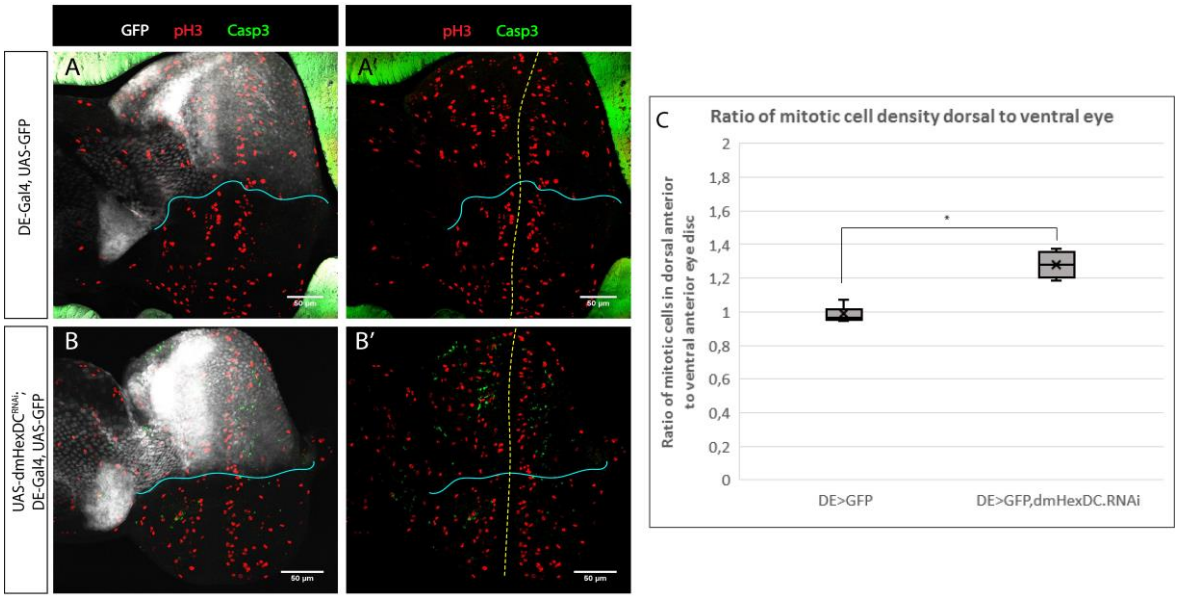

Figure 4.20. Dorsal-knockdown of dmHexDC. GFP (Gray), phosphohistone H3 (red), and caspase 3 (green) staining of control (A and A'), and dorsal knockdown dmHexDC (B and B') third instar larval eye. Blue line shows D-V boundary, and dashed yellow line shows MF. C) Quantification of mitotic cell density ratios. *: p>0.05

4.3.3. External Morphology of Eyes in Which dmHexDC Has Been Downregulated

To analyze the effect of dmHexDC downregulation on adult eye morphology, dmHexDC was downregulated by using the eye-specific driver ey-Gal4. Adult eyes showed no observable defect in external eye morphology (Figure 4.21A and B). The color change was not taken into consideration, because it results from the presence of the *white* gene marker in the UAS-*dmHexDC^{RNAi}* construct. To enhance downregulation efficiency, a

stronger driver eyGMR-Gal4 and overexpression of RNAi processor protein dicer2 (UAS-Dicer2) were used in addition to UAS-*dmHexDC*^{RNAi}. Again, no external defects were observed (Figure 4.21C and D). More than 20 flies for each experimental group were analyzed under the light microscope.

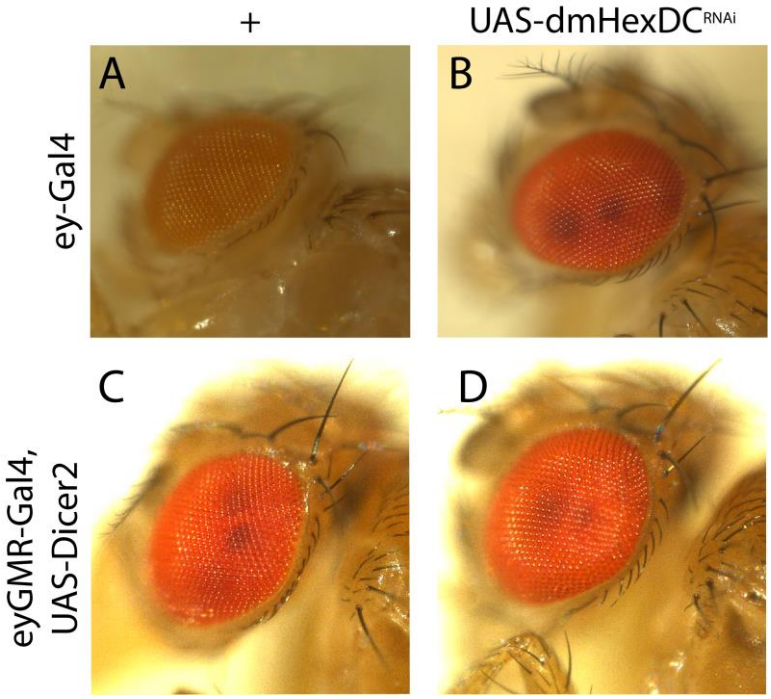

Figure 4.21. Light microscopy images of dmHexDC down regulated eyes. Control (A), ey>dmHexDC^{RNAi} (B), eyGMR>Dicer2 (C), and eyGMR>Dicer2, dmHexDC^{RNAi} (D) eyes of adult flies.

4.4. Analysis of dmHexDC Function in Autophagy

Degradative lysosomal enzymes can play a role in autophagy, and dmHexDC is a degradative enzyme and can be found in lysosomes. To investigate dmHexDC function in autophagy, fat body tissues were stained with a fluorescent dye called LysoTracker®, which labels acidic organelles including lysosomes and autolysosomes. Lysotracker has previously been used to detect autophagy-associated lysosomal activity in *Drosophila* tissues (DeVorkin and Gorski, 2014).

Autophagy was stimulated by starvation conditions. Starved and fed larva overexpressing dmHexDC ubiquitously (ubi-Gal4) were compared to larva carrying only the ubi-Gal4 transgene. No or very little formation of autolysosomes was observed in fat body tissues isolated from fed larvae, as expected (Figure 4.22, A and C), while starvation induced autolysosome formation in control and experimental tissues (Figure 4.22, B). However, autolysosome formation was drastically reduced in fat body tissues isolated from starved larvae that overexpress dmHexDC (Figure 4.22, D). Fat bodies were isolated from four larvae.

As a conclusion, dmHexDC have a role in autophagy pathway in *Drosophila*.

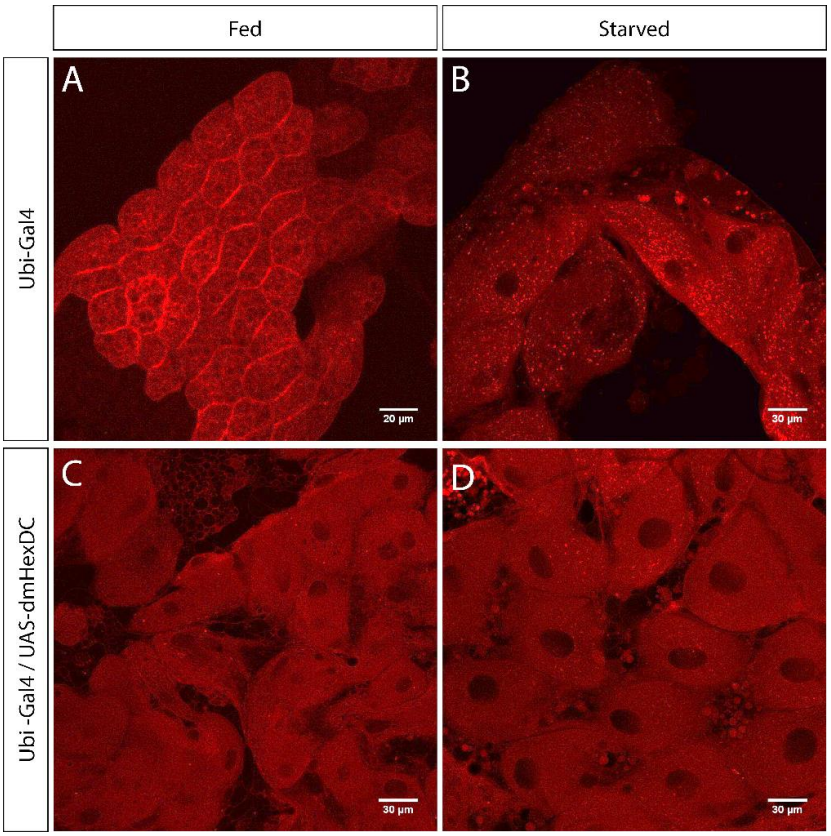

Figure 4.22. Effect of dmHexDC on autolysosome formation. Lysotracker staining of starved (A and C) and fed (B and D) fat body tissues from control (A and B) and dmHexDC overexpressed (C and D) third instar larva.

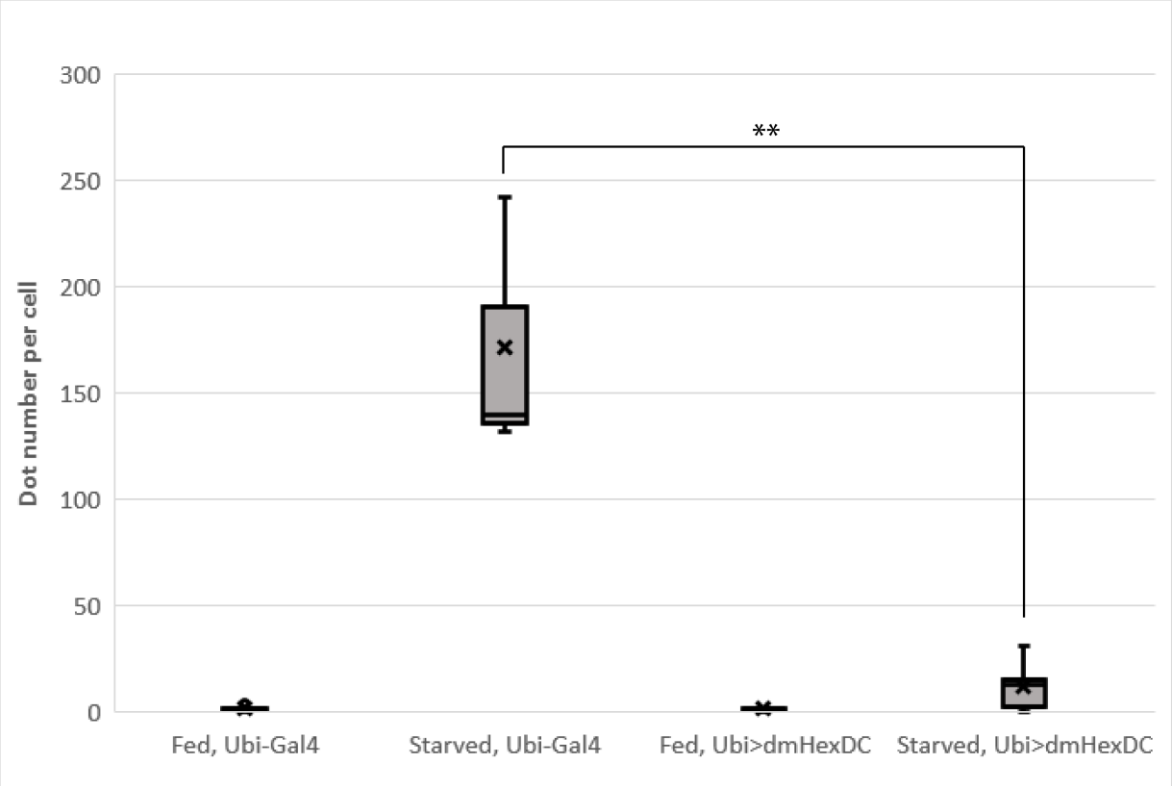

Figure 4.23. Quantification of autolysosome number per cell. Autolysosome formation significantly decreased dmHexDC overexpressed and starved fat body cells. **: p>0.005

4.5. Sub-cellular localization of dmHexDC

One way to understand the function of dmHexDC is to acquire knowledge about the sub-cellular localization of the protein in the cell. Previously, Golgi and endosomal localization of dmHexDC was reported by our lab (Kıral, 2015). However, these results were obtained by using mis-expression constructs. There is a considerable amount of error margin for the experiments, because labeling organelles with mis-expression construct may have a high error rate due to in efficient localization of the reporter protein. On the other hand, a conflicting result, mitochondrial localization of protein trap allele of dmHexDC has also been reported (Lye *et al.*, 2014). Different from previous experiments, organelle-specific antibodies for *Drosophila* were obtained and used in localization studies.

To detect sub-cellular localization of dmHexDC, posterior region of eye imaginal discs of GFP fused dmHexDC (dmHexDC::eGFP) line generated by BAC recombineering (Kaçmaz, 2013) was used. Endoplasmic reticulum, Golgi, lysosomes, early endosome, and

late endosome organelles were marked using organelle-specific antibodies which mark Calnexin99a, Golgin84, Arl8, Hrs, and Rab7 antigens respectively in *Drosophila* (Riedel, Gillingham, Rosa-Ferreira, Galindo, and Munro, 2016). Results show that dmHexDC::eGFP signals co-localize partially with all analyzed organelles. Quantification of sub-cellular localization of dmHexDC::eGFP was carried out by counting co-localized and total GFP-positive signals in the posterior side of the eye imaginal disc for each marker separately. For each marker, three images from at least three eye imaginal discs were quantified. Average percentages of GFP signals were obtained in Golgi, lysosome, ER, early endosome, and late endosome as 8.70%, 7.18%, 23.25%, 9.38%, and 10.05% respectively (Figure 4.24).

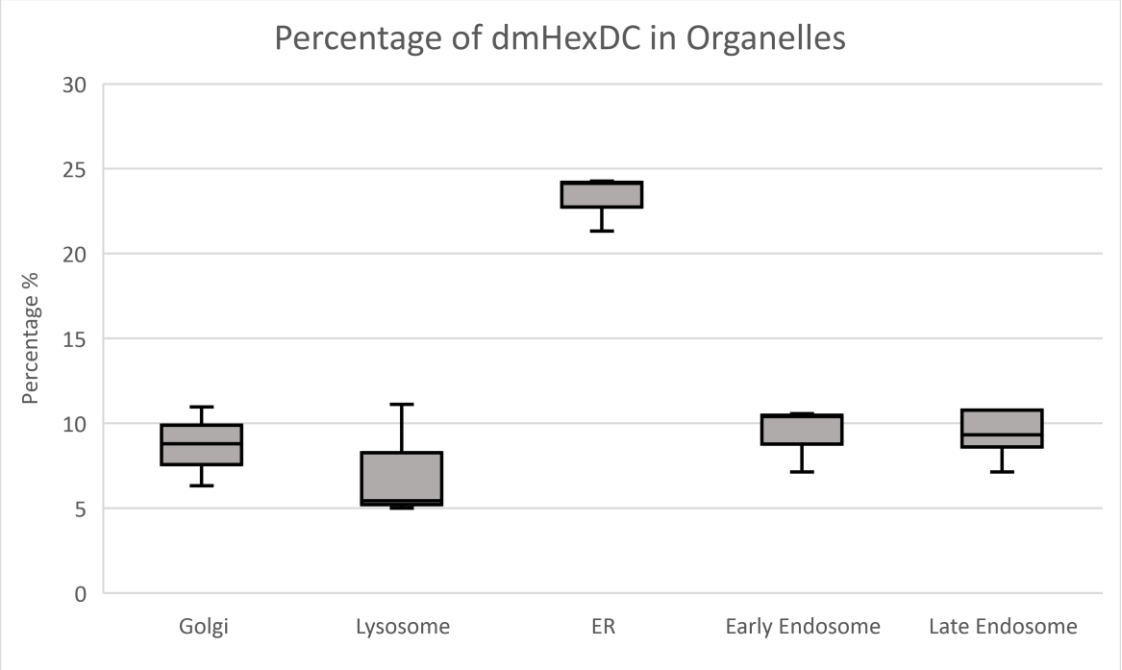

Figure 4.24. Quantification of colocalized GFP signals with Golgi, lysosome, ER, early endosome and late endosome. Quantification results are showed with box plot (n=3) with whiskers extending to ±1.5 x IQR. Median value is showed with a line across the box.

Contrary to our expectation, a small number of GFP signals co-localized with the Golgi and lysosome. After the quantification of GFP signals, more than 90% of GFP clusters were observed outside the Golgi (Figure 4.25A-A'' and Figure 4.24) and lysosome (Figure 4.25B-B'' and Figure 4.24).

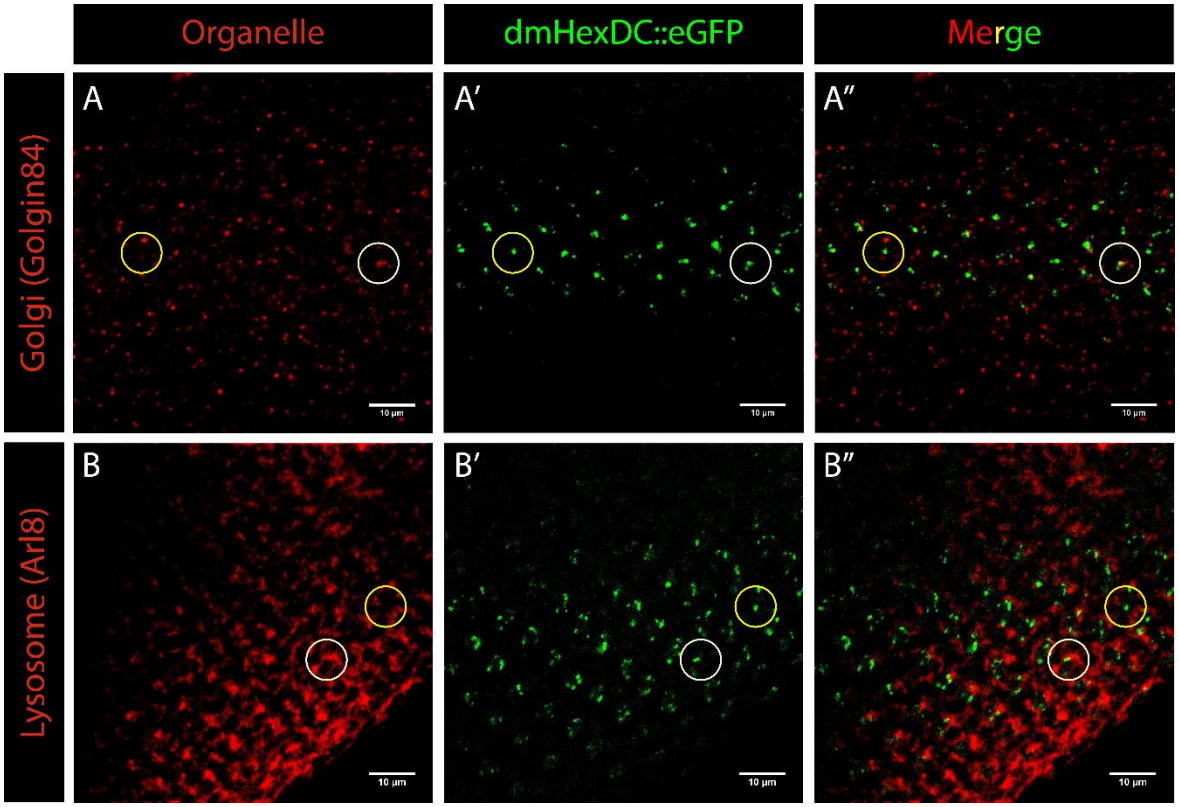

Figure 4.25. Localization analysis of dmHexDC to lysosomes and Golgi apparatus. GFP (green), and organelle-specific antibody against Golgi (A-A’’), and lysosome (B-B’’) staining of dmHexDC::eGFP of third instar eye imaginal discs. White circles indicate examples of co-localized signal sites, and yellow circles indicate examples of no co-localization sites.

Surprisingly, almost 25% of dmHexDC::eGFP signals colocalized with the endoplasmic reticulum (Figure 4.26A-A’’ and Figure 4.24). Similar to Golgi and lysosome, the percentage of localization of dmHexDC::eGFP puncta to early and late endosomes were limited to around 10% (Figure 4.26B-C’’ and Figure 4.24). As a conclusion dmHexDC mainly localizes to ER.

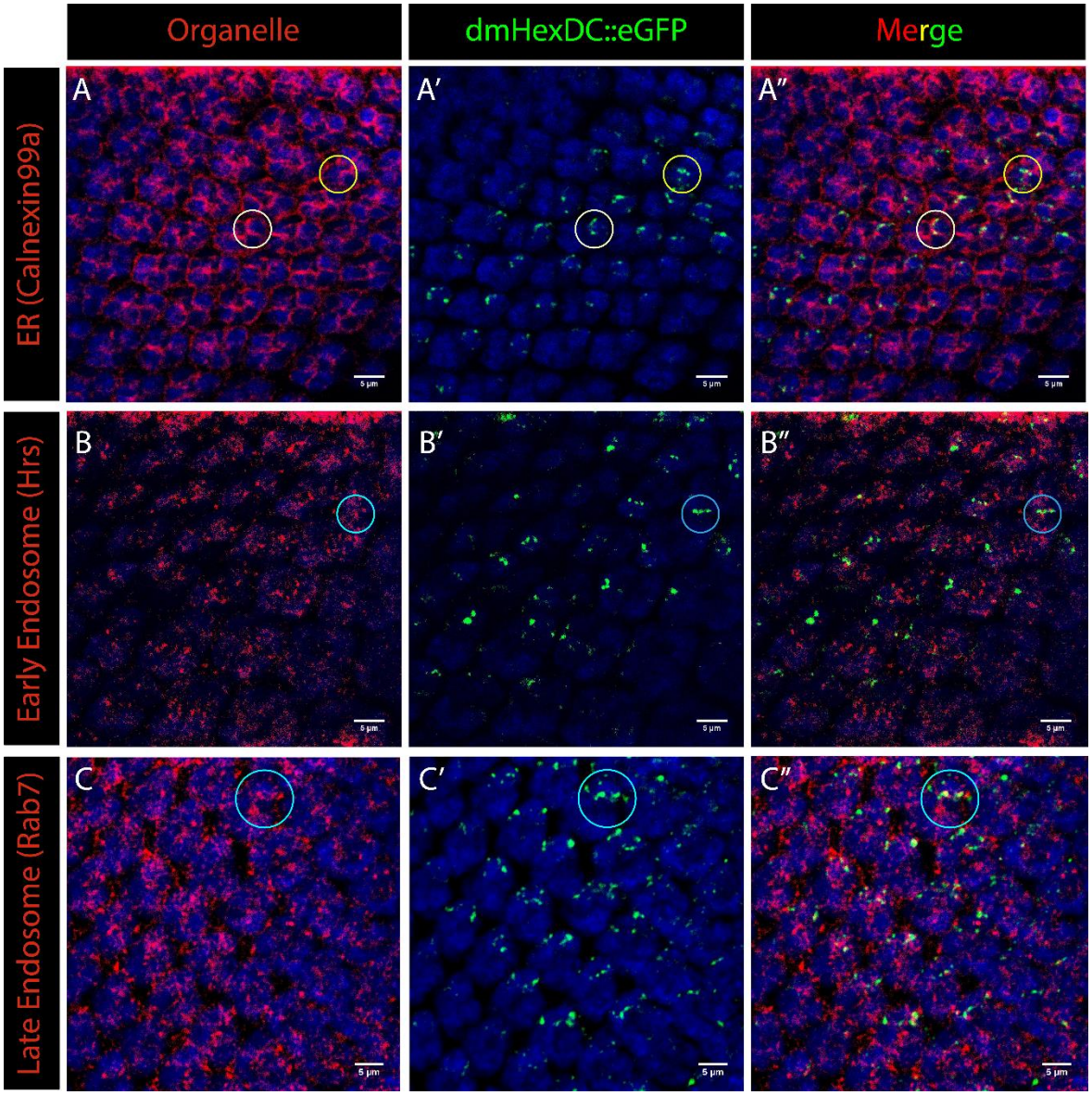

Figure 4.26. Localization analysis of dmHexDC to ER and endosomes. GFP (green), Elav (blue), and organelle-specific antibody (red) against ER (A-A''), early endosome (B-B''), and late endosome (C-C'') staining of dmHexDC::eGFP third instar eye disc. Circles indicate examples of co-localization (white circles) or not localization (yellow circles) or both (light blue circles) with organelle marker.

5. DISCUSSION

dmHexDC is a novel hexosaminidase enzyme expressed in the developing *Drosophila* eye that has role in the recycling of specific saccharides such as sulfated GAGs and gangliosides. The common feature of those saccharides is that they containing N-acetyl-galactosamine residues. dmHexDC has an affinity to hydrolyze terminal N-Acetyl-D-galactosamine residues. Hexosaminidase D is the mammalian homolog of dmHexDC. It is known that the hexosaminidase D is a nucleo-cytoplasmic protein involved in sulfated GAG degradation. However, the insect homolog, dmHexDC contains a highly hydrophobic region in a close proximity near to N-terminus. Therefore, sub-cellular localization and effect of dmHexDC can be different in compare with mammalian.

5.1. Catalytic Domain of dmHexDC is Essential for Survival

Several mutants were generated via CRISPR/Cas9 and their analysis indicates that the catalytic domain of dmHexDC is important for the survival of the organism. Mutants lacking the catalytic domain were lethal at embryonic stages. The only exception was observed in the $dmHexDC^{35}$ mutant, because homozygous $dmHexDC^{35}$ allele was viable. This unexpected result could be caused by a contamination in the stock line.

The used balancer chromosomes couldn’t protect dmHexDC genomic region from the recombination. Because of that, all stock mutant lines were lost.

5.2. Loss of dmHexDC Induces Autophagy, Apoptosis, and Compensatory Proliferation

Loss of dmHexDC leads to the accumulation of lipids and lysosomes (Kıral, 2015). In order to investigate whether dmHexDC has an effect on autophagy, we induced autophagy in dmHexDC overexpressed larva and control larva by the starvation assay. However, although autophagy was activated, still those molecules might not be degraded because

dmHexDC is the only enzyme for complete degradation of sulfated GAGs and gangliosides. Thus, the accumulation problem may turn into a lysosomal storage disorder, and cells enter programmed cell death. The relationship between autophagy and apoptosis has been described in mammals and happens through interaction between the autophagy protein Atg5 and pro-apoptotic protein bcl-2.

Apoptosis-induced CP is a phenomenon that is observed in imaginal discs of *Drosophila* (Fan & Bergmann, 2008a). Dying cells induce additional proliferation of neighboring cells by secreting a short-range signal such as wg and dpp (Fan & Bergmann, 2008b). In *dmHexDC*^{null} mutants, apoptotic cells cause apoptosis-induced CP in the anterior proliferative zone of the eye disc and neuronal differentiation of the cells generated by CP was delayed. It has been reported that autophagy protein Atg1 plays a role in CP (Li et al., 2016). So autophagy and apoptosis is related pathways to each other. In our case relation of autophagy and apoptosis pathways might be linked to each other via dAtg1, dAtg5 and debcl.

Thus, our findings suggest that the observed CP might be indirectly induced by the autophagy pathway in the *dmHexDC*^{null} mutant.

To observe CP more efficiently, undead cells were generated by using the caspase inhibitor, p35, which caused an increase in CP and impairment in MF progression. So, it means generated cells by CP prevents the MF progression. A similar mechanism to CP has been described in mammals, where p53-dependent apoptosis is induced in the intestinal epithelium of conditional *mdm2* knockout mice. In mice, dying cells are compensated by an increase in proliferation of non-mutant cells (Fan and Bergmann, 2008b). So, mammalian hexosaminidase D might have similar role to dmHexDC in mammalian compensatory proliferation or regeneration.

Thus, the revealing role of glycosylation on this mechanism can help to understand the effect of glycosylation on tissue regeneration. In apoptosis inhibited *dmHexDC*^{null} mutant eye, tumor-like over-proliferation was observed (Figure 4.11 B, arrowhead). It indicates that changing saccharide composition of cells can affect the cell proliferation rate. The effect of

dmHexDC on cell proliferation may help to understand the importance of enzymatic degradation of saccharides for tumor suppression.

5.3. Saccharide Accumulation in ECM Prevents Notch Activity

Impairment in neuronal differentiation and glial migration were observed near the equator of *dmHexDC*^{null} eye disc. The equator is the region where Notch is active. It is known that Notch is important in neuronal and glial cell fate determination (Fanto and Mlodzik, 1999). We postulate that loss of dmHexDC might somehow be modulating Notch activity, which would explain the observed phenotypes. ECM and membrane molecules can physically affect the interaction of membrane receptors and ligands. In our case, modification in the glycosylation pattern of molecules in the ECM, membrane proteins/lipids or Notch itself might change Notch activity and thus prevent its proper function (Figure 5.1).

Notch activity is required for normal migration of peripheral glial cells. Interruption of glial migration and increasing number of glial cells reported in Notch mutant Drosophila development (Edenfeld et al., 2007). The observed result in dmHexDC^{null} mutant show consistency with Notch mutants.

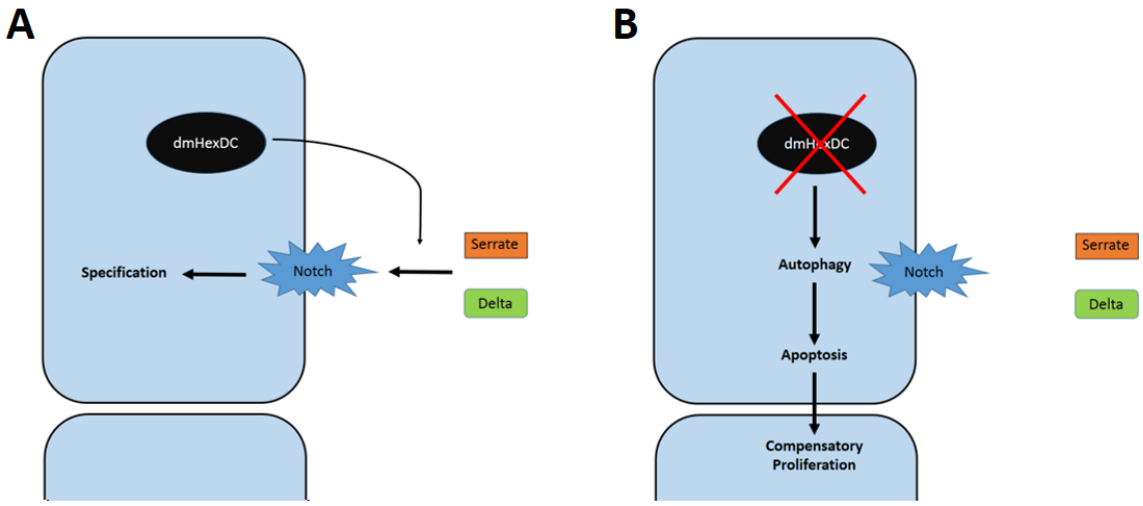

Figure 5.1. Representation of dmHexDC function in cellular specification.
A) dmHexDC provides cell specification via Notch activation. B) Loss of dmHexDC causes compensatory proliferation via autophagy and apoptosis.

5.4. dmHexDC is an Endosomal Protein Found in Organelle Membranes

In a previous study in our laboratory, subcellular localization of dmHexDC was investigated using reporter lines that localize RFP to subcellular locations utilizing the Gal4-UAS system and indicated the localization of dmHexDC to the Golgi and endosomes (Kıral, 2015). The recent development of *Drosophila*-specific antibodies that mark different organelles (Riedel et al., 2016) prompted us to use these to get more accurate information about the localization of dmHexDC.

Punctuated distribution of dmHexDC signal and partial co-localization of dmHexDC dots with several organelle markers show that the dmHexDC is an endosomal protein. dmHexDC seems to localize mostly to the ER. From the stainings, it is unclear to which membrane surface dmHexDC localizes. The first explanation is that, dmHexDC is found on the cytoplasmic side of the organelle membranes, because of the hydrophobic transmembrane domain. This probability can be an explanation for co-localization of dmHexDC mostly with ER, because it is the organelle with the most membrane surface area. The second probability is that the catalytic domain of dmHexDC is primarily found in the ER lumen. Catalytic function of dmHexDC takes place in ER, Golgi, and endosomes. However, the first explanation is more coherent with the mammalian homolog of dmHexDC. Furthermore, only around 60% of dmHexDC signals co-localized with the investigated organelles. Thus, it is unknown to which organelles the other 40% of dmHexDC signal localizes. Sub-cellular localization to the mitochondrial membrane is a possibility because mitochondrial localization of dmHexDC was previously reported in embryos (Lye *et al.*, 2014).

In mammalian, hexosaminidases generally localizes to lysosomes and cytoplasm. ER localization of dmHexDC is surprising, because GAG deglycosylation occur in lysosomes and cytosol. However, fused GFP domain may cause the ER localization of dmHexDC in the subcellular localization analysis, proteins stuck in the ER.

These results need to be treated with some caution. All experiments for sub-cellular localization were carried out by analyzing GFP tagged dmHexDC BAC construct. It should

be kept in mind that the GFP tag can affect the localization of the protein. In particular, the dmHexDC::GFP fusion generated here is not able to rescue the mutant phenotype, indicating that either the localization is not correct or some of the regulatory sequences are missing and the endogenous expression pattern is not recapitulated. Thus, the localization studies should be repeated once a reliable antibody against dmHexDC is generated.

5.5. Sulfated GAG Accumulation Prevents Puparium Formation

The major observed phenotype of homozygous *dmHexDC*^{null} flies is their deth by cuticle darkening during the puparium formation. This indicates that dmHexDC is important for puparium formation. It is known that the dmHexDC involves in enzymatic degradation of sulfated GAGs. These molecules are generally enriched in ligaments, cartilage, and skin tissues for providing flexibility and resistance to compression (Lindahl *et al.*, 2017). The cuticle of *Drosophila* larva is highly flexible tissue, but during puparium formation cuticle tissue loses its flexibility and becomes a rigid structure. For this transformation, dmHexDC may have a role in degrading sulfated GAGs in cuticle tissue and providing rigidness to the pupal cuticle. It can be the reason of the dying of *dmHexDC*^{null} flies during puparium formation.

5.6. dmHexDC Regulates Spinster Function

Spinster is a membrane protein involves many cellular process such as cell death and differentiation. In the literature, spinster knockout mutant *Drosophila* shows similar phenotypes to *dmHexDC*^{null} flies. Spinster knockout flies are lethal at the pupal stage, and Spinster is expressed in eye imaginal disc. Furthermore, it is a membrane protein localizes to lysosome and late endosome. Loss of spinster causes overmigration of glial cells in eye disc (Yuva-Aydemir *et al.*, 2011) similar to *dmHexDC*^{null} eye disc. Also, interfering of spinster mutation to apoptosis, lysosomal storage disorder and neuronal degeneration is reported (Nakano *et al.*, 2001). Those observed phenotypes are highly similar to *dmHexDC*^{null} phenotypes, which indicates dmHexDC function may regulates the effect of spinster.

5.7. Future Directions

The relation between Notch and dmHexDC is not clear enough. How can they affect each other? By overexpressing dominant negative Notch in D-V midline of the eye disc, the phenotypes can be compared with loss of dmHexDC phenotypes. Similar phontypes are expected, because it seems that the Notch activation regulated by dmHexDC. On the other hand, activation of Notch in *dmHexDC*^{null} eye discs can be analyzed by IHC.

The starvation-induced autophagy test should be repeated, and autophagy in the eye disc should be analyzed using autophagy reporter transgenic constructs. To prove that apoptosis is induced by autophagy atg5 and debcl protein localization should be analyzed by dmHexDC mutant clones. Furthermore, another possible CP signal, dpp, which has not been investigated so far should be analyzed in *dmHexDC*^{null} clones.

A relation between spinster and dmHexDC can be a new mechanism for regulation of glial migration. Further studies for determining how dmHexDC acts on spinster should be performed.

To clarify sub-cellular localization of endogenous dmHexDC, a better dmHexDC-specific antibody should be generated. Alternatively, endogenously tagged dmHexDC could be generated. dmHexDC localization to other organelles that have not been analyzed eg. mitochondria should be analyzed. Colocalization experiments could also be performed in S2 *Drosophila* cell cultures for better resolution. Also, higher resolution imaging could be used for better resolution of subcellular localization such as two-photon microscopy (Riedel *et al.*, 2016).

REFERENCES

Cagan, R. (2010). Principles of Drosophila Eye Differentiation, *2153*(9). https://doi.org/10.1016/S0070-2153(09)89005-4.Principles

Chondroitin Sulfate Degradation (Metazoa). (n.d.). https://targetexplorer.ingenuity.com/pathway/ING/ING:7l5yb, accessed at January 2018.

Çelik, A., & Wernet, M. F. (Eds.). (2017). *Decoding Neural Circuit Structure and Function*. Springer. https://doi.org/10.1007/978-3-319-57363-2

Dermatan Sulfate Degradation (Metazoa). (n.d.). https://targetexplorer.ingenuity.com/pathway/ING/ING:7l68z, accessed at January 2018.

Dermaut, B., Norga, K. K., Kania, A., Verstreken, P., Pan, H., Zhou, Y., … Bellen, H. J. (2005). Aberrant lysosomal carbohydrate storage accompanies endocytic defects and neurodegeneration in Drosophila benchwarmer. *Journal of Cell Biology*. https://doi.org/10.1083/jcb.200412001

Edenfeld, G., Altenhein, B., Zierau, A., Cleppien, D., Krukkert, K., Technau, G., & Klämbt, C. (2007). Notch and Numb are required for normal migration of peripheral glia in Drosophila, *301*, 27–37. https://doi.org/10.1016/j.ydbio.2006.11.013

Estella, C., & Baonza, A. (2015). Cell proliferation control by Notch signalling during imaginal discs development in *Drosophila*. *AIMS Genetics*, *2*(1), 70–96. https://doi.org/10.3934/genet.2015.1.70

Fan, Y., & Bergmann, A. (2008a). Apoptosis-induced compensatory proliferation. The Cell is dead. Long live the Cell! *Trends in Cell Biology*, *18*(10), 467–473. https://doi.org/10.1016/j.tcb.2008.08.001

Fan, Y., & Bergmann, A. (2008b). Distinct mechanisms of apoptosis-induced compensatory proliferation in proliferating and differentiating tissues in the Drosophila eye. *Developmental Cell*, *14*(3), 399–410. https://doi.org/10.1016/j.devcel.2008.01.003

Fanto, M., & Mlodzik, M. (1999). Asymmetric Notch activation specifies photoreceptors R3 and R4 and planar polarity in the Drosophila eye. *Nature*, *397*(6719), 523–526. https://doi.org/10.1038/17389

Gerhold, A. R., Richter, D. J., Yu, A. S., & Hariharan, I. K. (2011). Identification and characterization of genes required for compensatory growth in Drosophila. *Genetics*, *189*(4), 1309–1326. https://doi.org/10.1534/genetics.111.132993

Gratz, S. J., Rubinstein, C. D., Harrison, M. M., Wildonger, J., & O'Connor-Giles, K. M. (2016). Crispr-Cas9 Genome Editing in Drosophila, (May), 1–27. https://doi.org/10.1002/0471142727.mb3102s111.CRISPR-Cas9

Greenspan, R. J. (1997). *Fly Pushing*. New York, NY: Cold Spring Harbor Laboratory Press.

Greenwood, S., & Struhl, G. (1999). Progression of the morphogenetic furrow in the Drosophila eye : the roles of Hedgehog , Decapentaplegic and the Raf pathway, *5808*, 5795–5808.

Gutternigg, M., Rendic, D., Voglauer, R., Iskratsch, T., & Wilson, lain B. H. (2010). Mammalian cells contain a second nucleocyoplasmic hexosaminidase. *The Biochemical Journal*, *419*(1), 83–90. https://doi.org/10.1042/BJ20081630.MAMMALIAN

Hales, K. G., Korey, C. A., Larracuente, A. M., & Roberts, D. M. (2015). Genetics on the fly: A primer on the drosophila model system. *Genetics*, *201*(3), 815–842. https://doi.org/10.1534/genetics.115.183392

Jeibmann, A., & Paulus, W. (2009). Drosophila melanogaster as a model organism of brain diseases. *International Journal of Molecular Sciences*, *10*(2), 407–440. https://doi.org/10.3390/ijms10020407

Kaçmaz, G. (2013). *Characterization of a Novel R7-Specific Gene in the Drosophila Visual System* (Master's thesis). Retrieved from YÖK Ulusal Tez Merkezi

Kıral, F. R. (2015). *Functional Characterization of a Novel Hexosaminidase, CG7985, In Drosophila Eye Development* (Master's thesis). Retrieved from YÖK Ulusal Tez Merkezi

Kondo, S., Senoo-Matsuda, N., Hiromi, Y., & Miura, M. (2006). DRONC Coordinates Cell Death and Compensatory Proliferation. *Molecular and Cellular Biology*, *26*(19), 7258–7268. https://doi.org/10.1128/MCB.00183-06

Lee, J. D., & Treisman, J. E. (2002). Regulators of the Morphogenetic Furrow. *Drosophila Eye Development: Results and Problems in Cell Differentiation*, (212), 21–33.

Legent, K., & Treisman, J. E. (2009). Wnt Signaling in Drosophila eye development, *469*(10), 1–18. https://doi.org/10.1007/978-1-60327-469-2

Li, M., Lindblad, J. L., Perez, E., Bergmann, A., & Fan, Y. (2016). Autophagy-independent function of Atg1 for apoptosis-induced compensatory proliferation. *BMC Biology*, *14*(1), 1–15. https://doi.org/10.1186/s12915-016-0293-y

Lindahl, U., Couchman, J., Kimata, K., & Esko, J. D. (2017). Proteoglycans and Sulfated Glycosaminoglycans. In *Essential of Glycobiology*. https://www.ncbi.nlm.nih.gov/books/NBK453033/#_NBK453033_pubdet_, accesed at January 2018

Lye, C. M., Naylor, H. W., & Sanson, B. (2014). Subcellular localisations of the CPTI collection of YFP-tagged proteins in Drosophila embryos. *Development*. https://doi.org/10.1242/dev.111310

Martín, F. A., Peréz-Garijo, A., & Morata, G. (2009). Apoptosis in Drosophila: Compensatory proliferation and undead cells. *International Journal of Developmental Biology*, *53*(8–10), 1341–1347. https://doi.org/10.1387/ijdb.072447fm

Mayer, L. R., Diegelmann, S., Abassi, Y., Eichinger, F., & Pflugfelder, G. O. (2013). Enhancer trap infidelity in Drosophila optomotor-blind. *Fly*, *7*(2). https://doi.org/10.4161/fly.23657

McPhee, C. K., & Baehrecke, E. H. (2010). Autophagy in Drosophila melanogaster. *Biochim Biophys Acta*, *1793*(9), 1452–1460. https://doi.org/10.1016/j.bbamcr.2009.02.009.Autophagy

Nagy, P., Varga, Á., Kovács, A. L., Takáts, S., & Juhász, G. (2015). How and why to study autophagy in Drosophila: It's more than just a garbage chute. *Methods*, *75*, 151–161. https://doi.org/10.1016/j.ymeth.2014.11.016

Nakano, Y., Fujitani, K., Kurihara, J., Ragan, J., Usui-Aoki, K., Shimoda, L., … Yamamoto, D. (2001). Mutations in the novel membrane protein spinster interfere with programmed cell death and cause neural degeneration in Drosophila melanogaster. *Molecular and Cellular Biology*. https://doi.org/10.1128/MCB.21.11.3775-3788.2001

Ou, C. Y., Pi, H., & Chien, C. T. (2003). Control of protein degradation by E3 ubiquitin ligases in Drosophila eye development. *Trends in Genetics*, *19*(7), 382–389. https://doi.org/10.1016/S0168-9525(03)00146-X

Öztürk, A. (2010). *Characterization of genes involved in photoreceptor differentiation* (Master's thesis). Retrieved from YÖK Ulusal Tez Merkezi

Pastor-Pareja, J. C., & Xu, T. (2013). Dissecting Social Cell Biology and Tumors Using *Drosophila* Genetics. *Annual Review of Genetics*, *47*(1), 51–74. https://doi.org/10.1146/annurev-genet-110711-155414

Pennybacker, M., Liessem, B., Moczall, H., Tifft, C. J., Sandhoff, K., & Proia, R. L. (1996). Identification of domains in human beta-hexosaminidase that determine substrate specificity. *The Journal of Biological Chemistry*, *271*(29), 17377–17382.

Posse de Chaves, E., & Sipione, S. (2010). Sphingolipids and gangliosides of the nervous system in membrane function and dysfunction. *FEBS Letters*, *584*(9), 1748–1759. https://doi.org/10.1016/j.febslet.2009.12.010

Riedel, F., Gillingham, A. K., Rosa-Ferreira, C., Galindo, A., & Munro, S. (2016). An antibody toolkit for the study of membrane traffic in *Drosophila melanogaster*. *Biology Open*, *5*(7), 987–992. https://doi.org/10.1242/bio.018937

Sandhoff, K., & Harzer, K. (2013). Gangliosides and Gangliosidoses: Principles of Molecular and Metabolic Pathogenesis. *Journal of Neuroscience*, *33*(25), 10195–10208. https://doi.org/10.1523/JNEUROSCI.0822-13.2013

Scott, R. C., Schuldiner, O., & Neufeld, T. P. (2004). Role and regulation of starvation-induced autophagy in the Drosophila fat body. *Developmental Cell, 7*(2), 167–178. https://doi.org/10.1016/j.devcel.2004.07.009

Seyrantepe, V., Demir, S. A., Timur, Z. K., Von Gerichten, J., Marsching, C., Erdemli, E., … Miyagi, T. (2018). Murine Sialidase Neu3 facilitates GM2 degradation and bypass in mouse model of Tay-Sachs disease. *Experimental Neurology*, *299* (September 2017), 26–41. https://doi.org/10.1016/j.expneurol.2017.09.012

Sineshchekova, O. O., Kawate, T., Vdovychenko, O. V., & Sato, T. N. (2004). Protein-trap version 2.1: Screening for expressed proteins in mammalian cells based on their localizations. *BMC Cell Biology*. https://doi.org/10.1186/1471-2121-5-8

Toyoda, H., Kinoshita-Toyoda, A., & Selleck, S. B. (2000). Structural analysis of glycosaminoglycans in Drosophila and Caenorhabditis elegans and demonstration that tout-velu, a Drosophila gene related to EXT tumor suppressors, affects heparan sulfate in vivo. *Journal of Biological Chemistry*, *275*(4), 2269–2275. https://doi.org/10.1074/jbc.275.4.2269

Trowbridge, J. M., & Gallo, R. L. (2002). Dermatan sulfate: new functions from an old glycosaminoglycan. *Glycobiology*, *12*(9), 117R–125R. https://doi.org/10.1093/glycob/cwf066

Urbanelli, L., Sagini, K., Polidoro, M., Brozzi, A., Magini, A., & Emiliani, C. (2013). Therapeutic approaches for lysosomal storage diseases: a patent update. *Recent Patents on CNS Drug Discovery*, *8*(2), 91–109. https://doi.org/10.2174/1574889813089990002

Vijayalakshmi, M. (2012). *Drosophila melanogaster-Life Cycle*. *School of Chemical and Biotechnology SASTRA University*.

Voas, M. G., & Rebay, I. (2004). Signal Integration during Development: Insights from the Drosophila Eye. *Developmental Dynamics*, *229*(1), 162–175. https://doi.org/10.1002/dvdy.10449

Wernet, M. F., & Desplan, C. (2014). Homothorax and Extradenticle alter the transcription factor network in Drosophila ommatidia at the dorsal rim of the retina. *Development*, *141*(4), 918–928. https://doi.org/10.1242/dev.103127

Werth, N., Schuette, C. G., Wilkening, G., Lemm, T., & Sandhoff, K. (2001). Degradation of membrane-bound ganglioside GM2 by β-hexosaminidase A. Stimulation by GM2 activator protein and lysosomal lipids. *Journal of Biological Chemistry*, *276*(16), 12685–12690. https://doi.org/10.1074/jbc.M007970200

Yuva-Aydemir, Y., Bauke, A.-C., & Klambt, C. (2011). Spinster Controls Dpp Signaling during Glial Migration in the Drosophila Eye. *Journal of Neuroscience*, *31*(19), 7005–7015. https://doi.org/10.1523/JNEUROSCI.0459-11.2011

APPENDIX A: IMMUNOHISTOCHEMISTRY OF AC887 ENHANCER TRAP DEVELOPING ORGANS

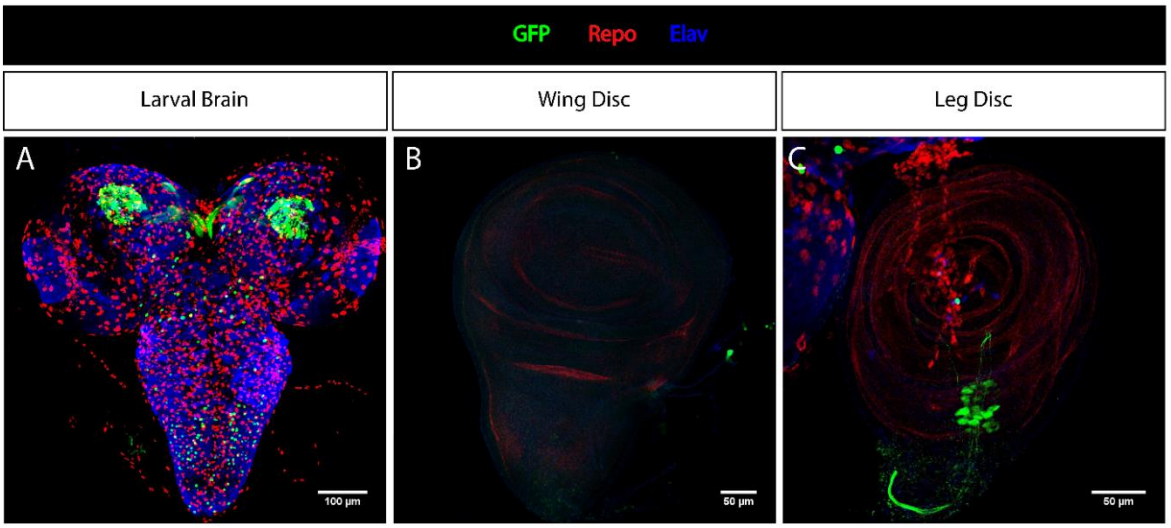

Figure A.1. Immunohistochemistry staining of developing organs; larval brain (A), wing disc (B), and leg disc (C) of AC887>GFPnls line.

APPENDIX B: PHALLOIDIN STAINING OF *DMHEXDC*^{NULL} CLONE ADULT EYE CRYOSECTIONS

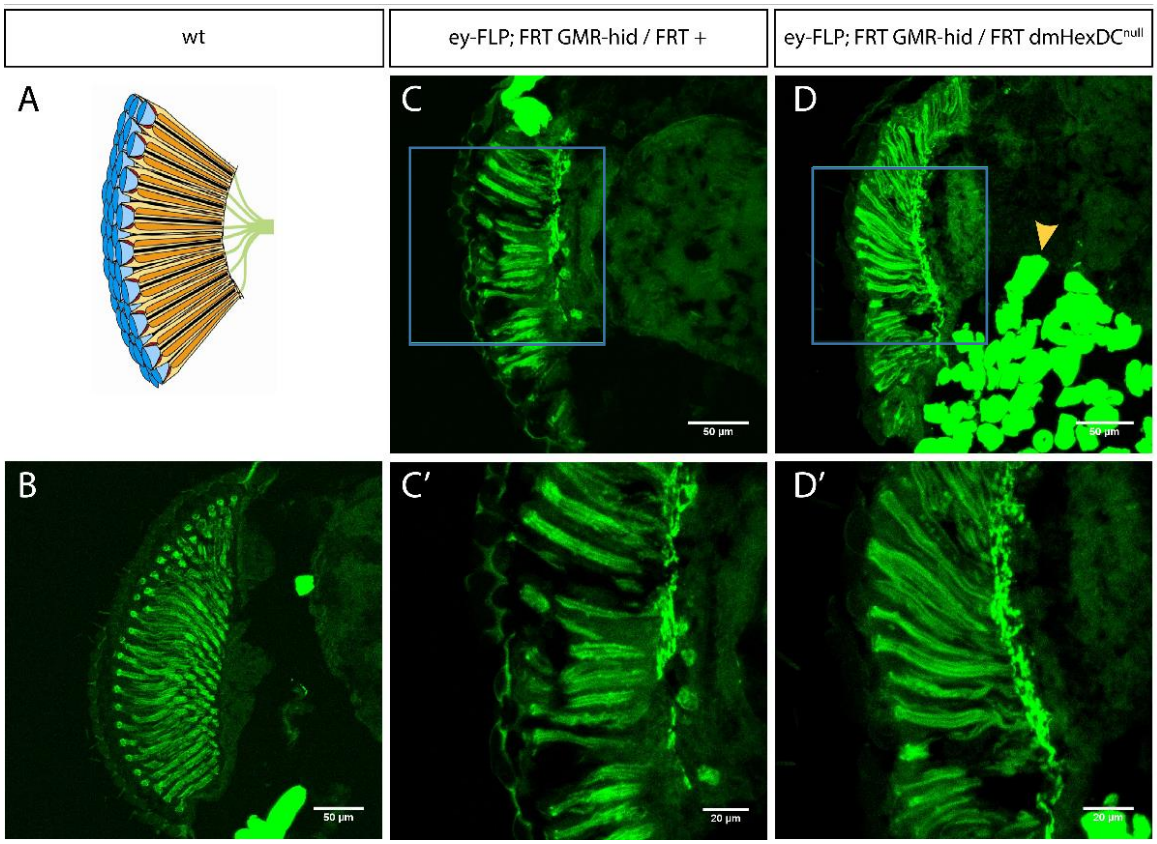

Figure B.1 Photoreceptor morphology of adult whole eye clones. A) Schematic representation of section of an adult eye. Phalloidin (green) staining of cryosection of wt (B), wt-clone (C) and higher magnification (C'), *dmHexDC*^{null}-clone (D) and higher magnification (D') adult eye. Yellow arrowhead marks accumulated fat tissue. Light blue square shows zoom in region.